Hot tearing of Mg-Y and Mg-Y-Zn alloys

Doctoral Thesis
(Dissertation)

to be awarded the degree
Doctor of Engineering (Dr.-Ing.)

submitted by

Zhi Wang

from Liaoning/VR China

approved by the Faculty of Natural and Materials Science,

Clausthal University of Technology

Date of oral examination

07.08.2014

Chairperson of the Board of Examiners

Prof. Dr. Diethelm Johannsmann

Chief Reviewer

Prof. Dr.-Ing. Babette Tonn

Reviewer

Prof. Dr.-Ing. habil. Karl Ulrich Kainer

Name, Vorname
Wang, Zhi

Datum:
14.08.2014

EIDESSTATTLICHE ERKLÄRUNG

Hiermit erkläre ich an Eides Statt, dass ich die bei der Fakultät für Natur- und Materialwissenschaften der Technischen Universität Clausthal eingereichte Dissertation selbständig und ohne unerlaubte Hilfe verfasst und die benutzten Hilfsmittel vollständig angegeben habe.

Unterschrift

Name, Vorname
Wang, Zhi

Datum:
14.08.2014

EIDESSTATTLICHE ERKLÄRUNG

Hiermit erkläre ich an Eides Statt, dass die eingereichte Dissertation weder in Teilen noch in Ihrer Gesamtheit einer anderen Hochschule zur Begutachtung vorliegt oder vorgelegen hat und dass ich bisher noch keinen Promotionsversuch unternommen habe.

Unterschrift

ACKNOWLEDGEMENTS

I gratefully acknowledge the financial assistance of Chinese-German Exchange Program organized by the Chinese Science Council (CSC) and German Helmholtz-Gemeinschaft.

This thesis work would not have been finished without the contribution of the following people that I deeply want to acknowledge.

I would like to thank my supervisor Prof. Dr. Karl Ulrich Kainer for all his help, guidance and insistence during my research work. I also specially thank Prof. Dr. Babette Tonn for her agreement to be the chief reviewer of this work and her valuable suggestions to complete this study.

I sincerely want to thank Dr. Norbert Hort and Dr. Yuanding Huang for their scientific and fruitful discussions during this work. I learned a lot from the discussions on castability of magnesium alloys with them.

Many thanks also to Dr. Amirthalingam Srinivasan, Dr. Felix Beckmann and Dr. Haifeng Liu for their helps in experiments and helpful discussions. Moreover, I would like to thank Dr. Chamini Mendis for her help in English grammar for my thesis.

Many thanks to Willi Punessen, Günter Meister, Gert Wiese, Petra Fischer and Sabine Schubert for their excellent technical help. I also gratitude all the staffs of WZP group for their assistance and the great working atmosphere during my stay.

Finally I would like to thank my parents and all my friends, especially my husband Ben Ma. Without their support, encouragement and the great times we spent together I would not have come so far!

ABSTRACT

Hot tearing is known as one of the most fatal solidification defects commonly encountered during casting. Although it has been investigated for decades, the understanding still stands at a qualitative level. So far, the investigations on hot tearing are mainly focused on the aluminum alloys and steel. Only a little work has been reported on the hot tearing of magnesium alloys. Recently, Mg-Y-Zn alloys have become as one of the most promising wrought magnesium alloys for practical applications. Therefore, it is extremely important to investigate the hot tearing susceptibility (HTS) of Mg-Y and Mg-Y-Zn alloys.

In the present work, the HTS of binary Mg-Y alloys is investigated using thermodynamic calculations based on Clyne and Davies model. The results indicate that the HTS as a function of Y content follows the "λ" shape. Based on predicted results, the HTS of Mg-Y and Mg-Y-Zn alloys are investigated at different initial mould temperatures using a constrained rod casting (CRC) apparatus with a load cell and a data acquisition system. Numerical simulations of HTS are calculated with ProCAST software. The HTS is characterized by quantifying the volume of the cracks and measuring the contraction force during solidification. Microstructures and fracture surfaces are investigated using XRD, OM and SEM.

The experimental results show that HTS decreases with increased mould temperature from 250 to 450 °C. The initiation of hot cracks is monitored during experiments and it corresponds with a drop in increment of load on the force-time curves. The critical solid fraction at which hot cracks form is determined according to the thermodynamic calculation with the Pandat software using the Scheil model. A study of macro-and microstructures of the alloys is performed and a relationship is found between the microstructures and HTS. The microstructures and fracture surfaces of Mg-Y alloys and Mg-Y-Zn alloys show that the hot cracks propagate along the dendritic or grain boundaries through the inter-dendritic separation or tearing of interconnected dendrites. The results also show that the grain size and type, second phases, freezing range of the alloys and the amount of eutectic phases are important factors that contribute to HTS. The HTS of binary Mg-Y alloys and ternary Mg-Y-Zn alloys is simulated using hot tearing indicator (HTI) model based on the accumulated plastic strain in the last stage of solidification and implemented in the ProCAST software. The predictions of HTS are validated by comparison with the experimental measurements.

LIST OF ABBREVIATIONS

BN	Boron nitride
CDI	Cumulated damage index
CRC	Constrained rod casting
CSC	Cracking susceptibility coefficient
EDS	Energy dispersive X-ray spectroscopy
HTS	Hot tearing susceptibility
HTI	Hot tearing indicator
ICP-OES	Inductively coupled plasma optical emission spectroscopy
LVDT	Linear variable differential transformer
OM	Optical microscopy
SEM	Scanning electron microscopy
SPV	Maximum volumetric flow rate per unit volume
SRG	Velocity of volumetric solidification shrinkage
TFR	Terminal freezing range
wt.%	Weight percent
XRD	X-ray diffraction

LIST OF SYMBOLS

D_{crit}	Critical diameter
X_{cr}	Fractional area of cracking
R_{100}^{av}	Average resistance reading for the 100 mm length
R_{40}^{av}	Average resistance reading for the 40 mm length
σ_{fr}	Fracture stress
γ	Surface tension
b	Liquid film thickness
F_z	Required force to increase the film thickness
η	Dynamic viscosity
R	Radius
f_s	Volume fraction of solid
f_l	Volume fraction of liquid
d	Average thickness of alloy solidifying grain
ε	Strain
m_p	Microstructure parameter
ρ_l	Liquid mass density
ρ_s	Solid mass density
v_l	Velocity of liquid
v_s	Velocity of solid
p_l	Pressure of liquid phase
p_s	Pressure of solid phase
σ_s'	Deviatoric stress tensor of solid
σ_l'	Deviatoric stress tensor of liquid
M	Interfacial momentum transfer
g	Acceleration of gravity
C_l	Heat capacity of liquid
C_s	Heat capacity of solid
λ_s	Heat conductivity in the solid phase

λ_l	Heat conductivity in the liquid phase
H	Latent heat
β	Shrinkage factor
$\dot{\varepsilon}_p$	Deformation rate
v_T	Solidification velocity
$\dot{\varepsilon}^{\max}$	Maximum deformation rate
$\dot{\varepsilon}^c$	Critical strain rate for hot tearing
l	Gage length
a	Length of tear
P_C	Cavitation pressure
P_M	Metallostatic pressure
K	Constitutive parameter
m	Strain rate sensitivity
κ	Permeability of mushy zone
η_L	Viscosity of liquid
λ_2	Secondary dendrite arm spacing
P_s	Effective feeding pressure
L	Length of porous network
c	Tortuousity constant of dendrite network
ρ_0	Density of liquid at melting point
$\overline{\rho}$	Average density
k	Partition coefficient
$\dot{T}$	Average cooling rate
m_l	Liquidus slope
C_0	Alloy with initial composition
t_V	Vulnerable time period
t_R	Time available for stress relief process
$t_{0.99}$	Time when the volume fraction of solid is 0.99
$t_{0.9}$	Time when the volume fraction of solid is 0.9
$t_{0.4}$	Time when the volume fraction of solid is 0.4

t_{coh}	Time when the volume fraction of solid at the coherency point
t_{cr}	Time when feeding becomes inadequate
$\bar{\varepsilon}_{ht}^{P}$	Critical accumulated effective plastic strain for the initiation of hot tearing
$\dot{\varepsilon}^{P}$	Effective plastic strain rate
t_C	Time when the coherency temperature is reached
t_S	Time when the solidus temperature is reached
$f_{p,d}$	Volume fraction of porous damage
I	Identity tensor
$\dot{\varepsilon}_s^{vp}$	Viscoplastic strain rate
T_{mold}	Mould temperature
V_{cr}	Hot crack volume
M_1	Weight of sample before injection of wax
M_2	Weight of sample after injection of wax
ρ_{wax}	Density of paraffin wax
C_L	Composition of the liquid at solid-liquid interface
T_M	Melting temperature of the pure base metal
T_E	Eutectic temperature
T_L	Liquidus temperature with alloy of initial composition
T	Temperature
ρ	Density
C	Specific heat
t	Time
Q	Heat flow
T_i	Critical temperature
f_{si}	Solid volume fraction at which hot crack initiation
F_r	Force release
T_f	Temperature at which the crack does not propagate
f_{sf}	Solid fraction at which the propagation of cracks stops
t_P	Propagation time

V_P	Force release rate
A	Conversion factor
ΔT	Temperature difference
S	Area
V	Volume

TABLE OF CONTENTS

1 INTRODUCTION

Various industries including automotive and aerospace, are showing greater interests in magnesium alloys, as they have a high specific strength when compared with aluminum alloys or steel [1-2]. More industries use magnesium alloys as a major component of new designs, thus, it is important to produce castings free of defects. Unfortunately, the newly developed magnesium alloys or the casting become increasingly thin and complicated, the alloys show a high susceptibility to defects known as hot tearing [3]. In order to enhance the magnesium alloy applications, it is extremely important to investigate the hot tearing susceptibility (HTS) of magnesium alloys.

Hot tearing, also known as hot cracking, hot shortness or hot brittleness, is one of the most severe solidification defects commonly encountered during casting [4-6]. It is defined as a failure occurring in the mushy zone of a freezing alloy. Hindered contraction and lack of feeding in the wide mushy zone are the main phenomena leading to the initiation of hot tearing [7-14]. It is a problem commonly encountered during the casting of alloys having a long freezing range. The cracks that form may be large enough to rupture entire section of casting. Such tears generally consist of a main tear and numerous minor offshoots, which follow inter-granular paths. The failure surface reveals a dendritic morphology.

The subject of hot tearing has been studied extensively. Many testing techniques and computational models to characterize HTS were developed. Numerous investigations show that hot tearing is a complex phenomenon, caused by the interactions between heat flow, fluid flow and mass flow. Various intrinsic and extrinsic factors influence hot tearing [15-16]. Although, it has been investigated for decades, the understanding still stands at a qualitative level. The quantitative information on hot tearing behaviour in alloys still remains somewhat unclear.

The factors affecting the tendency of hot tearing include: alloying elements, freezing range, grain size, amount of eutectic phases and initial mould temperature etc. [17-19]. So far, the investigations on hot tearing mainly focus on the steel and aluminium alloys. A comprehensive review on hot tearing behaviour of aluminum alloys has been published by Eskin et al. [5]. In contrast, only a little work has been reported on the hot tearing of magnesium alloys. For the hot tearing of magnesium alloys, most of the previous inspections

were conducted only for Mg-Al and Mg-Zn alloys [8-13, 20-23]. The additions of alloying elements such as Ca, Zn, Sr and rare earth (RE) elements to Mg-Al alloys were also investigated [8-13, 21]. Recently, Mg-Y-Zn system attracts significant to interest because they have both high strength at room and elevated temperatures [24]. Therefore, it is very important to investigate the castability of the alloys, especially hot tearing behaviour.

Hot tearing of any size scale can severely influence the performance and lifespan of parts. In order to understand the fundamental mechanisms responsible for the formation of hot tearing in magnesium alloys, it is very important to investigate the HTS using a quantitative and qualitative method under different casting conditions. Meanwhile, the application of numerical simulation techniques in metal casting provides insight into interpreting and understanding the formation of defects. Numerical simulation has been used to reduce the time required in new product design cycles and as a tool for quality assurance. To predict the susceptibility of hot tearing in a casting, a hot tearing indicator (HTI) is used in the present investigation which is based on Gurson's constitutive model and implemented in the ProCAST software. The numerical modeling of hot tearing formation is validated by experiments.

2 LITERATURE REVIEW

2.1 Methods for assessing HTS

Many techniques have been developed over the years to investigate hot tearing and assess HTS. This section summarizes some experimental methods used to study hot tearing.

2.1.1 Ring mould

A ring mould test is one of the simplest and classic hot tearing test methods. It has been used in numerous studies [25-27]. The ring mould was shown in Fig. 2.1 [16]. The relatively simple experimental setup consists of a ring and a core, both concentrically resting on a flat plate. The core can be made with a slight taper to be separated easily after casting. The ring, core and flat plate are made of materials with low thermal expansion coefficients and melting points much higher than those of the tested alloy. The alloy cast into the annular space between the ring and the core. The molten metal is readily poured into the space between the ring and the core. During solidification, the core resists solidification shrinkage and thermal contraction of the solidifying alloy. Consequently, a tensile stress is imposed onto the solidifying alloy, which causes hot tearing if the stress on the solidifying body exceeds its strength.

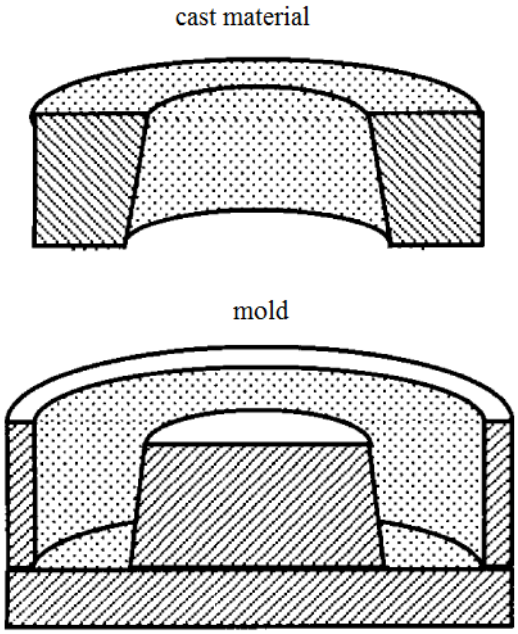

Fig. 2.1 A ring mould for hot tearing assessment [16].

Singer and Jennings [28] reported that the pouring temperature of the melt considerably influences the results of the ring mould test. They suggest that the pouring temperature should be 100 °C above the liquidus. The mould temperature is not critical. However, it is suggest that it is kept slightly higher than the room temperature. Since the top of the mould is open, the whole process of solidification can be visually observed. The main limitation of this technique is that it is difficult to control the solidification rate. Furthermore, this test gives only a qualitative value for the HTS. The HTS is usually measured by the length of the main crack. Sometimes, it is also defined as the sum of all crack lengths on all surfaces divided by the perimeter of the radial section. The disadvantage in this method is that the crack width or depth is not taken into account, but it is simple and appears to work quite well.

Wang et al. [8] investigated HTS of Mg-9Al-xZn alloys using crack-ring moulds as shown in Fig. 2.2. A round mould diameter of 108 mm was used. Chills were used to regulate the sequence of solidification. A round block of steel was located in the centre of the mould to hamper the solidification shrinkage of alloys. The diameter of the steel block is proportional to the degree of hindrance to an alloy. The critical diameter of the round steel block is inversely proportional to the HTS of magnesium alloys. The diameter of the round steel block is changed at an interval of 5 mm, such that the diameter 98, 93mm, etc. A crack susceptibility coefficient (CSC) is proposed, which is expressed as:

$$CSC = \frac{108 - D_{crit}}{108} \tag{2-1}$$

where D_{crit} is the critical diameter of the round steel block.

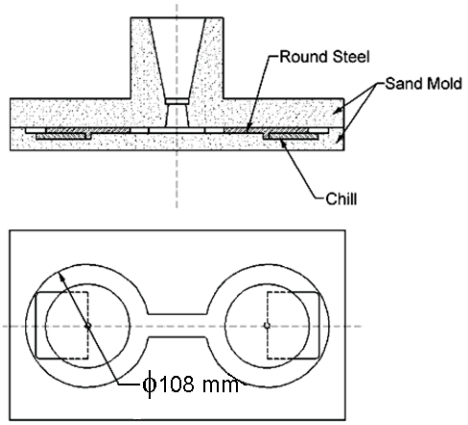

Fig. 2.2 Mould of crack rings [8].

Warrington and McCartney developed a so-called cold-finger test for the HTS [29-30]. The experimental conditions are reproducible and can be carefully controlled during this test. The test is likely to be particularly relevant to study the problem of shell zone hot tearing. The experimental setup, shown in Fig. 2.3, consists of an internally tapered steel crucible placed in an open furnace and a water cooled copper chill with a tapered conical portion. A copper chill has dimensions of maximum diameter 60 mm, minimum diameter 20 mm and 17.5° taper angle and its diameter is such that a wall thickness of the solidified ingot is approximately 10 mm. The molten alloy is poured into the crucible and held at the desired temperature for a given time. The chill is inserted into the alloy melt to a pre-determined depth. The insertion of the chill freezes the melt in a direction perpendicular to the chill surface. The crack is initiated on the top of a casting layer as it corresponds to the largest diameter of a specimen, and the highest retained stress. The hot tearing propagates downwards and then stops. After the solidification, the chill and the adhering ingot are removed. The melt temperatures and the copper chill can be precisely controlled using this technique. The length of cracks forms to determine the HTS.

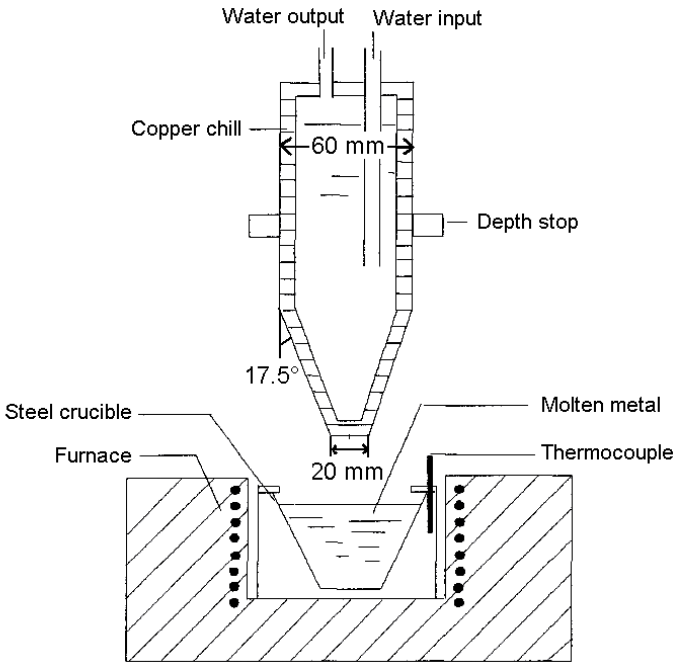

Fig. 2.3 Schematic illustration of the cold finger test system [30].

The limitation of these moulds is that it is difficult to control the cooling rate and the results cannot be duplicated accurately. Additionally, the techniques give only a qualitative value for HTS.

2.1.2 Restrained bar tests

These tests are developed to examine the HTS in one experiment by combining several restrained bar moulds, which are different in length and diameter, in a single setup. Novikov and Grushko [31] reported a harp type testing for 12 samples of 2×7 mm cross-section and different lengths from 10 to 120 mm. The melt is poured into the mould through a filling hole. Due to the progressively elevating constrained stress, hot tearing occurs in the longer samples. The HTS is taken as the minimum critical length of the samples in which hot tearing appears. An example of a harp shape mould is shown in Fig. 2.4 (a) [16]. Fig. 2.4 (b) demonstrates another configuration with variation of sample dimensions [16]. Here, the diameter of the samples is varied from 4 to 16 mm for a constant sample length of 40 mm. The hot tearing grade is determined as the square of the maximum value of bar diameter at which the hot tearing occurs. The higher the value of hot tearing grade, the worse the hot tearing resistance of the alloy investigated.

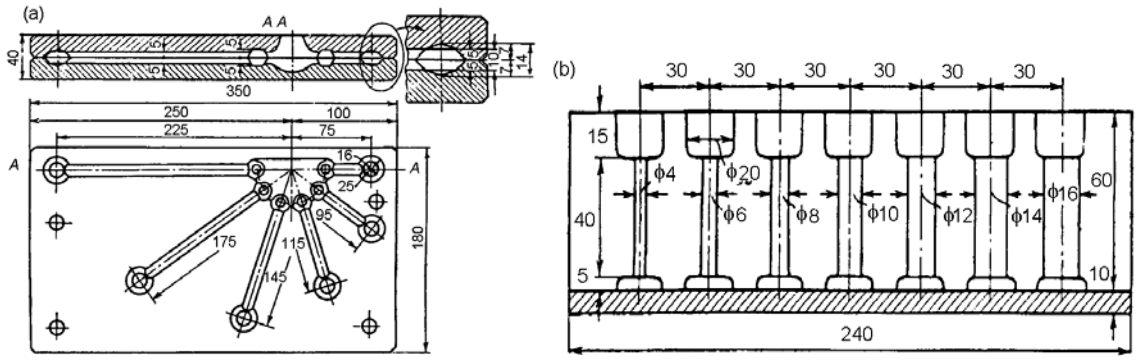

Fig. 2.4 Combination of several backbone moulds for evaluation of HTS with variation of cast length (a) and diameter (b) [16].

P. Gunde et al. [32] evaluated the HTS of Mg-Y-Zn alloys using a harp shape steel mould. The geometry of the cast component is shown in Fig. 2.5. The rod length variations (head to head distance) are as follows: 25, 45, 65, 95, 125 and 175 mm; all are 10 mm in diameter. The rods cannot freely contract during solidification. The mould was opened approximately 5 min after pouring, and the castings are examined for cracks with the naked eye and a 10× magnifying glass. A number representing the HTS was allocated to each investigated alloy. This number is obtained by examining each rod and assigning a value between 0 and 1 according to the following scheme: 1 for completely broken rods; 0.5 for obviously cracked

rods; 0.25 for rods with cracks detectable only with the magnifying glass; and 0 if no cracks are observed.

Fig. 2.5 Component cast in permanent steel mould for evaluation of HTS [32].

The electrical resistance method involves the measurement of total cracks on the surface and sub-surface. Clyne and Davies developed an elaborated restrained bar mould which contained a heater in the centre of mould and coolers at each end, as shown in Fig. 2.6 [33-34]. This allows for greater control of the thermal gradient during solidification. A steel mould is placed beneath an inductively heated graphite crucible that contains the alloy to be cast. It is cooled by water at both ends of the steel mould. The HTS is determined by comparing the electrical resistivity of the bars after solidification.

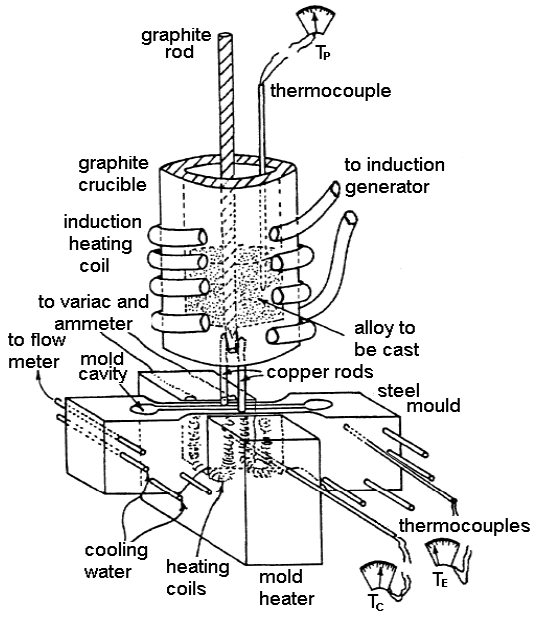

Fig. 2.6 The experimental setup of electrical resistance test [34].

The cross sectional area is reduced from the initial value to a final value due to presence of cracks. It is expressed as fractional area of cracking ($X_{cr,}$) and related to the measured resistance. It can be expressed as:

$$X_{cr} = 1 - \frac{R_{40}^{av}}{2(R_{100}^{av} - 2R_{40}^{av})} \tag{2-2}$$

where R_{100}^{av} and R_{40}^{av} are the average resistance readings for the 100 mm and 40 mm lengths, respectively. This gives $X_{cr} = 1$ for a completely cracked section. Clyne and Davies have used this method to measure the HTS of Al-Mg alloys. The results were broadly in agreement with those reported by Pumphrey and Lyons [26] using the ring casting tests.

These apparatuses are widely used to study the hot tearing behaviours due to that they are simple and have a good reproducibility. However, it is difficult to observe the formation of hot tearing during solidification.

2.1.3 Instrumented restrained bar tests

In recent years, a hot tear testing apparatus has been developed that incorporate the in-situ measurements of both the load and temperature. In order to assess the HTS quantitatively, a hot tearing setup based on the previous constrained rod testing was developed by Zhen et al. [35], as shown in Fig. 2.7. The system consists of a constrained rod casting (CRC) mould, a contraction force measurement system with a load cell, a data logging unit and a data recording program.

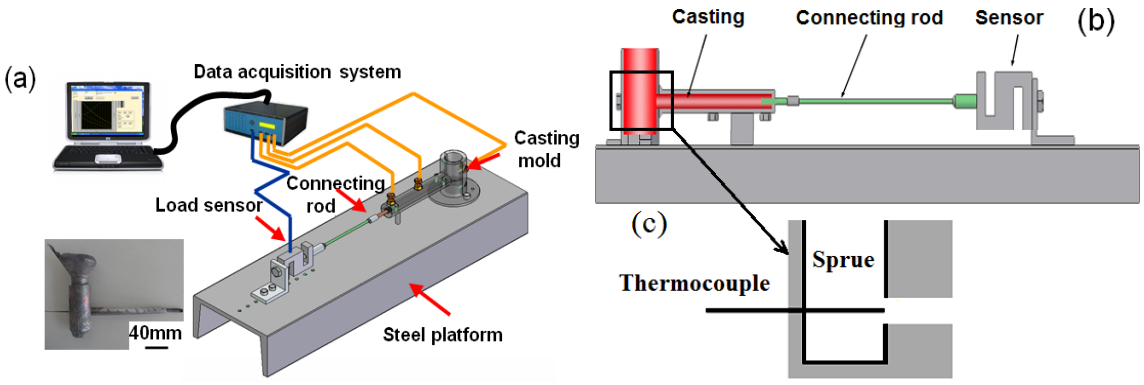

Fig. 2.7 Schematic of the experimental setup: (a) the whole setup, (b) the device for detecting temperature and force during the casting, (c) the position of thermocouple for obtaining the temperature at which the hot cracking initiates [35].

The mould consists of two parts: vertical sprue and horizontal round rod with a length of 148 mm. The sprue is open to air at the top and connected to the rod portion of the mould near the bottom. The diameter of the horizontal rod is 12.5 mm at sprue end and 10 mm at the opposite end. This slight taper is designed to reduce the friction between the mould and casting. At the opposite end to the sprue, a steel rod with 53 mm in length and 6 mm diameter is inserted into the rod portion of the mould and connected to a load cell (max. 2 kN) as illustrated Fig. 2.7. This steel rod provides a partial constraint to the movement of the casting in the mould during solidification. The force developed is monitored by the load cell. The data on the force retained, the mould temperature at different positions and temperature of the solidifying casting at the hot spot area are recorded on the attached computer. The force curve (force vs. time) and cooling curve (temperature vs. time) are used for the analysis of the hot tearing. Based on the recorded curves, the critical temperature and solid fraction at which the hot tears initiate can be determined.

The device shown in Fig. 2.7 (b) is used to measure the temperature and force at which cracking occurs during solidification. The hot tears occur at the junction of the sprue and the horizontal rod. At the sprue-rod junction, a thermocouple is placed along the centre axis of the rod, at a distance 3 mm from the junction (i.e. inside the sprue area) in order to avoid the influence of the needle tip on hot tearing initiation (Fig. 2.7 (c)). The setup monitors the evolution of hot tearing using the measurement of the contraction force induced during the solidification and thermal shrinkage. Fig. 2.8 shows the experimental curves for Mg-1 wt.% Al alloy with a mould temperature of 350 °C. When a hot tear occurs during solidification, the induced contraction stress is released, and a sudden drop is observed in the contraction force curve [35].

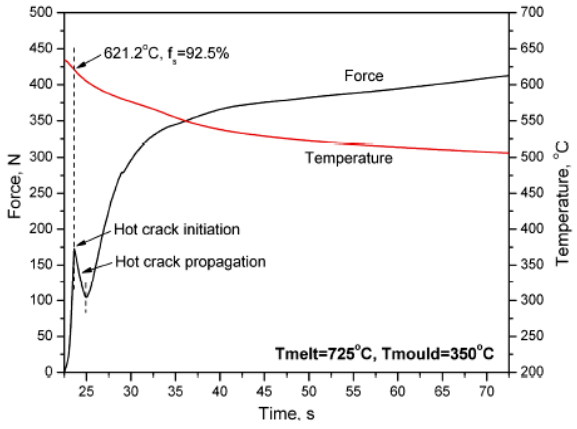

Fig. 2.8 Contraction force and temperature as a function of time for Mg-1wt.%Al alloy [35].

Cao et al. [10] developed an instrumented CRC method to investigate hot tearing and studied Mg-Al and Mg-Al-Ca alloys. The experimental setup is shown in Fig. 2.9. It consists of a steel mould, a load cell and a thermocouple. The six upper rods (165, 146, 127, 108, 89, and 70 mm in length) are used for testing the cracking susceptibility. All rods have a diameter of 9.5 mm. The bottom rod (length: 165 mm) is used to detect the onset of hot tearing. This rod is connected to the load cell at one end and a thermocouple is embedded at the junction area between the rod and the sprue, near the potential place of the crack. The mould is equipped with a graphite pouring cup and a graphite sleeve in order to maximize the reproducibility and minimize the interference of the increased tension near the sprue end of the rods during the test. After pouring the melt into the mould, the temperature, time and load are recorded with a computer data acquisition system.

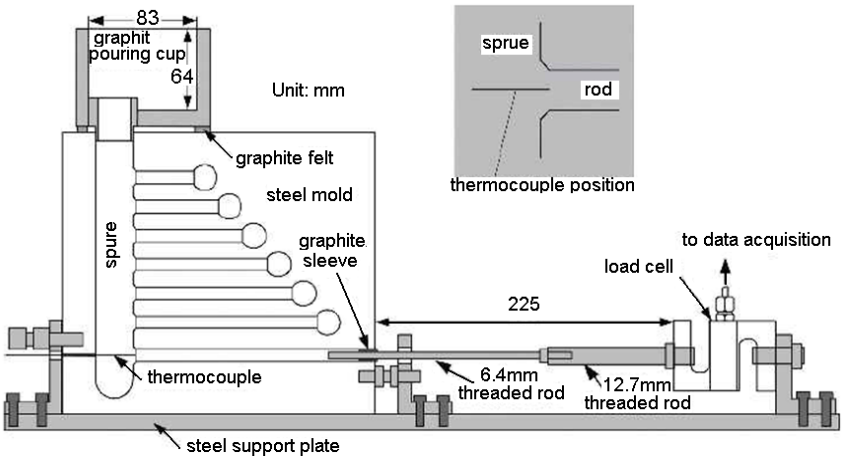

Fig. 2.9 Steel mould for instrumented constrained rod casting designed to detect the onset of hot tearing [10].

Recently, an instrumented constrained rod mould was developed by the Metal Processing Institute at WPI and CANMET Materials Technology Laboratory [36]. The principle is similar to Zhen's apparatus. The mould is designed to simultaneously measure the load/time/temperature during solidification for a restrained casting, as shown in Fig. 2.10. The mould has two arms. The arms are designed with a slight taper to decrease friction between the mould and the casting. One arm is constrained at one end with a steel bolt, which is embedded in the end of the casting. This end section will solidify first and fast due to lower temperature of the embedded bolt. A graphite stopper anchors the bolt, and since the bolt cannot move, this setup keeps the arm from contracting. This develops a tensile force and hence cracking may be induced during solidification. The other arm is used to measure the

temperature and load/displacement data. This end is connected to a rod, which has one end embedded in the arm and the other end connected to a load cell or linear variable differential transformer (LVDT). The LVDT is unrestrained and can move horizontally and freely while the load cell will offer a resistance to the contraction and cause cracking in the casting. The test results are reproducible and reliable.

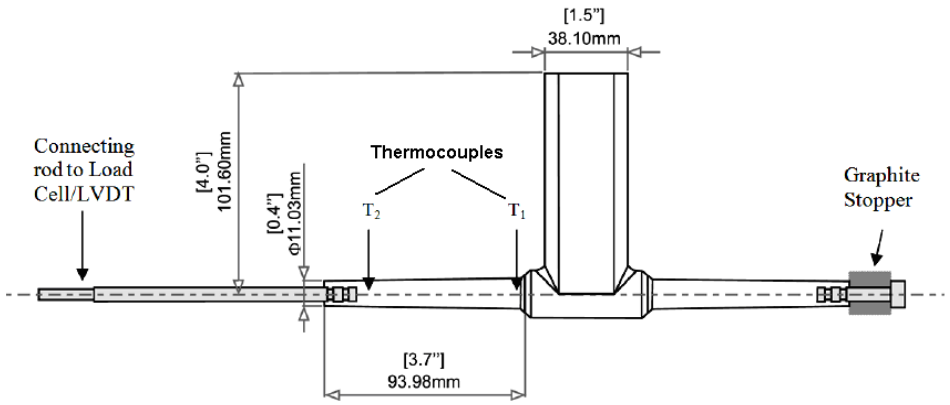

Fig. 2.10 Schematic diagram of the casting used for the WPI–CANMET hot tear test apparatus [36].

Another apparatus for measuring tensile stress observed during solidification was developed by Instone et al. [37-38]. It is a restrained bar test which incorporates a feeder located in the centre of the bar. The testing setup provides constraint during solidification and collect information on development of stress, strain accommodation and hot cracking behaviour of the mushy zone. A schematic plan view of the mould is shown in Fig. 2.11.

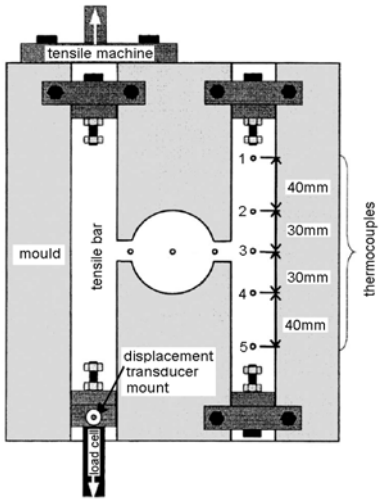

Fig. 2.11 Plan view of the test mould developed by Instone et al. [37].

In this setup one cast bar is used for tensile loading and the other for temperature measurements. The cast bar connects to the load cell and the displacement transducer. Temperature measurements are obtained from the other bar so that the microstructure of the tensile test bar is not influenced during solidification by the thermocouple. The steel mould has a combined centre pouring reservoir and a riser that feeds the cast bars during solidification. A schematic diagram of the setup is shown in Fig. 2.12.

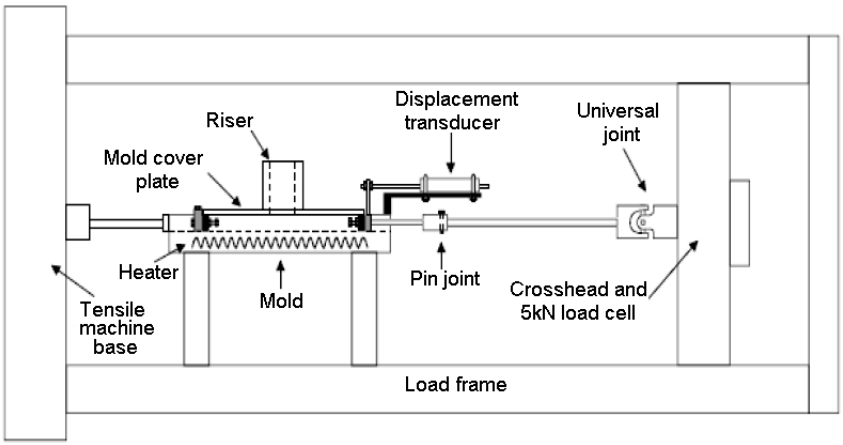

Fig. 2.12 Schematic diagram of the hot tear rig [38].

Similar to the previous setups, a load cell is attached in the setup so that the evolution of contraction force during solidification can be recorded, which shows when the hot tearing initiates and how it propagates.

2.2 Theories on hot tearing

Industrial and laboratory scale research on hot tearing phenomenon show that hot tearing occurs during the last stages of solidification when the solid fraction exceeds 0.85~0.95 [5]. According to Eskin et al. [5], four stages of solidification to characterize the permeability of the solid network:

- Mass feeding, where both liquid and solid are free to move;
- Inter-dendritic feeding, during which the dendrites start to form a solid skeleton and the liquid has to flow through the dendritic network;
- Inter-dendritic separation, during this stage the liquid network becomes fragmented and pore formation or hot tearing may occur;
- Inter-dendritic bridging or solid feeding, during which the ingot has developed a considerable strength and solid state creep compensates further contraction.

The last two stages are important for the formations of pores and hot tears. With increasing solid fraction, permeability of the solid network becomes very low and liquid feeding ceases. Further, strain due to thermal contraction, can develop simultaneously. If the strain imposed on the solid network is exceeds a critical value, then hot tearing occurs [15]. Large volume of works has been conducted to understand the hot tearing phenomenon. Many theories on hot tearing have been proposed in the past few decades. Some of the main theories are briefly described below.

2.2.1 Theories based on stress, strain and strain rate

2.2.1.1 Stress-based theory

The stress-based theory of hot tearing is based on the viewpoint that a semi-solid body will fracture if the applied stress exceeds the maximum stress of the body. The first stress-based theory provides that a material can obtained a limited amount of stress. In the second stress-based theory, the HTS is originated from an assumption that the material contains defects. Whether the defect cause fracture or not depends on stress, defect dimensions etc. The influence of grain size, viscosity and liquid fraction on hot tearing can be explained using this theory.

Novikov [16] and Dickhaus et al. [39] reported a stress-based hot tearing theory that uses the strength of liquid trapped between grain boundaries. As shown in Fig. 2.13, they refer to the stress needed to pull apart two parallel plates separated by a thin liquid film as the strength of semisolid metals.

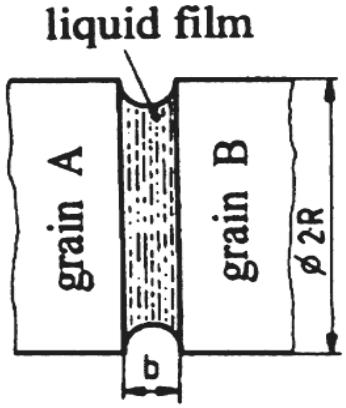

Fig. 2.13 Model of two grains separated by a liquid metal film in the assumption of complete wetting between grains and melt [39].

This theory is expressed as:

$$\sigma_{fr} = 2\gamma / b \tag{2-3}$$

where σ_{fr} is the fracture stress, γ is the surface tension, and b is the film thickness. The model is neglects viscosity and wetting angle.

Dickhaus et al. [39] modified the model to involve viscosity. The separation force of the parallel plates separated by a liquid film is given as:

$$F_z = \frac{3\pi\eta R^4}{8t}\left(\frac{1}{b_1^2} - \frac{1}{b_2^2}\right) \tag{2-4}$$

where F_z is the force required to increase the film thickness from b_1 to b_2; η is the dynamic viscosity; R is the plate radius; t is the time required to increase the film thickness from b_1 to b_2.

The liquid film thickness can be written as:

$$b = \frac{(1 - f_s)d}{2} \tag{2-5}$$

where f_s is the solid fraction and d is the average thickness of alloy solidifying grain.

Lahaie and Bouchard [40] proposed a new hot tearing model based on equation (2-4). The model involves solid fraction f_s, strain ε, liquid film thickness b and microstructure parameter m_p. It is written as:

$$\sigma_{fr} = \frac{4\eta}{3b}\left(1 + \left(\frac{f_s^{m_p}}{1 - f_s^{m_p}}\right)\varepsilon\right)^{-1} \tag{2-6}$$

The equation can be applied for both equiaxed and columnar grains by adjusting the m_p value. The value of m_p is $1/2$ and $1/3$ for columnar and equiaxed grains, respectively.

The calculated fracture stress and strain for a semisolid body are shown in Fig. 2.14. It can be seen that the stress to fracture varies from near zero when solid fractions is around 0.9 to less than 10 MPa for very high solid fractions approaching 1 in Fig. 2.14 (a). In previous work, a similar drop in strength is observed as a function of increasing temperature in the semisolid state [41-42]. The influence of grain size on fracture stress and strain is shown in Fig. 2.14 (b).

The fracture stress decreases with increasing grain size. The fracture stress calculated using this model could explain the low the HTS for a fine grained structure.

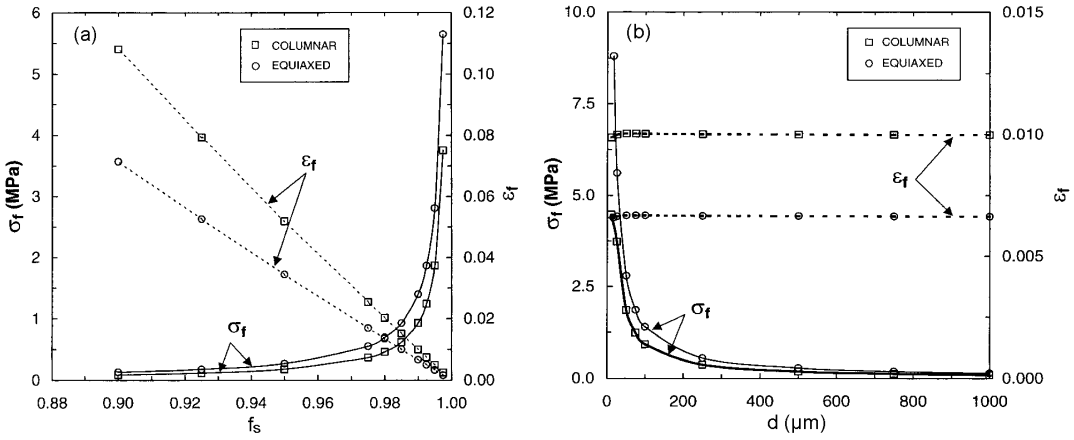

Fig. 2.14 The calculated fracture stress and strain of a semisolid body as a function of solid fraction (a) and grain size (d) for columnar and equiaxed microstructures [40].

A two-phase model of mushy zone parameters associated with hot tearing was investigated by Farup and Mo [43]. It focuses on the pressure decreasing in the mushy zone. This approach treats the pressure in the solid phase as higher than the pressure in the liquid phase close to the end of solidification. Momentum transport in the liquid phase was assumed to follow Darcy's law. The equation for conservation of mass, momentum and energy are expressed as:
Conservation of mass in the solid and liquid:

$$\frac{\partial(f_s\rho_s)}{\partial t} + \nabla\cdot(f_s\rho_s v_s) = \Gamma \tag{2-7}$$

$$\frac{\partial(f_l\rho_l)}{\partial t} + \nabla\cdot(f_l\rho_l v_l) = -\Gamma \tag{2-8}$$

where f_s and f_l are the volume fractions of solid and liquid respectively, ρ_s and ρ_l are the solid and liquid mass densities respectively, v_s and v_l are velocities of the solid and liquid respectively, Γ is the interfacial mass transfer due to phase change.

The momentum balance in the solid and liquid expressed by:

$$p_l\nabla f_s - \nabla(f_s p_s) + \nabla(f_s\sigma_s^{'}) + M + f_s\rho_s g = 0 \tag{2-9}$$

$$-f_l\nabla p_l - M + f_l\rho_l g = 0 \tag{2-10}$$

where p_l and p_s are the pressure of solid and liquid phases respectively, $\sigma_s^{'}$ is the deviatoric stress tensor, M is the interfacial momentum transfer, g is the gravitational acceleration.

Conservation of energy:

$$(f_s\rho_s C_s + f_l\rho_l C_l)\frac{\partial T}{\partial t} + (f_s\rho_s C_s v_s + f_l\rho_l C_l v_l)\cdot\nabla T = \nabla\cdot\left[(f_s\lambda_s + f_l\lambda_l)\nabla T\right] + H\Gamma \quad (2\text{-}11)$$

where C_s and C_l are the heat capacity of solid and liquid phases respectively, λ_s and λ_l are the heat conductivity in the solid and liquid phases respectively, and H is the latent heat.

It is assumed that the solid skeleton is an incompressible in the coherent regime, only the deviatoric parts of the solid and liquid stress tensors contribute to deformation of the sample. Farup and Mo proposed the two-phase stresses according to the deviatoric single-phase stress tensor, associated with the experimental measurements. It is expressed as [43]:

$$\sigma' = f_s\sigma'_s + f_l\sigma'_l \quad (2\text{-}12)$$

Where f_s and f_l are the volume fractions of solid and liquid respectively, σ'_s and σ'_l are the deviatoric stress tensor of solid and liquid phases respectively.

This model assumes that the liquid density is constant and no pore form. Farup and Mo [43] applied this model to a one dimensional direct chill casting process of binary Al-Cu alloys. The results indicate that both liquid pressure drop due to feeding difficulties and tensile stress caused by thermal contraction of the solid phase are necessary for the formation of hot tears.

2.2.1.2 Strain-based theory

A semi-empirical criterion has been derived by Magnin et al. [42], computes the viscoplastic strain accumulated in the mushy zone. Tensile tests in the solidification range have revealed a U-shaped ductility-temperature curve which does not depend on strain rate. This leaded them to formulate a hot cracking criterion in terms of critical plastic strain. They chose the greatest positive principal plastic strain to introduce non-symmetrical rupture behaviour. The maximum value of strain was obtained at the centre of billet and depends on the casting speed as shown in Fig. 2.15. When the maximum principal strain accumulated in the mushy zone is larger than the experimental ductility, the risk of hot cracking is high.

This theory was implemented in direct chill casting simulation code which allowed computing the strain field generated during the simulation process. When the strain generated remained below the experimental ductility, no crack forms at lower casting speed. At the higher casting speed, experimental ductility is exceeded and hot cracks form.

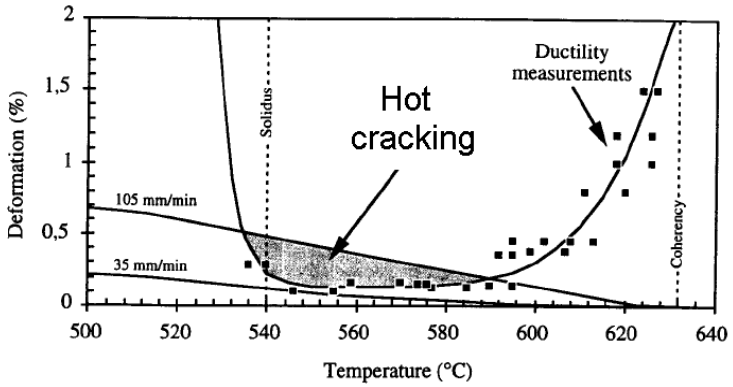

Fig. 2.15 Prediction of hot cracking risk by comparison of ductility in semisolid state with computed strain in the centre of the billet for two different casing speeds [42].

The same approach was also used by Zhao et al. [44] for hot tearing prediction in an Al–4.5% Cu alloy. They measured the shrinkage stress of casting, which is transformed to a critical strain for formation of hot tearing. The strain determined from their test is compared with the ductility from the work of Magnin et al. [42]. The temperature range where the ductility is less than the strain induced by solidification contraction is regarded as a region of potential risk for hot tearing.

Recently, Commet and Larouche [45] proposed a similar criterion of cumulated damage index (CDI). Damage is expressed as the infinitesimal viscoplastic strain $d \in (T)$ divided by the experimental ductility $\in_{rupt} (T)$. HTS is defined as the damage integral between traction coherency (T_{tc}) and solidus (T_{sol}) temperatures.

$$CDI = \int_{T_{tc}}^{T_{sol}} \frac{d \in (T)}{\in_{rupt} (T)} \tag{2-13}$$

This criterion is applied when a new alloy is being developed to optimize the composition with respect to castability, but does not bring information on hot tearing mechanisms.

2.2.1.3 Strain rate-based theory

Hot tearing is a strain controlled phenomenon, which occurs when the strain accumulated within the hot spot reaches a critical value [46]. At a later stage, the liquid film is thinner and the overall extension is concentrated in these hot zones to produce a high unit strain. Total strain developed during film life depended on two factors: (1) strain rate; (2) film life time [36]. According to this theory, the liquid film provided the condition that causes hot tearing [47-48]. However, the actual occurrence of hot tearing is determined by mechanical factors

inherent to the rate of deformation. The hot tearing of semisolid metal is not possible unless the strain rate is sufficiently high [49].

A new hot tearing theory was proposed by Rappaz et al. [50] based on strain rate. It is based on a mass balance performed over the semisolid mixture. In the mass balance equation, the deformation rate is introduced as the main factor for hot tearing. The mass balance equation for columnar microstructures with liquid fluid and solidification growth only along the x direction is provided as:

$$\frac{d(f_l v_l)}{dx} + (1+\beta) f_s \dot{\varepsilon}_p - v_T \beta \frac{df_s}{dx} = 0 \tag{2-14}$$

where f_l and f_s are the liquid and solid fraction respectively; v_l is the liquid velocity; β is the shrinkage factor; $\dot{\varepsilon}_p$ is the deformation rate in the solid phase perpendicular to the direction of solidification growth; v_T is the velocity of solidification.

This model introduces a critical deformation rate for the formation of cavities. The critical value is that increase with function the thermal gradient and permeability and function of decreasing viscosity. The first occurrence of the cavity is considered as a hot tear. The model is derived from columnar dendrites. The HTS is expressed as:

$$HTS = 1/\dot{\varepsilon}^{\max} \tag{2-15}$$

where $\dot{\varepsilon}^{\max}$ is the maximum deformation rate.

An extension of this model is proposed by Braccini et al. [51] who complement Rappaz et al.'s model [50] with the rheological behaviour of the mushy zone. Braccini et al. proposed that critical strain rate for hot tearing is expressed as:

$$\dot{\varepsilon}^c = (1-\frac{b}{l})\left[\frac{\lambda-a}{\lambda}(\frac{\frac{2}{3}P_C - P_M}{K_s})\right]^{1/m} + \frac{b}{l}\frac{2\kappa}{(\lambda-a)^2}\frac{P_c}{\eta_L} \tag{2-16}$$

where b is the liquid film thickness, l is the gage length, a is the length of the tear, P_c is the cavitations pressure, P_M is the metallostatic pressure, K is the a constitutive parameter, m is the strain-rate sensitivity, κ is the permeability of the mushy zone, and η_L is the viscosity of the liquid. Their model maybe applied to both columnar and equiaxed microstructures.

2.2.2 Theories based on other principles

2.2.2.1 Feurer's theory

Feurer's theory is a non-mechanical criterion that mainly focuses on feeding rather than stress due to solidification shrinkage [52]. It considers that hot tearing occurs due to lack of feeding, which relates to the difficulties of fluid flow through the mushy zone as a permeable medium. The theory focuses on the effect of alloy composition and solidification conditions on the dendrite arm spacing, the feeding shrinkage, and the hot tearing properties of aluminum alloys. Two terms proposed by Feurer are SPV and SRG. SPV is the maximum volumetric flow rate per unit volume through a dendritic network. SRG is the velocity of volumetric solidification shrinkage caused by the density difference between solid and liquid phase. SPV is expressed as:

$$SPV = \frac{f_l^{\,2}\lambda_2^2 P_s}{24\pi c^3 \eta_L L^2} \tag{2-17}$$

where f_l is the liquid volume fraction in the dendrite network; λ_2 is the secondary dendrite arm spacing; P_s is the effective feeding pressure; L is the length of porous network that is determined as the distance between the location at coherency and solidus temperature; c is the tortuousity constant of dendrite network; η_L is the viscosity of the liquid phase.

SRG is formulated as:

$$SRG = \left(\frac{\partial \ln V}{\partial t}\right) = -\frac{1}{\rho}\frac{\partial \overline{P}}{\partial t} = \frac{(\rho_0 - \rho_s + akC_L)\cdot \dot{T} \cdot f_l^{(2-k)}}{\overline{\rho}(1-k)m_l C_0} \tag{2-18}$$

$$\overline{\rho} = \rho_l f_l + \rho_s (1 - f_l) \tag{2-19}$$

where ρ_0, ρ_s and ρ_l are the densities of liquid aluminum at the melting point, the solidus and the liquidus; $\overline{\rho}$ is the average density; a is the composition coefficient of liquid density; k is the partition coefficient; C_L is the composition of the liquid at the solid-liquid interface; $\dot{T}$ is the average cooling rate during solidification of the primary solid phase; f_l is liquid volume fraction; m_l is the liquidus slope; C_0 is the alloy composition.

Feurer's theory states that hot tearing can occur when:

$$SPV < SRG \tag{2-20}$$

The theory only considers compensation for solidification shrinkage but not for thermal contraction of the solid phase.

2.2.2.2 Clyne and Davies' theory

A hot tearing model proposed by Clyne and Davies is based on the Feurer's theory during the last stage of freezing [53]. It is difficult for liquid to move freely and mass feeding cannot accommodate the strains developed during this stage. This theory considers the last stage of solidification to be the most susceptible stage for hot tearing. However, the increase in the solid fraction, bridging between adjacent dendrites is established so that inter-dendritic separation is prevented. The cracking susceptibility coefficient (CSC) is defined by the ratio of the vulnerable time period t_V and time available for stress-relief process t_R:

$$CSC = \frac{t_V}{t_R} = \frac{t_{0.99} - t_{0.9}}{t_{0.9} - t_{0.4}} \tag{2-21}$$

where $t_{0.99}$ is the time when the volume fraction of solid, f_s is 0.99; $t_{0.9}$ is the time when f_S is 0.9; $t_{0.4}$ is the time when f_s is 0.4.

The hot tearing susceptibility for Mg-Zn and Mg-Al binary alloys has been predicted using thermodynamic calculations based on this model [22, 54]. Comparison between the predicted CSC and experimental HTS for binary magnesium alloys show that the thermodynamic calculation results are generally in agreement with experimental results. Thus, Clyne and Davies' model can give a theoretical prediction on the influence of alloy composition on the hot tearing behaviours of an alloy.

2.2.2.3 Katgerman's theory

In Katgerman's model, theoretical considerations of Clyne and Davies' and Feurer's are combined [55], and supposed to predict HTS during direct chill casting of aluminum. In this model, the effect due to the casting speed, the ingot diameter, and the alloy composition are considered. The model can be applied for binary and commercial alloys. HTS is defined as:

$$HTS = \frac{t_V}{t_R} = \frac{t_{0.99} - t_{cr}}{t_{cr} - t_{coh}} \tag{2-22}$$

where t_{coh} is the time when f_s at the coherency point; t_{cr} is the time when feeding becomes inadequate. The time t_{cr} is determined from Feurer's theory. It is uncertain which coherency temperature, shear or tensile, was used as it was simply defined as the temperature where the dendritic network starts to form.

2.2.3 Summary of hot tearing theory

The subject of hot tearing is not simple, and two sets of theories proposed are generally summarized as [56]:

- The group of mechanisms based on stress, strain and strain rate, and these are related to thermo-mechanical properties of the alloy.
- The group of mechanisms based on liquid film, cavity formation and lack of feeding which are related to metallurgical factors.

It has been widely acknowledged that existing hot tearing theories cannot adequately predict hot tearing universally. It is a complex phenomenon which combines both the metallurgical and the thermo-mechanical interactions. Even though, the basic phenomena involved in hot tearing is understood, there is still no agreement on the controlling factors that gives rise to it.

2.3 Factors affecting hot tearing

The phenomenon of hot tearing in metal castings has been experimentally investigated for many years with reference to factors that influence of hot tearing. The factors include alloying elements, freezing range, amount of eutectic phase that forms during the solidification, and the initial mould temperature.

2.3.1 Alloy composition

Alloy composition is mainly dictated by the desired final product mechanical properties, it is one parameter that controls hot tearing. The majority of the investigation considers the effect alloy composition on hot tearing [57-58]. The previous investigation indicates that the most important feature of the alloy composition is the amount of eutectic liquid. HTS has been related to the amount of residual eutectic liquid present during the last stage of solidification. The presence of even a small amount of eutectic liquid has shown to worsen the HTS. The HTS increases with increasing the eutectic liquid. When the amount of eutectic liquids increases to a critical amount, the maximum HTS of the alloys is observed. With further increase the amount of eutectics liquid in alloys, HTS decreases.

Hot tearing behaviour of an alloy has been also considered to be related to the freezing range of the alloy. For most binary alloys, the relationship between HTS and alloy composition is considered to follow the so called lambda curve [15, 59], as shown in Fig. 2.16. Generally, the larger the freezing range, the more is the alloy prone to hot tearing [5, 34]. The reason for this is that the alloy spends a longer time in the vulnerable stage, and its interaction with the

geometry and the stresses of a particular casting configuration. In other words, if the alloy has low melting point phases distributed at the grain boundaries, the strength of the metal would be reduced because of the liquid film remaining at low temperature during the solidification, so hot tearing can occur.

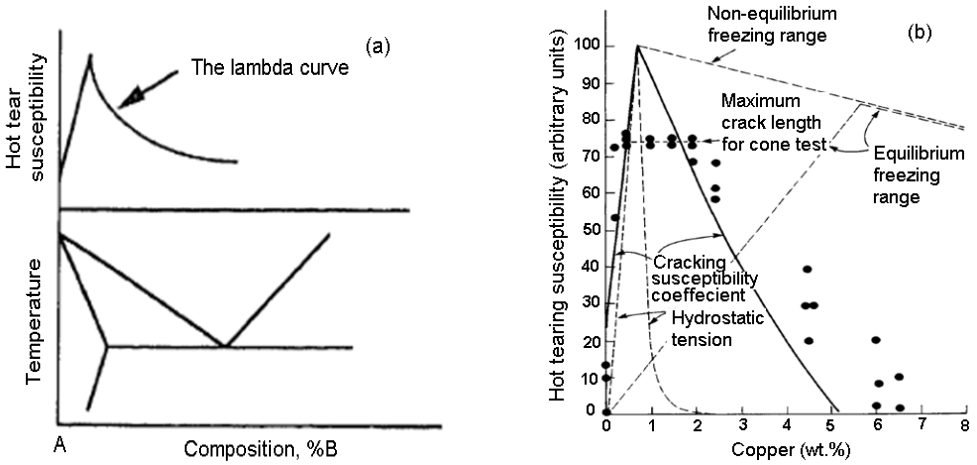

Fig. 2.16 (a) Schematic illustration of HTS as a function of composition for a binary alloy, shown as a lambda curve; (b) Hot tearing for Al-Cu alloys, showing a peak at approximately 0.7%Cu from the conical ring die test [15, 59].

The effect of grain refinement on hot tearing has been investigated by many [58, 60-62]. Most of results show that grain refinement improves the resistance to hot tearing by better accommodating local strains. Thus, a fine equiaxed grain structure is normally desired in castings. The type and size of grains are determined by the composition of the master alloys (grain refiners) containing intermetallic particles which provide sites for heterogeneous nucleation. A simple and easy way to control the grain size is by the addition of grain refiners.

Easton et al. [61-62] investigated the effect of grain refinement on hot tearing. A CAST (CRC for Cast Metals Manufacturing) hot tearing rig was used in their study and the load development with temperature in the test bars was measured. Alloy 6061 was studied with additions of 0.001 (no addition), 0.005, 0.01, and 0.05% Ti as a grain refiner morphology. They proposed three mechanisms, by which the grain refinement affecting hot tearing.

- Grain refinement changes grains from columnar to equiaxed morphology, and as a result the permeability length scale is changed from secondary dendrite arm spacing (for columnar grain) to grain size (for equiaxed grains).
- Changing the region over which feeding occurs.

- Changing the capillary pressure. The liquid film between grains become thinner at a given fraction solid due to smaller grain size, and therefore capillary pressures to be overcome before a crack can propagate become larger.

Clyne and Davies [33] studied the effect of grain refinement on two Al-Mg alloys. One was Al-2 wt.% Mg, which had low cracking susceptibility, and another was Al-1 wt.% Mg, which had high cracking susceptibility. Both alloys had a columnar grain structure when no grain refiner (Ti) was added. It was found that the low susceptibility alloy showed an increased cracking tendency over a narrow range of Ti content despite the grain structure became finer and equiaxed. However, the high susceptibility alloy was unaffected by the Ti additions except at high level (>0.2 wt.% Ti) even though the grains altered from columnar to equiaxed morphology. Thus, there is a complex interaction between element content, grain structure, and cracking susceptibility.

2.3.2 Processing parameters

The process parameters, such as superheat, influence the HTS at a given alloy composition. Clyne and Davies [33] utilized electrical resistance measurements to establish a relationship between the susceptibility of tearing and melt superheat. Their results on Al-Mg alloys with different amounts of superheating are shown in Fig. 2.17. The results indicate that HTS is dependent on both the composition and the pouring temperature. When the amount of superheating is high, the maximum value in HTS curve is increased and moves to lower magnesium contents.

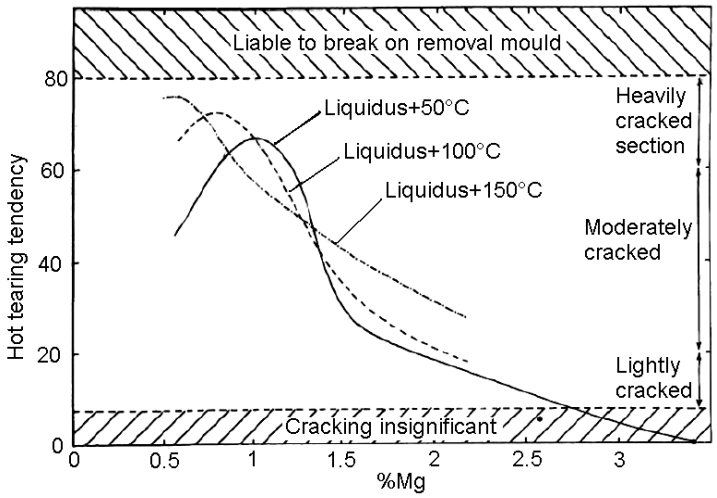

Fig. 2.17 The variation of hot tearing susceptibility of Al-Mg alloys with different amounts of superheat [33].

Middleton et al. [63] showed that hot tearing was likely to occur and was more severe at higher casting temperatures than at lower temperatures. Pumphrey et al. [26] studied six binary aluminum alloy systems, and showed that at any given alloying content the cracking susceptibility decreased with decreasing superheat. However, Bichler et al. [64] found that the variation of pouring temperature did not have a significant effect in a magnesium alloy. Other factors in the casting process such as metal fluidity, cooling rate and healing phenomena etc., should also be considered. Generally, the influence of mould temperature on hot tearing is through its effect on cooling rate. Mould temperature directly affects the cooling rate. In other words, controlling cooling rate is generally through controlling mould temperature. In fact, most of studies on hot tearing that involve mould temperature was used it to control the cooling rate or the solidification pattern as Clyne et al. [33] and Spittle et al.'s [65].

Recently, Zhen et al. [66] investigated the effect of mould temperature in the range of 250 to 500 °C on hot tearing for binary Mg-Al alloys. They found that increasing the mould temperature decreased HTS. Meanwhile, the higher mould temperature led to higher crack onset temperature and longer propagation time. The initiation of hot cracks occurred at all the mould temperatures conditions, but the cracks could be refilled by the remaining liquid and healed at higher mould temperature. With a higher mould temperature, a lower propagation rate for the hot crack is detected. This is due to the remaining liquid favoured to refill the initiated hot crack, and consequently interrupting the propagation or possibly resulting in complete healing of the cracks.

2.4 Hot tearing of magnesium alloys

2.4.1 Binary alloys

The results of investigations on the HTS of Mg-Al, Mg-Zn and Mg-Gd alloys were reported previously. The HTS of these binary alloy systems, with respect to the alloy compositions, follows a so-called "λ" curve (Fig. 2.16 (a)).

2.4.1.1 Mg-Al

For the hot tearing of magnesium alloys, most previous studies were conducted for Mg-Al series. Dodd et al. [67] investigated the HTS of binary Mg-Al alloys up to 8 wt.% Al by ring casting in a steel mould and found the peak susceptibility was at 0.75 wt.% Al. Rosenberg et al. [68] studied hot tearing of binary Mg-Al alloys up to 17 wt.% Al by restrained bar casting with a sand mould and observed the peak susceptibility at around 2.5 wt.% Al. Cao et al. [54] performed detailed work on the HTS of Mg alloys containing 0.25 to 8 wt.% Al. The HTS

was evaluated using CRC in a steel mould, in which cracking was induced by enlarging the ends of the rods to keep them from contracting freely during solidification. The HTS was evaluated based on both the widths and locations of cracks in the castings. The curve of the crack size versus Al content shows the existence of the peak susceptibility to hot tearing near 1 wt.% Al, which is similar to that reported by Dodd et al. [67].

2.4.1.2 Mg-Zn

Recently, Zhou et al. [22-23, 69] used thermodynamic calculations and quantitative experimental methods to evaluate the hot tearing of Mg-Zn alloys, which are the base alloy system used for the development of wrought Mg alloys such as Mg-Zn-RE, Mg-Zn-Zr. As shown in Fig. 2.18, the hot tearing influenced by both the Zn content and the mould temperature. The influence of Zn content on the HTS follows the "λ" shape. The initial mould temperature also played a very important role in HTS, as the HTS decreases with increasing in the initial mould temperature from 200 to 500 °C.

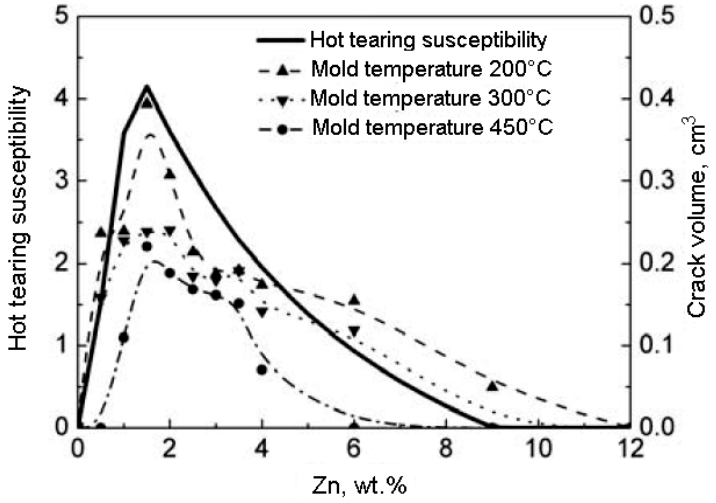

Fig. 2.18 Comparison of predicted CSC and experimental HTS for Mg-Zn binary alloys [22].

2.4.1.3 Mg-Gd

Hot tearing characteristics of binary Mg-Gd alloys were investigated in an instrumented CRC mould apparatus by Srinivasan et al. [70]. The susceptibility increases with increasing in Gd content to reach a maximum at 2 wt.% Gd and then reduces with further increment in Gd content. The high susceptibility observed in Mg-2 wt.% Gd was attributed to cellular or columnar grain structure, which facilitated easy tear propagation, high stress at the onset with little amount of remaining liquid. The results also indicated that the increase in mould

temperature significantly reduce the HTS. In addition to the improved feeding characteristics, higher mould temperatures reduced the cooling rate that resulted in a lower thermal gradient and decreases the hot spot size.

The compositions of primary alloy elements corresponding to the maximum HTS of typical binary magnesium alloys are given in Table 2-1. The experimental observations demonstrate that the binary alloys with these alloy compositions are the most prone to hot cracking.

Table 2-1 Chemical compositions of binary magnesium alloys having the maximum HTS

Alloy system	Maximum HTS at a composition (wt.%)	Ref.
Mg-Al	1.0	[54]
Mg-Zn	1.5	[22]
Mg-Gd	2.0	[70]

2.4.2 Ternary alloys

The hot tearing of three ternary systems Mg-Al-Zn, Mg-Al-Ca and Mg-Al-Sr was investigated.

2.4.2.1 Mg-Al-Zn

Wang et al. [8] investigated the HTS of Mg-9Al alloy with Zn (x=0~1 wt.%) addition. The hot tearing originated along the grain boundary at the end of solidification for these alloys. They concluded that Zn additions increased the HTS of Mg-9Al-xZn alloys. The reason is that Zn decreased the end solidification temperature and increased the quantity of low melting point phases at grain boundaries.

The cracking tendency in the Mg-xAl-1.5Zn (x=0.5, 3, 6 wt.%) and Mg-0.5Al-xZn (x=0.5, 1.5, 2.5, 4 wt.%) alloys was examined using CRC mould testing by Zhou et al. [22]. For the Mg-xAl-1.5Zn (x=0.5, 3, 6 wt.%) alloys, the HTS decreases with increasing Al content. When the content of Al is fixed, the HTS curve of Mg-0.5Al-xZn (x=0.5, 1.5, 2.5, 4 wt.%) alloys has two peaks: one is at about 1.0 to 1.5 wt.% Zn, and another at about 3.0 wt.%.

2.4.2.2 Mg-Al-Ca

Investigation on the HTS of Mg-4Al-xCa (x=0.5, 1.5, 2.5, 3.5 wt.%) and Mg-xAl-2.5Ca (x=4, 5, 6 wt.%) alloys were performed by Cao et al. [10] using CRC mould. The HTS, based on the

measurements of crack widths and crack locations, decreases significantly with increasing Ca content, but do not change much with the Al content, as shown in Fig. 2.19. The serious susceptibility observe in these alloys is attributed to its wide freezing range and the low eutectic amount.

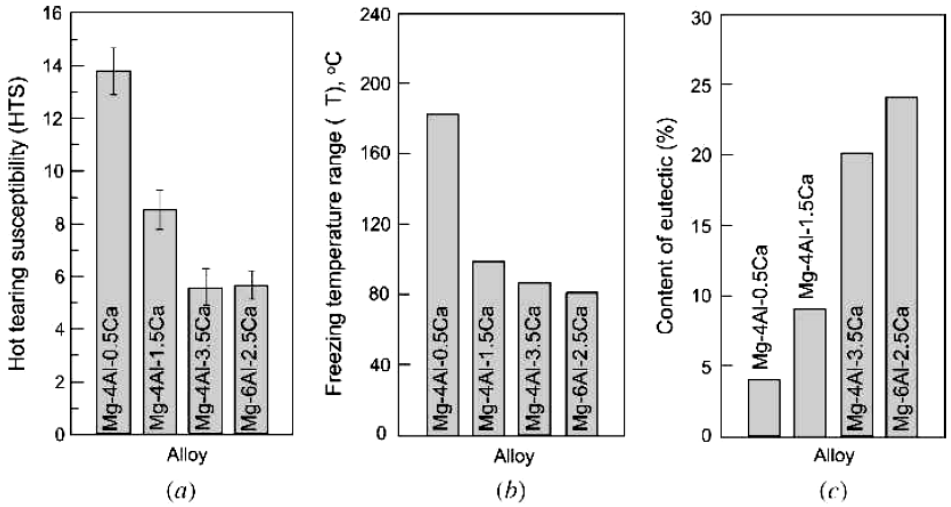

Fig. 2.19 Correlations between HTS and freezing temperature range and amount of eutectic: (a) HTS, (b) freezing temperature range and (c) amount of eutectic [10].

2.4.2.3 Mg-Al-Sr

The susceptibility of Mg-Al-Sr alloys to hot tearing was also investigated by Cao et al. [9] who used CRC mould test. The results show that an addition of Al to Mg-Sr alloys causes the pronounced decrease in hot tearing sensitivity. It also shows that an increase in the content of Sr at a constant content of Al results in a decrease in HTS. It is also reported that the HTS increases with increasing in fraction solid at the end of primary solidification.

2.4.3 Multi-component alloys

There are several multi-component magnesium alloy systems for which the HTS was investigated, for example, Mg-Al-Mn-Sr, Mg-Y-Zn-Zr, Mg-Al-Zn-RE and Mg-Al-Mn-RE systems. The HTS is not always shown by a certain characteristic value but is rather represented comparatively, showing the effect of various additions on a certain alloy.

2.4.3.1 Mg-Al-Mn-Sr

In Mg-6Al-0.5Mn-Sr alloys, the HTS decreases with increasing the content of Sr (≤0.2 wt.%). These results were reported by Li et al. [71] who used a critical diameter method. The

decrease in hot tearing was due to Sr refining the grain size which improves the filling capacity.

2.4.3.2 Mg-Y-Zn-Zr

The influence of Y additions on the HTS of Mg-3Zn-0.5Zr alloys was investigated by Gunde et al. [32] with a dog bone-shaped steel mould. The addition of a small amount of Y results in a significant reduction of HTS. As shown in Fig. 2.20, the addition of Y increases the solidus temperature of the multi-component system and thus shortens the terminal solidification path, which in turn reduces the freezing range.

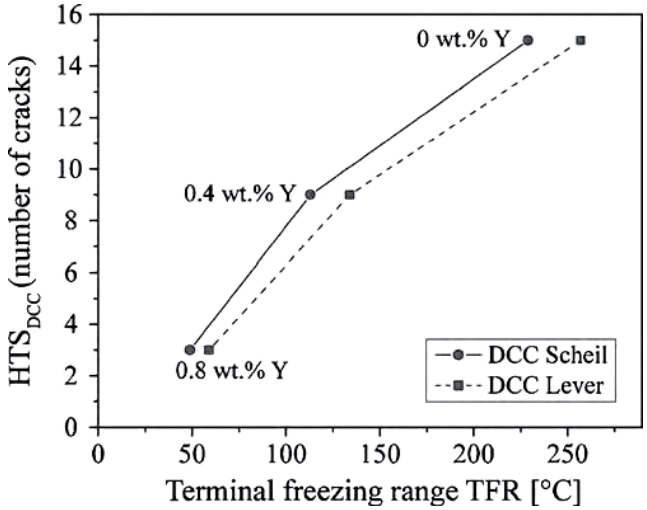

Fig. 2.20 HTS of Mg-3Zn-xY-0.5Zr alloys in direct chill casting (HTS_{DCC}) represented as a function of the terminal freezing range (TFR) [32].

2.4.3.3 Mg-Al-Zn-RE and Mg-Al-Mn-RE

Effect of Zn and RE additions on the HTS of Mg-9 wt.% Al alloy were studied with a crack ring mould [20]. Zn and RE elements were added to a maximum amount of 1.2 and 1.6 wt.%, respectively. The results show that the RE addition has little effect on HTS of Mg-9Al alloys with low or no Zn content. However, when Zn content is exceeded 0.8 wt.%, the RE distinctly decrease the HTS of Mg-9Al alloys.

The effect of RE content ranging from 0.1 to 1.2% (mass fraction) on the hot tearing resistance of Mg-Al-Zn and Mg-Al-Mn were investigated by Zheng et al. [21] using the critical diameter method. The hot tearing resistance of these alloys remarkably reduces with

an increase of RE addition. The addition of RE coarsens the grain, reduces the feeding ability and increases the shrinkage ratio discrepancy between the second phases and matrix.

2.5 Numerical simulations of hot tearing for magnesium alloys

Solidification involves many physical phenomena such as fluid flow, heat transfer, phase changes, microstructure and macrostructure development, deformation, formation of defects, etc. [72]. The application of numerical simulation techniques in metal casting has provided insights into understanding the effects of alloy chemistry, thermal-fluid transport phenomena, and their relationship to the alloy microstructure and the formation of defects. Numerical modeling can also answer some of the critical questions concerning mould filling, microstructure formation, mechanisms of casting defect formation, and the final shape of casting [73-77]. It can be used to reduce the time required for new product design cycles and as a tool for quality assurance.

2.5.1 Hot tearing indicator

The commercial numerical simulation software ProCAST, which simulates the process of casting and solidification based on finite elemental method, has been used extensively in foundries to understand the physical phenomena occurred during solidification. In this software, a module called HTI was developed to predict the HTS [78].

The HTI is a strain-driven model based upon the total strain which develops during solidification. The model compute the elastic and plastic strains at a given node when the fraction of solid is between the critical solid fraction (usually 50%) and 99%. The model is based on Gurson's constitutive model, which was developed to investigate the progressive micro-rupture through nucleation and growth of micro-voids in a material of ductile and porous solids [79]. In order to describe the material behaviour in the semi-solid state, a modified Gurson's constitutive model was used for the HTI [77, 79-82]. It is assumed that the casting is isotropic (although at the final stage of the solidification, the castings may exhibit localized anisotropic behaviour), the HTI (e_{ht}) was obtained as follows:

$$e_{ht} = \bar{\varepsilon}_{ht}^{p} = \int_{t_c}^{t} \sqrt{\frac{2}{3}\dot{\varepsilon}^{p} : \dot{\varepsilon}^{p}}\, d\tau , \quad t_C \le t \le t_S \tag{2-23}$$

where $\bar{\varepsilon}_{ht}^{p}$ is the critical accumulated effective plastic strain for the initiation of hot tearing, $\dot{\varepsilon}^{p}$ is the effective plastic strain rate, t_C is the time when the coherency temperature is reached, and t_S denotes the time when the solidus temperature is reached, : is the dyadic tensor.

In fact, as shown by the above equation, HTI is the accumulated plastic strain in the semi-solid region that corresponds to the void nucleation. Therefore, it should provide a good indication for the susceptibility of the hot tearing occurred during solidification.

The numerical simulation of hot tearing formation in binary Mg-Al alloys was investigated by Zhu et al. [77] who used the HTI module. Fig. 2.21 shows a comparison between the predicted damage fields and experimental images. The results show that the simulations agree well with the experimental results. The hot tearing at the same location is less severe when the content of Al increases from 2 to 4% and then to 8%.

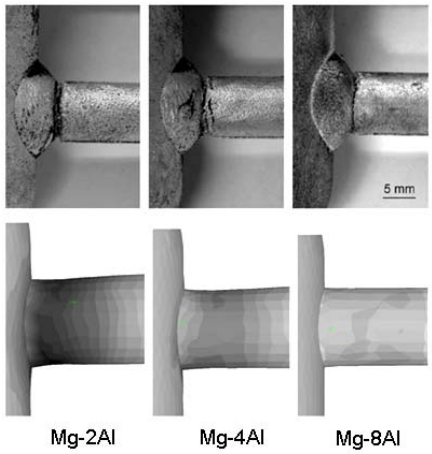

Fig. 2.21 Comparison between simulation and observed cracks in the experiments for Mg-Al alloys [77].

2.5.2 Viscoplastic deformation model

Another numerical simulation is the viscoplastic deformation model. It calculates the material damage as well as the solid deformation. It includes effect of both strain hardening and strain rate, and use the volume averaged solid momentum equation as well as a solid constitutive model. It is implemented as a new module in MAGMA soft by Monroe [83].

The viscoplastic deformation model calculates the porosity formed due to solid deformation or porous. The porosity formed was found by [84]:

$$f_{p,d} = \int_{t_s^{coh}}^{t} f_s \dot{\varepsilon}_s^{vp} : Idt \tag{2-24}$$

where $f_{p,d}$ is the volume fraction of porous damage, t_s^{coh} is the time at which the coherent solid fraction is reached, f_s is the solid volume fraction, $\dot{\varepsilon}_s^{vp}$ is the viscoplastic strain rate, I

is the identity tensor. In this module, the damage is coupled with the deformation calculation and the porous damage to determine hot tearing criterion.

Pokorny et al. [85] calculated the material damage using this viscoplastic deformation model. They predicted the stress and formation of hot tear in Mg-Al alloys. For the simulation, a trial-and-error method was used to determine the mould-metal interfacial heat transfer coefficient from experimental results.

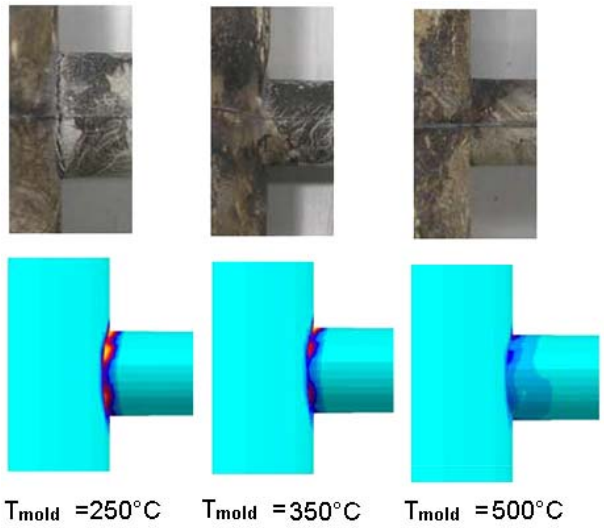

Fig. 2.22 Comparison between simulation and observed cracks in the experiments for Mg-9Al at different mould temperatures [85].

Fig. 2.22 shows the comparison between the predicted damage fields and experimental macrographs for Mg-9Al alloy at different mould temperatures. The predicted results are in agreement with the hot tears observed in the experimental castings. With decrease in the mould temperature, the amount of damage increases. The HTS of magnesium alloys can be accurately predicted with numerical simulation software.

3 MOTIVATION AND OBJECTIVES

Investigations on the castability of magnesium alloys indicated that castings are often prone to hot tearing. It is very important to study the HTS and understand hot tearing mechanism for magnesium alloys. Therefore, the present work investigates the HTS of Mg-Y-(Zn) alloys. In this work, firstly binary Mg-Y alloys are designed and investigated to optimize the Y content in the alloys according to thermodynamic calculation results. The Mg-Y-Zn alloys are designed and investigated based on the results of binary Mg-Y alloys. Y and Zn are selected as main alloying elements based on the following reasons.

- Magnesium alloys containing RE elements such as Y are interesting as light structural materials with high strength at both room and elevated temperatures [86-88]. The addition of Y not only improves the mechanical properties but also increases corrosion resistance [89].
- There is significant interest in the development of Mg-Y-Zn wrought Mg alloys with high strength, high corrosion resistance, and excellent formability at elevated temperatures for structural application [90-91]. In order to avoid defects, it is very important to investigate the HTS of Mg-Y-(Zn) alloys.
- The mechanisms of hot tearing in magnesium alloys containing Y and Zn still remaining somewhat unclear.

The HTS of binary Mg-Y and ternary Mg-Y-Zn systems are investigated by experimental methods and numerical simulation. The objectives of this study performed in five phases as given below:

- The first phase is to predict HTS of binary Mg-Y alloys by thermodynamic calculation using the Clyne and Davies' model.
- The second phase is to investigate HTS of binary Mg-Y and ternary Mg-Y-Zn alloys by an instrumented CRC mould apparatus.
- The third phase is to study the other factors, such as mould temperature, grain size and second phases on HTS of Mg-Y-(Zn) alloys.
- The fourth phase is to conduct computer simulations on temperature, solid fraction fields and HTI using casting simulation software ProCAST.
- The last phase is to observe hot tearing characteristics and propose mechanisms of hot tearing in various Mg-Y-(Zn) alloys.

4 EXPERIMENTAL PROCEDURE AND NUMERICAL SIMULATION

4.1 Experimental procedure

4.1.1 Hot tearing test experimental setup

To detect the hot tearing initiation, a system based on the measurement of contraction stress was developed by Zhen et al. [35]. This apparatus was used in the present study. The device uses a cylindrical steel mould that has a single arm branching out. This arm is connected to a load sensor that measures the force which acts on a rod attached at the end of the arm. A load cell is attached in the present setup so that the evolution of contraction force during solidification can be recorded. This is very important information to shows when the hot tearing initiates and how it propagates. This information is very important to understand the mechanism of hot tearing. The details of the apparatus setup are given literature review section. The advantage of the present evaluation system, which is mainly different from Cao's apparatus, is to eliminate the influence of friction between the mould and the casting rod [9].

4.1.2 Melting process

In the present work, the HTS of the as-cast Mg-Y and Mg-Y-Zn alloys was investigated at different mould temperatures. Their nominal compositions are listed in Table 4-1. The chemical compositions of the casting were analysed using inductively coupled plasma-optical emission spectroscopy ICP-OES (Spectroflame, Spectro, Kleve, Germany).

A cylindrical mild steel crucible coated with boron nitride (BN) was used for melting Mg alloy in an electrical resistance furnace. 350 g of magnesium alloy was molten under a protective gas mixture of high purity Ar+0.2% SF_6. Pure Zn, pure Y and Mg-30 wt.% Zr master alloys were added to the melt at 700 °C. After stirring at 80 rpm for 2 min and the temperature was increased to a pouring temperature 750 °C for 5 min, then the molten alloys were cast into a CRC mould, which was coated with a thin layer of BN. The mould was preheated to a temperature (T_{mould}) of 250 or 450 °C. The castings were extracted from the mould after solidification and then examined for cracks. Each test was repeated at least three times to ensure reproducibility. After acquiring the data, the cooling curve and force vs. time curve were processed to obtain the important information such as solidification process and hot tearing formation. Since hot tearing is a complex phenomenon when many variables are

involved, and it is attempted to control the casting process as well as possible, such as pouring speed and pouring temperature.

Table 4-1 Nominal compositions of tested alloys (wt.%)

Alloys	Zn	Y	Zr	Mg
Mg-0.2Y	-	0.2	-	Bal.
Mg-0.9Y	-	0.9	-	Bal.
Mg-1.5Y	-	1.5	-	Bal.
Mg-2Y	-	2	-	Bal.
Mg-4Y	-	4	-	Bal.
Mg-0.2Y-1.5Zn	1.5	0.2	-	Bal.
Mg-2Y-1.5Zn	1.5	2	-	Bal.
Mg-3Y-1.5Zn	1.5	3	-	Bal.
Mg-4.5Zn	4.5	-	-	Bal.
Mg-0.4Y-4.5Zn	4.5	0.4	-	Bal.
Mg-0.9Y-4.5Zn	4.5	0.9	-	Bal.
Mg-2Y-4.5Zn	4.5	2	-	Bal.
Mg-2Y-0.5Zn	0.5	2	-	Bal.
Mg-0.4Y-4.5Zn-0.5Zr	4.5	0.4	0.5	Bal.

4.1.3 Measurements of crack volume

4.1.3.1 Wax penetration method

In the present work, the volume of cracks was measured by a wax penetration method [66] for all Mg-Y-(Zn) alloys. The advantages of this method are simplicity and quickness, without damaging the samples.

After the hot tearing experiments, the sample was cut from the casting in a T-shape, and immersed into a molten wax bath at 80 °C, and stayed for 10 min to homogenize the temperature. Then the bath was put into a vacuum chamber to suck out the air entrapped in the wax and inside the cracks. The vacuum valve was then opened, and a pressure with a value of one bar was immediately applied to the wax and the sample. With this pressure, the molten wax was injected into the cracks. After that, the bath was cooled, and the solidified

wax on outside surfaces of the sample was removed, while the wax inside the cracks was retained. The volume of the cracks can be determined using the following equation:

$$V_{cr} = \frac{M_2 - M_1}{\rho_{wax}} \tag{4-1}$$

where V_{cr} is the volume of cracks; M_1 and M_2 are the weight of the magnesium casting before and after the injection of wax, respectively; ρ_{wax} is the density of the paraffin wax, $\rho_{wax} = 0.90 g/cm^3$. The schematic of this process is shown in Fig. 4.1.

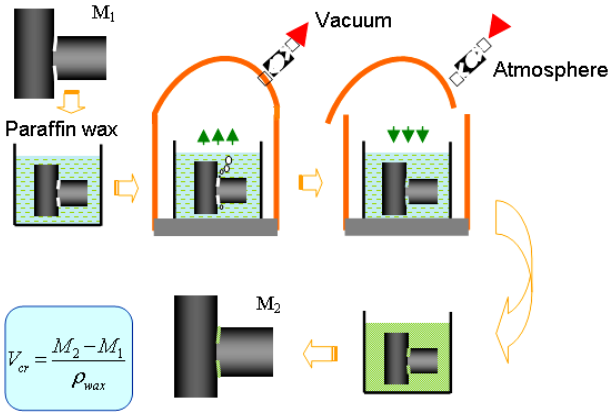

Fig. 4.1 Schematic of wax penetration method for the measurements of crack volume.

4.1.3.2 X-ray micro-tomography

The shortness of the wax penetration method was that the closed cracks inside the rod can not be measured. Therefore, the HTS was also characterized by measuring the volume of cracks using 3D X-ray micro-tomography, which can detect not only the surface cracks but also the internal cracks. The results obtained by this method were more reliable compared with the wax penetration method. However, it was difficult to prepare cylindrical sample for X-ray micro-tomography when the castings with serious hot cracks, such as some ternary Mg-Y-Zn alloys.

X-ray micro-tomography is a non-destructive, three dimensional characterization method that has been applied to a number of fields within materials science [92-97]. The principle of this method is to obtain a sequence of X-ray projections of the machined rod containing crack as it rotates on an axis perpendicular to the X-ray beam. The technique allows imaging the internal microstructural features by measuring variations in intensity of a transmitted x-ray beam through a rotating specimen.

In the present study, the HTS of the alloys were evaluated using X-ray micro-tomography in a X-ray tube-based high resolution micro-tomography (*nanotom® s* - phoenix, GE Measurement & Control Solutions, Germany). The scheme of such tomographic experiment was shown in Fig. 4.2. The 3D volume reconstruction was made from the 2D projections (with a filtered back-projection algorithm) using *datos/x 2.0* reconstruction software (phoenix, GE Measurement & Control Solutions, Germany). To improve reconstruction quality the automatic geometry calibration was applied during the reconstruction process. In order to reduce the final size of the data file, the output data resolution was reduced by 0.5. The resolution achieved after reconstruction of the volume in the region of interest was 20 µm. Further data processing, including normalization and alignment of the 3D-data sets, the segmentation and characterization of the crack volume was applied using the software IDL 8.1 (Exelis Visual Information Solutions, Inc.). Cylindrical samples with a diameter of approximately 12.5 mm machined from the CRC mould castings (Fig. 4.3), were used for the tomographic measurements. The average crack volume is calculated with minimum two samples for each hot tearing test.

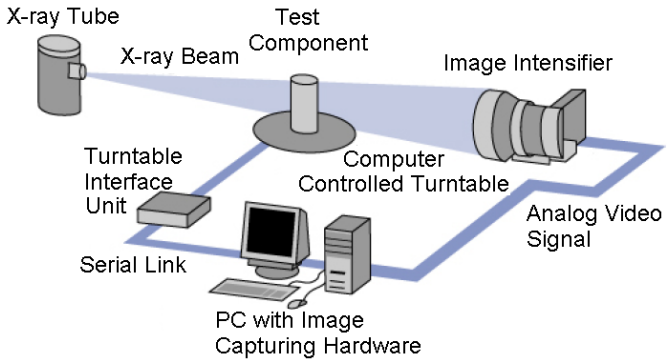

Fig. 4.2 Schematic diagram of the tomographic experiment.

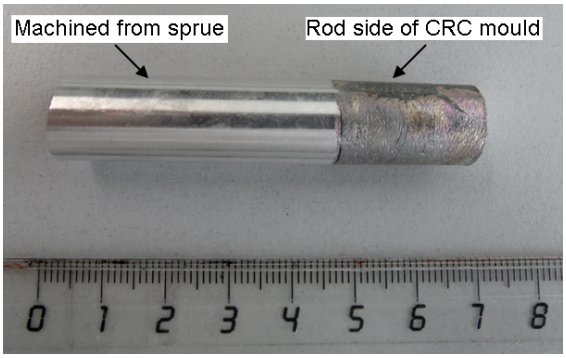

Fig. 4.3 Sample for X-ray tomographic investigations.

4.1.4 Microstructural observations

The morphologies of grains and cracks were observed on both the transversal and longitudinal sections of the rod samples cut from the locations near the sprue-horizontal rod junction. Polished samples were chemically etched in solution of 8 g picric acid, 5 ml acetic acid, 10 ml distilled water and 100 ml ethanol. The microstructures were observed using Reichert-Jung MeF3 optical microscope. A Zeiss Ultra 55 (Carl Zeiss GmbH, Oberkochen, Germany) Scanning Electron Microscope (SEM) equipped with Energy Dispersive X-ray Spectroscopy (EDS) was used to observe the fracture surfaces and also the crack propagations.

4.2 Numerical simulation

4.2.1 Geometry and meshing

The model includes four assembled parts: mould, ingot, steel rod and graphite stopper. The geometry used in the simulation includes a thermocouple (TC1) location as shown in Fig. 4.4. The figure shows dimensions on the mid-plane view of the casting and all dimensions are in mm. The overall dimensions were:

- Length=252.5 mm
- Width=80 mm
- Height=140 mm

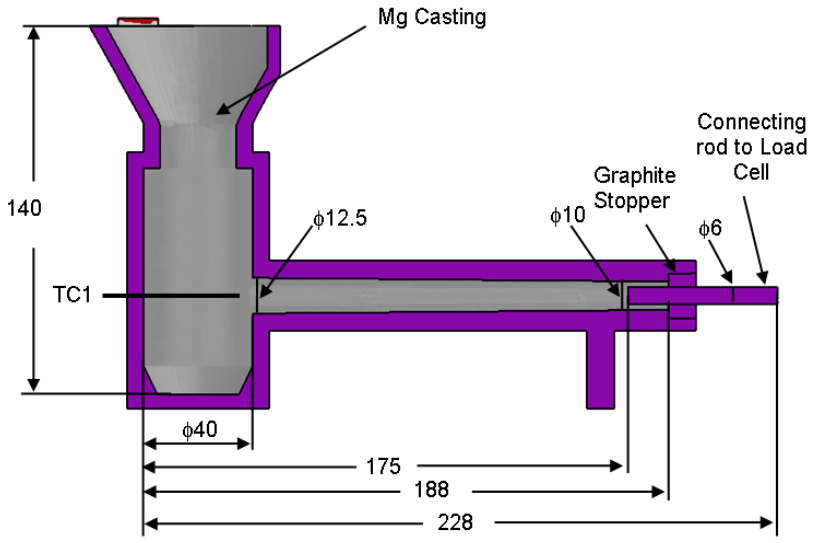

Fig. 4.4 Geometry of casting mould (unit: mm).

The mesh generator MeshCAST is used to construct the computational grid of the ingot and the mould. Construction of this mesh is an important as it determines the accuracy of the

computations and the time required for modeling. Fig. 4.5 shows computational mesh of the ingot and mould. Four node linear tetrahedral finite-elements were chosen for the ingot and the mould. A finer finite-element mesh is chosen for the ingot to increase the accuracy of the calculations, while a coarse mesh density was used for the mould. The computational mesh of ingot and mould consist of 168,627 elements and 35,708 nodes.

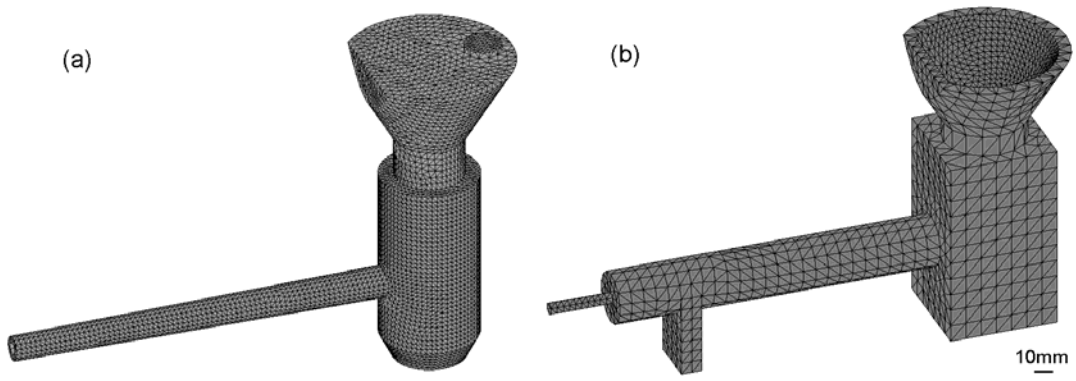

Fig. 4.5 Computational meshing of the ingot and mould: (a) ingot, (b) mould.

4.2.2 Material properties

The alloy composition, casting geometry, cooling history and mechanical properties of alloys influence hot tearing. In order to predict hot tearing, it is critical to have accurate data of thermo-physical and mechanical properties, especially for the mushy zone, as input for complex solidification processes. ProCAST has an automatic link to the thermodynamic databases to calculate these properties. Thus, it is possible to compute the enthalpy curve, density, viscosity and thermal conductivity based upon the chemical composition. Thus, in the present work, these material properties were computed in ProCAST using thermodynamic databases. In the Fig. 4.6 and Fig. 4.7, examples of calculated thermo-physical and thermodynamic properties are given for Mg-1.5Y alloy, as a function of temperature. The solidification path can be calculated with Scheil model in Pandat software using PanMg8.0 database. During ProCAST simulation, the castings are assumed to be solid undergoing elasto-plastic deformation.

In the assembly of model, the mould and steel rod are assigned steel_H13 and stopper is assigned graphite. The material properties of steel_H13 and graphite are taken from the materials database in ProCAST. The rigid and the vacant models are used to account for

contact interaction between the casting and the mould. An elasto-plastic stress model is used for the ingot and the rigid model is used for the mould.

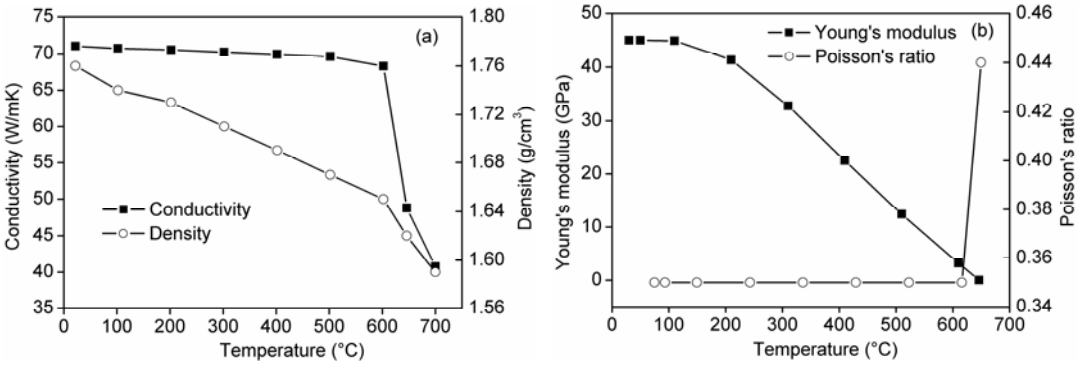

Fig. 4.6 Thermo-physical properties of the Mg-1.5Y alloy: (a) thermal conductivity and density, (b) Young's modulus and Poisson's ratio.

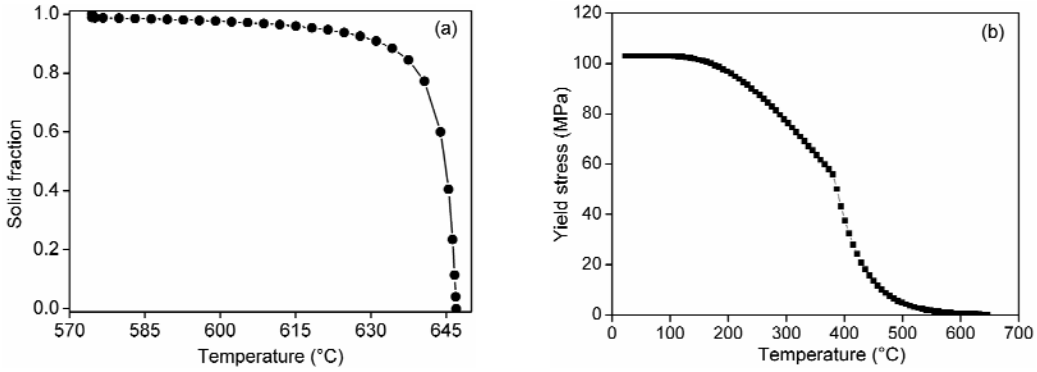

Fig. 4.7 Thermodynamic and thermo-physical properties of the Mg-1.5Y alloy: (a) solidification path, (b) yield stress and temperature curve of Mg-1.5Y alloy.

4.2.3 Boundary and initial conditions

The boundary and the initial conditions are assigned as follows:

- All components of the model, except for the ingot, are assigned as constrained by applying zero displacements in all directions. Zero displacement in the y direction is assigned to the rod end of the ingot.
- Heat transfer coefficient of 500 W/(m^2*K) is applied to the ingot-mould interface.
- Convection air cooling is applied to all surfaces which are surrounded by air. The ambient temperature of the surrounding air is 20 °C.
- The mould is preheated by applying an initial temperature of 250 or 450 °C.

- A gravity of 9.8 m/s^2 is applied to the ingot which kept the bottom surface in contact with the mould.

4.2.4 The calculation and the analysis of results

The thermal, fluid flow and stress modules operated simultaneously and calculations performed for the hydrodynamics of the casting operation (the filling of the mould with the alloy), crystallization and cooling of the casting, formation of stresses and strains in the casting are all executed simultaneously. The results of temperature, solid fraction and HTI fields can be displayed with the post-processor after the computation. These results are used to analyses the hot tearing formation.

5 RESULTS

5.1 Hot tearing behaviours of binary Mg-Y alloys

5.1.1 Prediction of HTS based on Clyne and Davies' model

5.1.1.1 Clyne and Davies' model

The existing hot tearing criteria [5-6, 53] can be divided into the two categories: non-mechanical and mechanical. The former criteria deal with vulnerable temperature range, phase diagrams and process parameters, which is represented by the criteria of Clyne and Davies [53], Feurer [52] and Katgerman [55]. The latter criteria involve critical stress, critical strain, or critical strain rate [53]. These hot tearing criteria are applied to different casting processes. In this work, the HTS of binary Mg-Y alloys are predicted with thermodynamic calculations based on Clyne and Davies' model.

In Clyne and Davies' model [53], CSC is proposed to describe the effects of alloy composition on hot tearing. The CSC can be defined as equation (2-21). In the present study, this equation is used to calculate the CSC value. A schematic diagram in Fig. 5.1 shows the calculation of CSC.

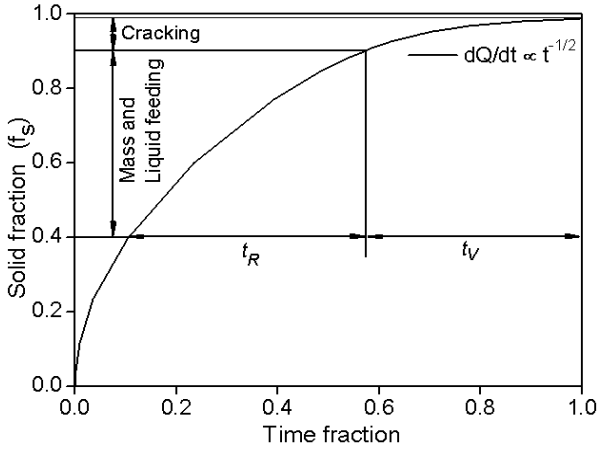

Fig. 5.1 Schematic diagram of solid fraction vs. time fraction showing the calculation of CSC.

In order to predict the variation of CSC with composition, it is necessary to obtain the solid fraction as a function of time during solidification for each specified alloy. For the

solidification conditions encountered in normal castings, the Scheil equation works well. Thus,

$$C_L = C_0 f_L^{k-1} \tag{5-1}$$

where C_L is the liquid composition after a fraction $(1-f_L)$ of the alloy with initial composition C_0 and partition coefficient k, has solidified. Assuming that the liquidus and solidus to be approximately straight lines. This is expressed as,

$$f_L = \left(\frac{T_M - T}{T_M - T_L}\right)^{1/(k-1)} \tag{5-2}$$

where T_M is the melting temperature of the pure base metal, T_L is the liquidus temperature of the alloys of composition, C_0, and T is the temperature at which the liquid fraction f_L, would exist. Using the start of solidification as the beginning, the initial boundary conditions are,

$$t = 0, T = T_L, f_L = 1 \tag{5-3}$$

At later stages of solidification, eutectic liquid will appear. The appearance of eutectic liquid was thus taken as the end point of the solidification process. In any event, this does not invalidate the analysis, as ratios of time are taken. Therefore, the final boundary conditions are,

$$t = 1, T = T_E, f_L = \left(\frac{T_M - T_E}{T_M - T_L}\right)^{1/(k-1)} \tag{5-4}$$

where T_E is the eutectic temperature.

In Clyne and Davies' model, three cooling paths were investigated:

(1) Rate of fall of temperature, $\frac{dT}{dt}$=constant,

(2) Rate of heat flow out of the volume element, $\frac{dQ}{dt}$=constant, and

(3) Rate of heat flow out of the volume element, $\frac{dQ}{dt} \propto t^{-1/2}$, where $dQ = (\rho H df_L + \rho C dT)$, ρ is the density and C is the specific heat (assumed the same for solid and liquid) and H is the latent heat of melting.

Of these, the first one is unrealistic but mathematically simple. In practice, thermal conditions are expected to fall somewhere between condition (2) and (3). For condition (1) equation (5-2) can be written in the form.

$$t_1 = (f_L^{k-1} - 1)(\frac{T_M - T_L}{T_L - T_E}) \tag{5-5}$$

For the other two modes, the expressions relating time and liquid fraction are obtained by substitution for dQ and integration. The resulting relationship for condition (2):

$$t_2 = \frac{\frac{H}{C}(1 - f_L) + (T_M - T_L)(f_L^{k-1} - 1)}{\frac{H}{C}\left[1 - (\frac{T_M - T_E}{T_M - T_L})^{1/(k-1)}\right] + (T_L - T_E)} \tag{5-6}$$

For condition (3):

$$t_3 = (\frac{\frac{H}{C}(1 - f_L) + (T_M - T_L)(f_L^{k-1} - 1)}{\frac{H}{C}\left[1 - (\frac{T_M - T_E}{T_M - T_L})^{1/(k-1)}\right] + (T_L - T_E)})^2 \tag{5-7}$$

The typical calculated cooling curves for Mg-1.5Y alloy under these three cooling conditions are shown in Fig. 5.2. After comparing with the experimental results, the calculated results using the mode (3) are found close to the reality. Thus, all CSC values are calculated using the mode (3) cooling condition in the present investigation.

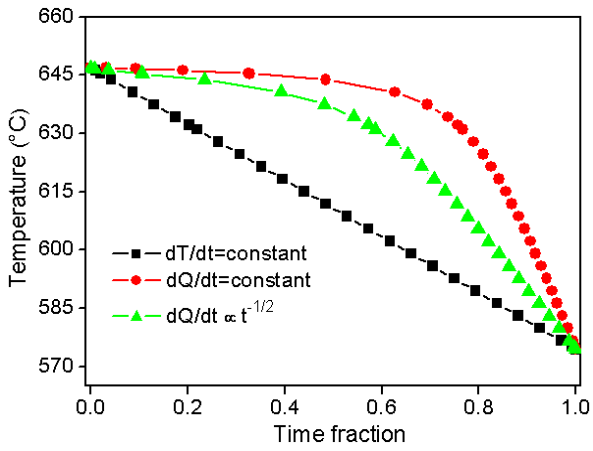

Fig. 5.2 Calculated cooling curves for Mg-1.5Y alloys under three different cooling conditions.

5.1.1.2 Results of thermodynamic calculations

As shown in equation (2-21) before calculating the CSC the variant fractional time at a specified solid fraction or liquid fraction should be known. This can be achieved through the following steps:

- Using Scheil model, the volume fraction of solid phase as a function of temperature is first calculated using thermodynamic software Pandat and PanMg8.0 thermodynamic database. In Clyne and Davies' model, the Scheil assumption was considered to be reasonable for the solidification conditions encountered during castings.
- The second step is the determination of temperature profile as a function of time, i.e. the cooling curve.

In order to predict the variation of the CSC with alloy composition, it is necessary to design a series of alloys with different Y contents, so a range of Y content from 0.2 to 8.0 wt.% which is less than its maximum solubility in magnesium at the eutectic temperature was chosen [98-99]. The volume fraction of solid phase as a function of temperature is shown in Fig. 5.3. The Y content has a large influence on both the freezing range and the melting point. Above 610 to 640 °C the solid fraction reduces quickly, and below 610 to 640 °C it changes slowly. The specific temperature above which the solid fraction changes quickly depends on the Y content. The melting points of Mg-Y alloys decrease from 650 to 632 °C when the content of Y increased from 0.2 to 8.0 wt.%.

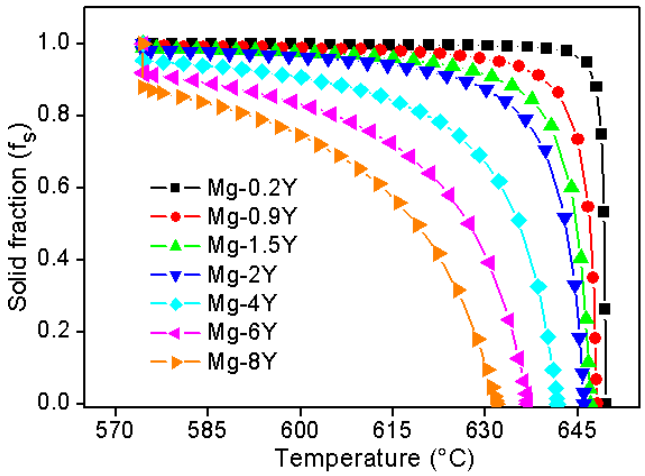

Fig. 5.3 Solid fraction and temperature curve for binary Mg-Y alloys calculated with using Scheil modeling.

In Clyne and Davies' model, the partition coefficient, liquidus and solidus slopes were assumed to be constant. Actually, this is not accurate. The liquidus and solidus in phase diagrams are normally not linear. In order to improve the accuracy of calculated results, in the present work the partition coefficient and liquidus slope were calculated using PanEngine

module in Pandat software based on thermodynamic database PanMg8.0. PanEngine is a collection of C++ classes, which performs some specified thermodynamic and equilibrium calculations in accordance with a specified metallurgical phenomenon [100]. The calculated partition coefficient and liquidus slope of the Mg-Y alloys are shown in Fig. 5.4, which indicates that both the partition coefficient k and liquidus slope m_L vary with temperatures. The value of the partition coefficient increases from 0.19 to 0.27 as the temperature decreases from 650 to 632 °C. The liquidus slope also changes from 6.8 to 8.5 in the temperature range from 650 to 632 °C.

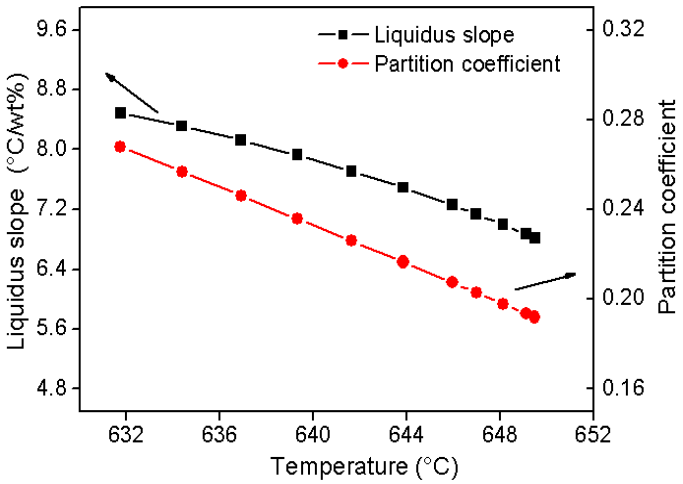

Fig. 5.4 Calculated partition coefficient of Y and liquidus slope for the Mg-Y binary system.

The calculated cooling curves using condition (3) are shown in Fig. 5.5. The cooling rate seems to depend on the alloy compositions.

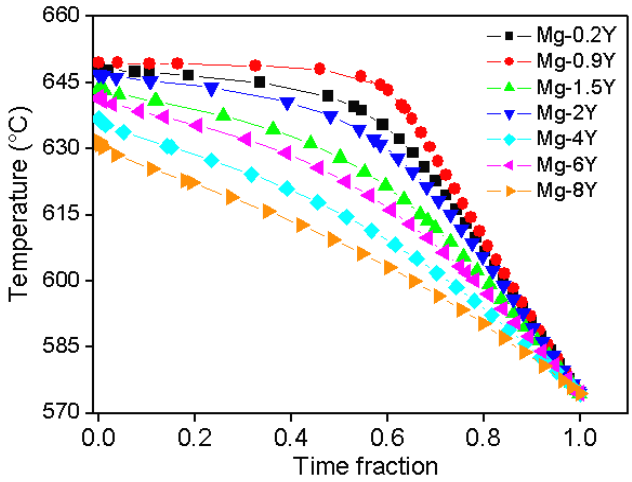

Fig. 5.5 Cooling curves calculated for Mg-Y alloys using condition mode (3).

5.1.1.3 CSC of Mg-Y alloys

The CSC value as a function of the Y content for binary Mg-Y alloys is shown in Fig. 5.6. The curve follows the typical "λ" shape expected for CSC. The CSC increases with the content of Y, reaches the maximum at 1.5 wt.% Y and then decreases with further increase in the Y content.

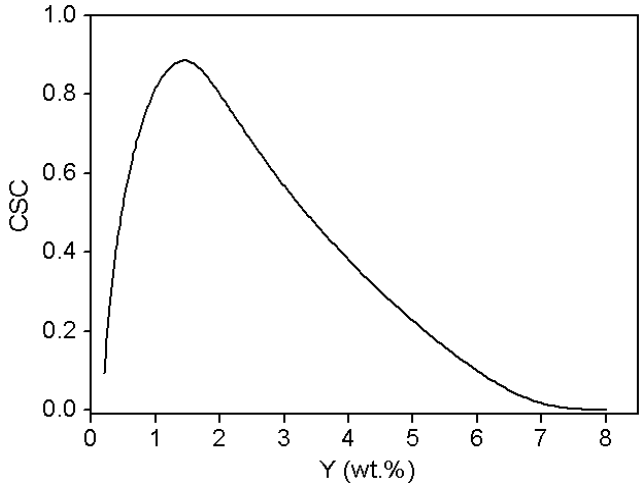

Fig. 5.6 Calculated CSC value as a function of the content of Y in binary Mg-Y alloys.

5.1.2 Experimental results of hot tearing tendency

To improve the hot tearing resistance of alloys, it is necessary to understand how a variety of factors effecting the hot tearing behaviour. The HTS of Mg-Y alloys predicted by the thermodynamic calculations in the previous section and provide a theoretical basis for alloy design. This section presents the experimental results, including the crack volume calculations and microstructure observations. The measurements of crack volume and analysis on crack initiation and propagation can help to understand the formation mechanism of hot tearing. Influences of mould temperature, alloy composition and thermal contraction on HTS of Mg-Y alloys are also investigated.

5.1.2.1 Chemical compositions

Table 5-1 shows the actual compositions of the experimental binary Mg-Y alloys, which are close to the nominal compositions.

Table 5-1 Actual chemical compositions of experimental alloys (wt.%)

Alloy	Y	Mn	Si	Fe	Mg
Mg-0.2Y	0.22	0.034	0.018	<0.001	Bal.
Mg-0.9Y	1.11	0.033	0.012	<0.001	Bal.
Mg-1.5Y	1.44	0.032	0.107	<0.001	Bal.
Mg-2Y	1.97	0.032	0.010	<0.001	Bal.
Mg-4Y	3.58	0.030	0.007	<0.001	Bal.

5.1.2.2 Hot tearing curves

Fig. 5.7 is a typical experimental curve, recording temperature and contraction force during casting of alloys. The red curve shows the temperature at the hot spot area, while the black curve shows the evaluation of contraction force during solidification. The contraction force develops in the rod during cooling due to the solidification shrinkage and thermal contraction.

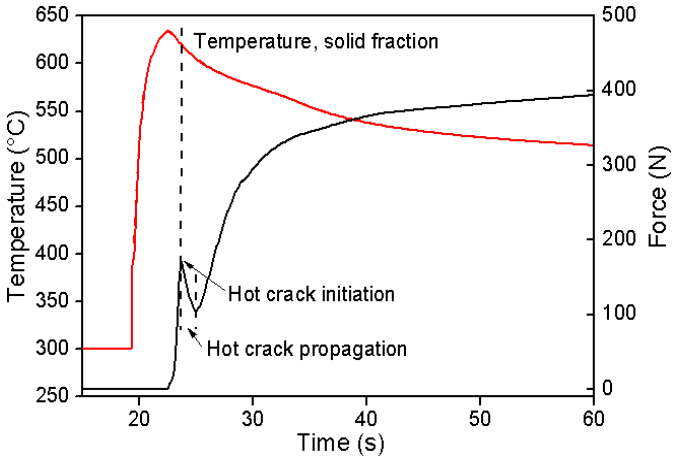

Fig. 5.7 Typical obtained contraction force and temperature as a function of time curve for Mg-1wt.% Al alloy at mould temperature of 350 °C [35].

At the early stages of solidification, the liquid is free to move, so the contraction can be accommodated by the liquid flow [5]. The hot tearing does not occur. However, this mass feeding stage is relatively short considering that a solid shell would form rapidly after pouring due to the high cooling rate observed in the present investigation. After the solid shell forms (dendrite coherency reaches), both the strains and stresses build up due to thermal contraction and impose on the shell and concentrate in the weak area of the casting. If strains and stresses are larger than a critical value, they may cause to tear apart the dendrites, and hot tearing

occurs. As shown in Fig. 5.7, the contraction force increases very sharply at the beginning of solidification, and then suddenly drops to a certain level and then further increasing again until the solidification finishes. The point when the contraction force begins to decrease indicates the initiation of hot tearing. Corresponding the point on the temperature, both the critical temperature (T_i) and solid fraction (f_{si}) at which the hot crack initiates can be obtained. The force dropping stage shown in Fig. 5.7 is regarded as the crack propagation. Therefore, by analyzing the curve, not only the initiation of hot tearing but also its propagation can be investigated.

Fig. 5.8 shows the experimental hot tearing curves of Mg-Y alloys with different contents Y at mould temperature of 250 °C. On all hot tearing curves, a slight reduction in the force contraction is observed at the beginning of pouring. This is possibly due to the fact that the molten melt pressure exerted on the stud that is connected to the load cell as the melt entered from sprue into the rod relatively fast, due to the sudden change in the cross sections. The load evolution is generally similar for all alloys, but some differences are observed at the beginning of solidification. With the solidification proceeding, the contraction force increases, and reaches maximum value and then decreases or becomes stable and increases again. This force drop indicates the formation of the hot tearing. The temperature corresponding to the start of the force drop is considered to be the initiation temperature of hot tearing.

The alloy compositions affect the hot tearing initiation temperatures. For Mg-0.2Y alloy, the hot cracks initiate at 606 °C, which corresponds to a solid fraction of 0.997 according to the thermodynamic calculation using Scheil model in Pandat software (Fig. 5.8 (a)). For Mg-0.9Y alloy, the hot cracks initiate at 598 °C, where the solid fraction is 0.989 (Fig. 5.8 (b)). The contraction force for Mg-0.9Y alloy remained lower after the initial drops for an extended time. It means that the hot cracks propagate for longer lengths in this alloy. Normally the sharper and longer the force drop, the longer is the crack size. Unlike aforementioned alloys, the contraction force curve of Mg-1.5Y does not show a decrease in force. However, the microstructural observations of the castings (shown in the next section) indicate that there is hot tearing in this alloy. Huang et al. [101] reported that the onset of hot tearing can be identified by locating the point at which the contraction force as a function time deviates from linear its. Therefore, the initiation temperature of Mg-1.5Y alloy is found to be 617 °C. This temperature corresponds to a solid fraction of 0.956, which that corresponds to the established principle hot tearing normally occurs at the last stage of solidification when approximately 5%

liquid is left [6]. In a similar way, the hot tearing initiation temperatures 614 °C and 594 °C for Mg-2Y and Mg-4Y can be calculated, respectively. The corresponding solid fractions for Mg-2Y and Mg-4Y are 0.942 and 0.918, respectively.

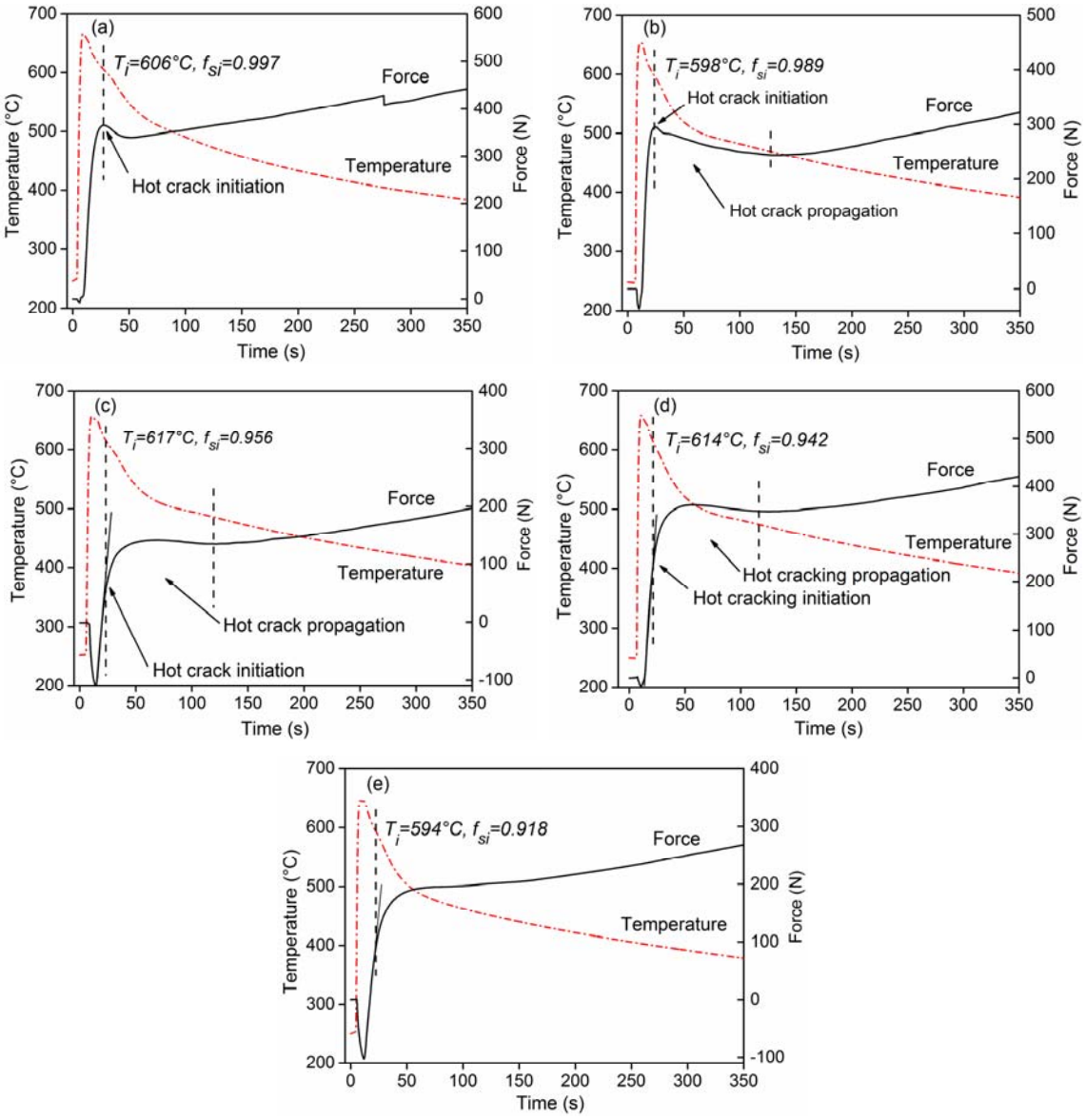

Fig. 5.8 Contraction force and temperature as a function of time for Mg-xY alloys at a mould temperature of 250 °C: (a) x=0.2, (b) x=0.9, (c) x=1.5, (d) x=2, (e) x=4.

Fig. 5.9 shows the experimental curves for Mg-0.9Y and Mg-1.5Y alloys at a mould temperature of 450 °C. On these curves, no apparent force drops are observed, indicating that no hot cracks occur in Mg-0.9Y and Mg-1.5Y alloys. This is in good agreement with the macrostructural observations of hot cracks (discussed in the following section). Combining

with the results at low mould temperature, this shows that the hot tearing decreases with increased the initial mould temperature.

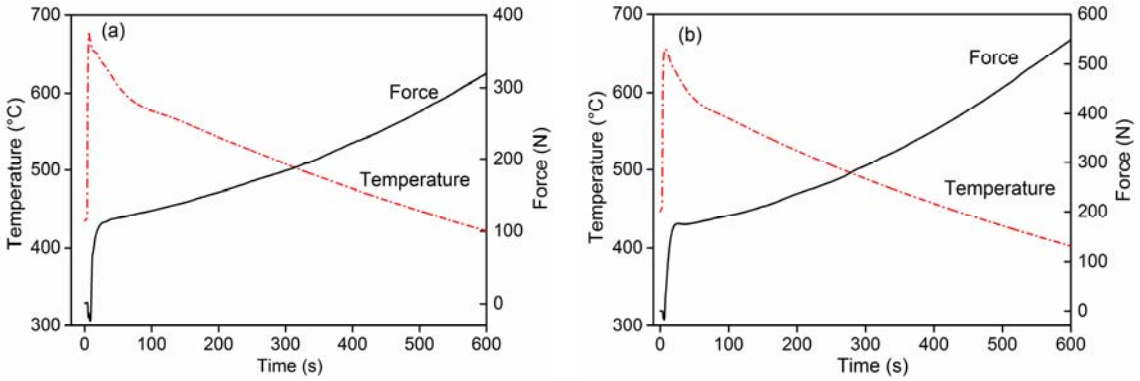

Fig. 5.9 Contraction force and temperature as a function of time for Mg-0.9Y and Mg-1.5Y alloys at a mould temperature of 450 °C: (a) Mg-0.9Y, (b) Mg-1.5Y.

5.1.2.3 Macro-structural observations

Table 5-2 Hot cracks of Mg-Y binary system under different mould temperatures

	Mg-0.2Y	Mg-0.9Y	Mg-1.5Y	Mg-2Y	Mg-4Y
250 °C					
450 °C					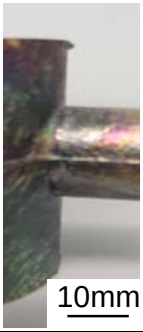

Table 5-2 shows the macrostructure of cracks on the surfaces of the restrained rods at different mould temperatures for the alloys investigated. Both the composition of alloys and mould temperature influence the formation of hot cracks. No macro-cracks are observed near the junctions of Mg-0.2Y and Mg-4Y alloys at a mould temperature of 250 °C. In contrast, the macro-cracks are clearly observed near the junctions of Mg-0.9 Y and Mg-1.5 Y alloys. The large open crack in Mg-0.9Y alloy shows that this alloy has the largest HTS at 250 °C from the compositions investigates. When the mould temperature was increased to 450 °C, no visible cracks are observed on the all the casting surfaces.

5.1.2.4 Microstructural observations

Fig. 5.10 shows the polarized optical micrographs of binary Mg-Y alloys taken from the region near the junction of the sprue and the horizontal rod at a mould temperature of 250 °C. When increasing the Y content, the microstructure changes from columnar grain to equiaxed grain structures. Among the alloys investigated, Mg-0.9Y alloy exhibits the largest grain size and a columnar morphology. In the Mg-4Y alloy, the equiaxed grains are dominant. This may be due to the enrichment in solute that promotes constitutional undercooling.

Fig. 5.11 shows the optical micrographs of binary Mg-Y alloys at the regions near the junction of the sprue and the horizontal rod at a mould temperature of 450 °C. At low Y contents, the cellular or/and columnar grain structures dominate. Whereas, the equiaxed grains can be seen in the alloys with high contents of Y. Comparison of Fig. 5.10 and Fig. 5.11 shows that the primary cellular grain sizes decreases with increased the mould temperature at low content of Y. During cellular mode of solidification, the undercooling at the tip of the dendrite decreases as the cooling rate increases. As a result, the tip radius increases, known as cell flattening, resulting in the start of columnar growth with substantial side branching [102]. Compared lower Y content alloy, Mg-4Y alloy exhibits a larger equiaxed structures.

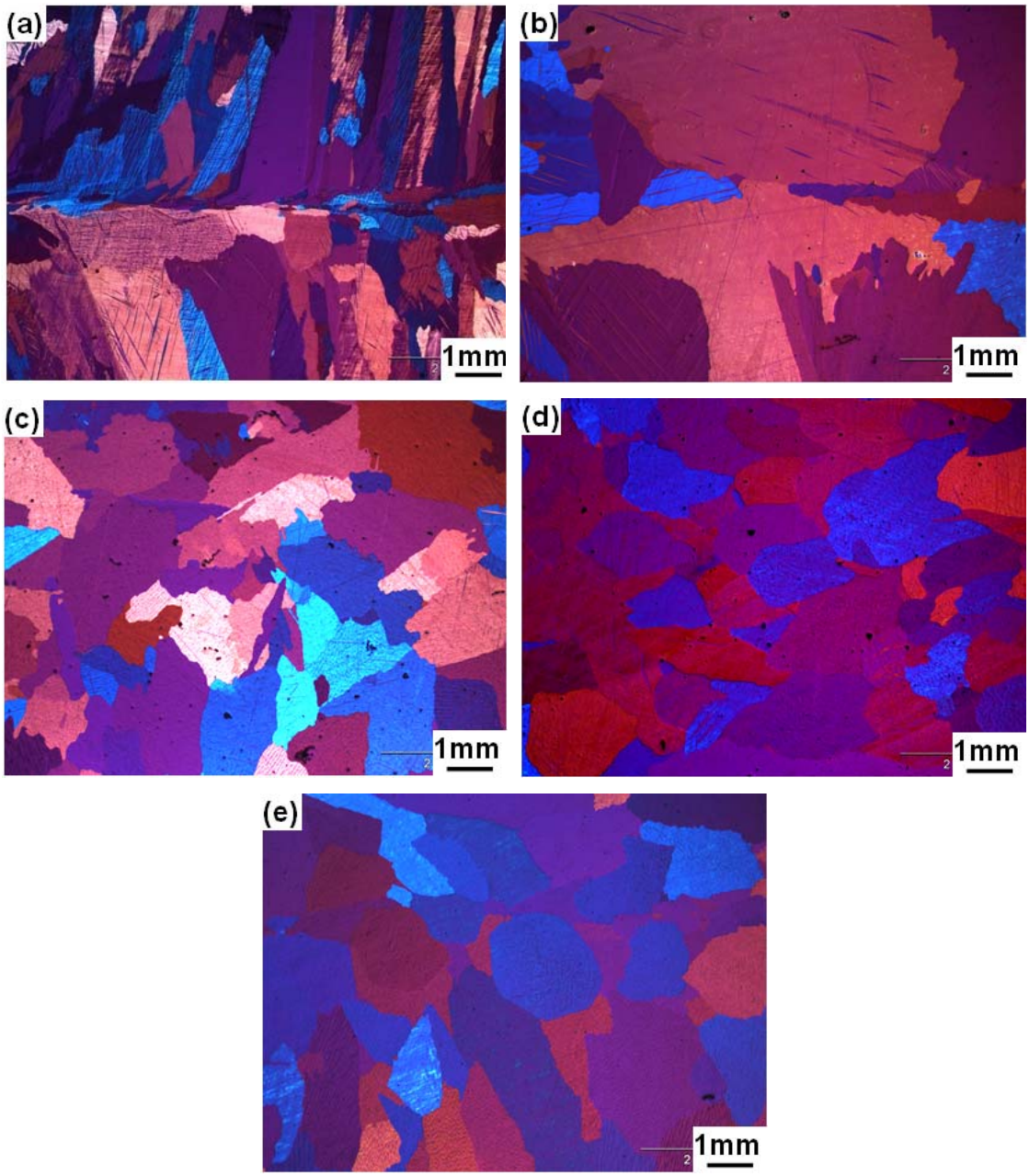

Fig. 5.10 Optical microstructures of binary Mg-Y alloys at mould temperature of 250 °C: (a) Mg-0.2Y, (b) Mg-0.9Y, (c) Mg-1.5Y, (d) Mg-2Y, (e) Mg-4Y.

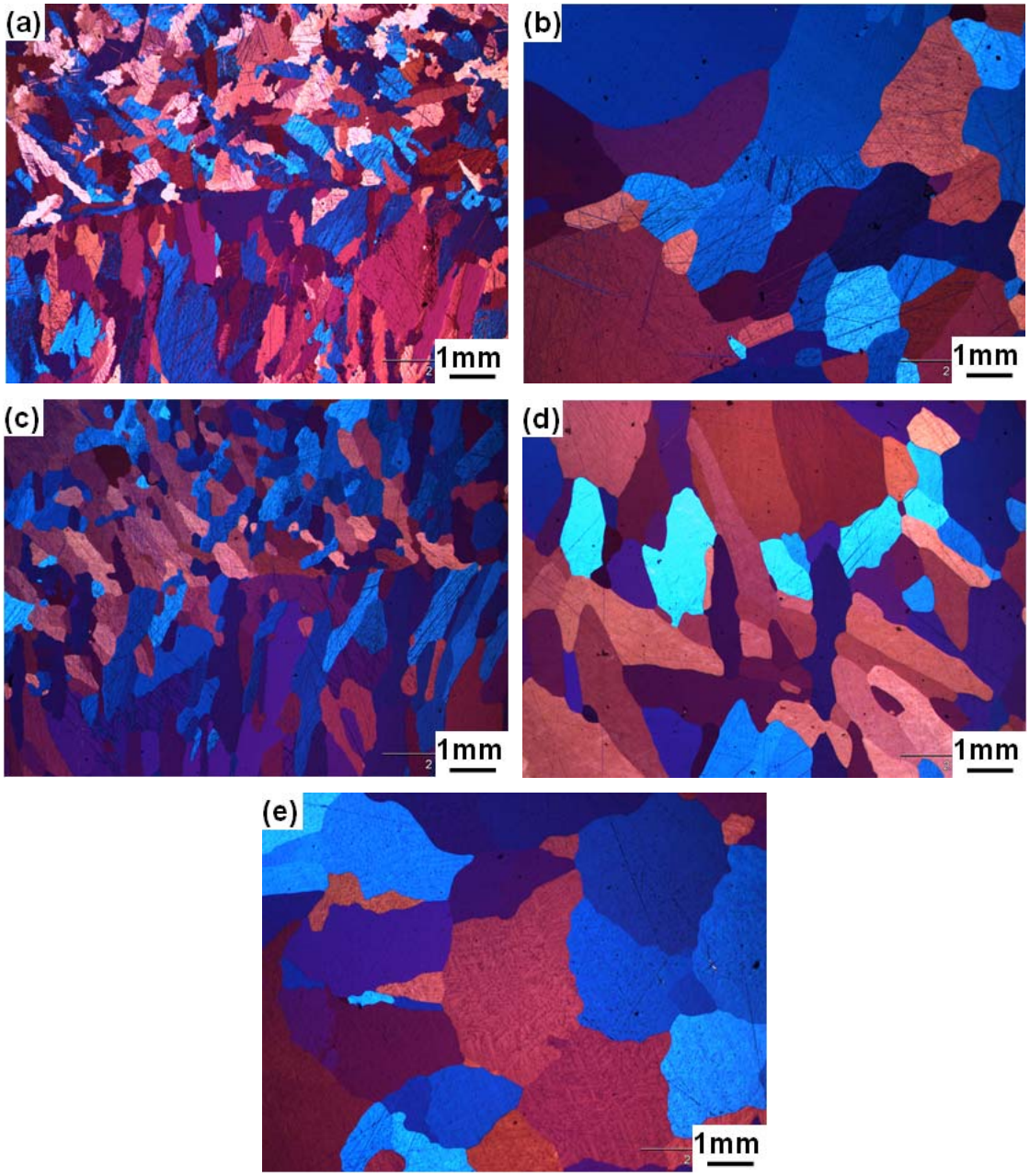

Fig. 5.11 Optical microstructures of binary Mg-Y alloys at a mould temperature of 450 °C: (a) Mg-0.2Y, (b) Mg-0.9Y, (c) Mg-1.5Y, (d) Mg-2Y, (e) Mg-4Y.

Fig. 5.12 shows SEM microstructures of hot cracks along the longitudinal surfaces at a mould temperature of 250 °C. All hot cracks propagate along the dendrite and grain boundaries. In general, the width of the tear reduces as it grows from the outer surface into the centre, which indicates that the tear initiates at the outer surface of the rod and develops toward the centre. The main cracks generally initiate at the sprue-rod junction.

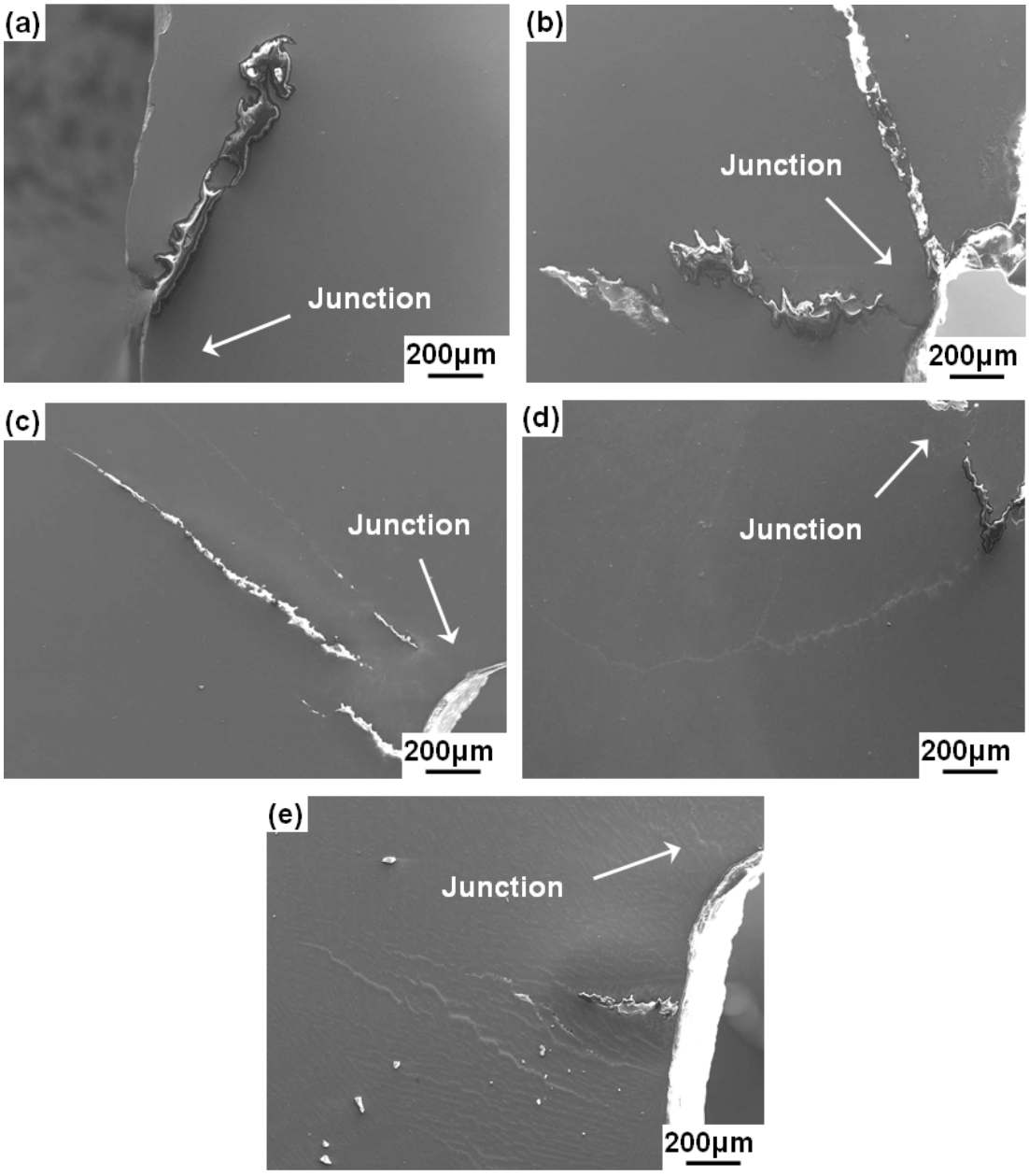

Fig. 5.12 SEM micrographs showing the cracks in the regions near the sprue and rod junction at a mould temperature of 250 °C: (a) Mg-0.2Y, (b) Mg-0.9Y, (c) Mg-1.5Y, (d) Mg-2Y, (e) Mg-4Y.

The SEM microstructures of hot cracks along the longitudinal surfaces at a mould temperature of 450 °C are shown in Fig. 5.13. The main cracks generally initiate at the sprue-rod junction. In both the Mg-2Y and the Mg-4Y alloys, secondary phases with different contrasts are observed in ahead of the main cracks. With increased Y content the amount of white contrast regions increases. With increment in the mould temperature to 450 °C, the cracks apparently reduced (compared Fig. 5.12 with Fig. 5.13).

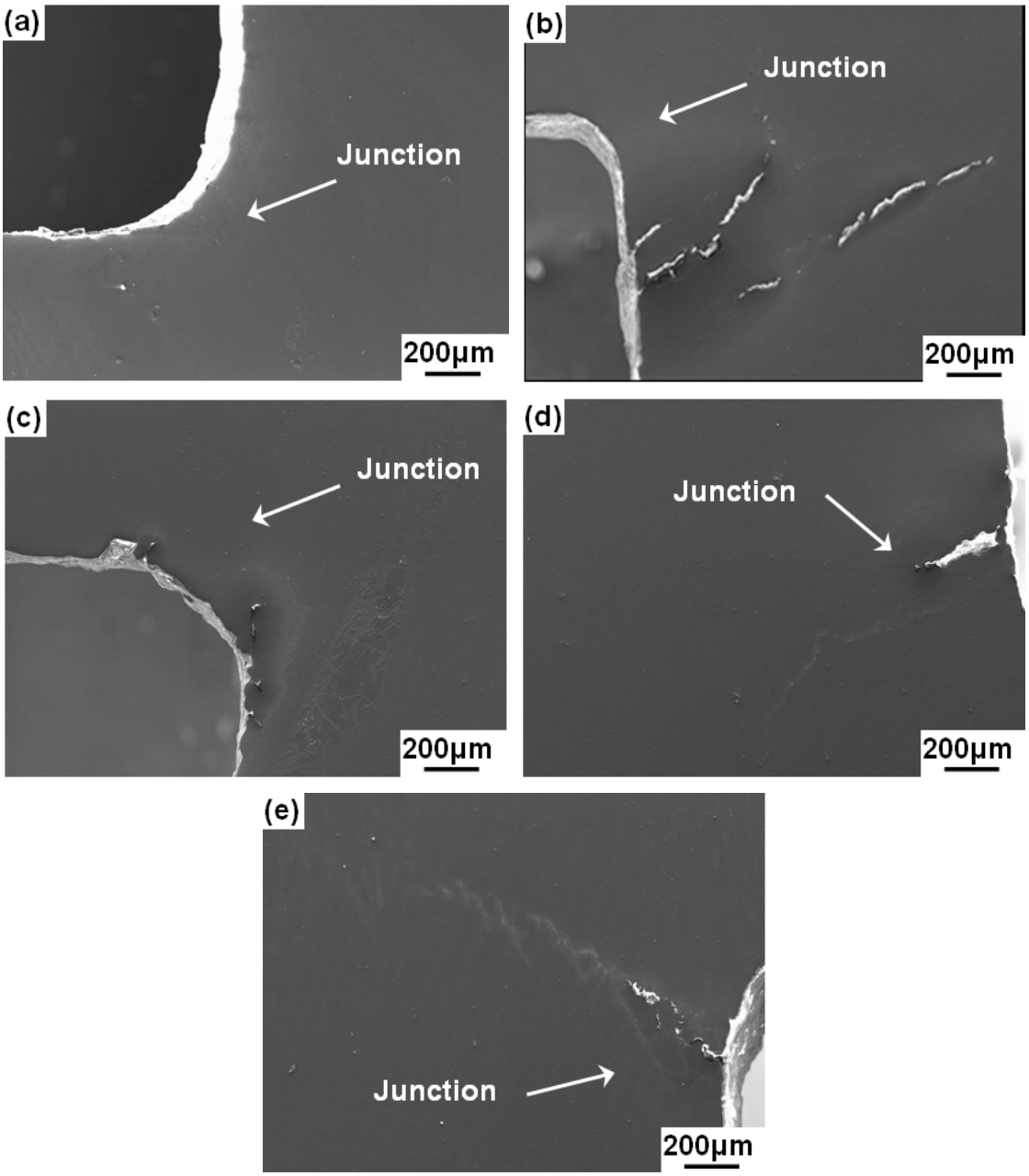

Fig. 5.13 SEM micrographs showing the cracks in the sprue-rod junction at a mould temperature of 450 °C: (a) Mg-0.2Y, (b) Mg-0.9Y, (c) Mg-1.5Y, (d) Mg-2Y, (e) Mg-4Y.

Fig. 5.14 shows the X-ray micro-tomography radiographs of hot cracks for Mg-Y alloys at a mould temperature of 250 °C. As with SEM observations, the hot cracks are located at the junction of rods (2D centre slice). Very few cracks are observed in the Mg-0.2Y and the Mg-4Y alloys. The alloy with 0.9 wt.% Y has a larger volume of cracks. In this sample, the initiation of hot cracks at the junctions can be traced from the outer surface to the centre of the rod. Compared with Mg-0.9Y alloy, the volume of cracks decreased in Mg-1.5Y alloy. Few

white river patterns due to the higher absorption of X-ray compared to the Mg matrix can be seen along with a tear in higher Y containing alloys. This indicates the presence of Y-rich phases or Y segregation. It is noticed that these white river patterns are normally observed near the main cracks. In addition, in all the rods the majority of the hot cracks are located near the surfaces. In contrast, the hot cracks are generally not observed in the centre of the rod.

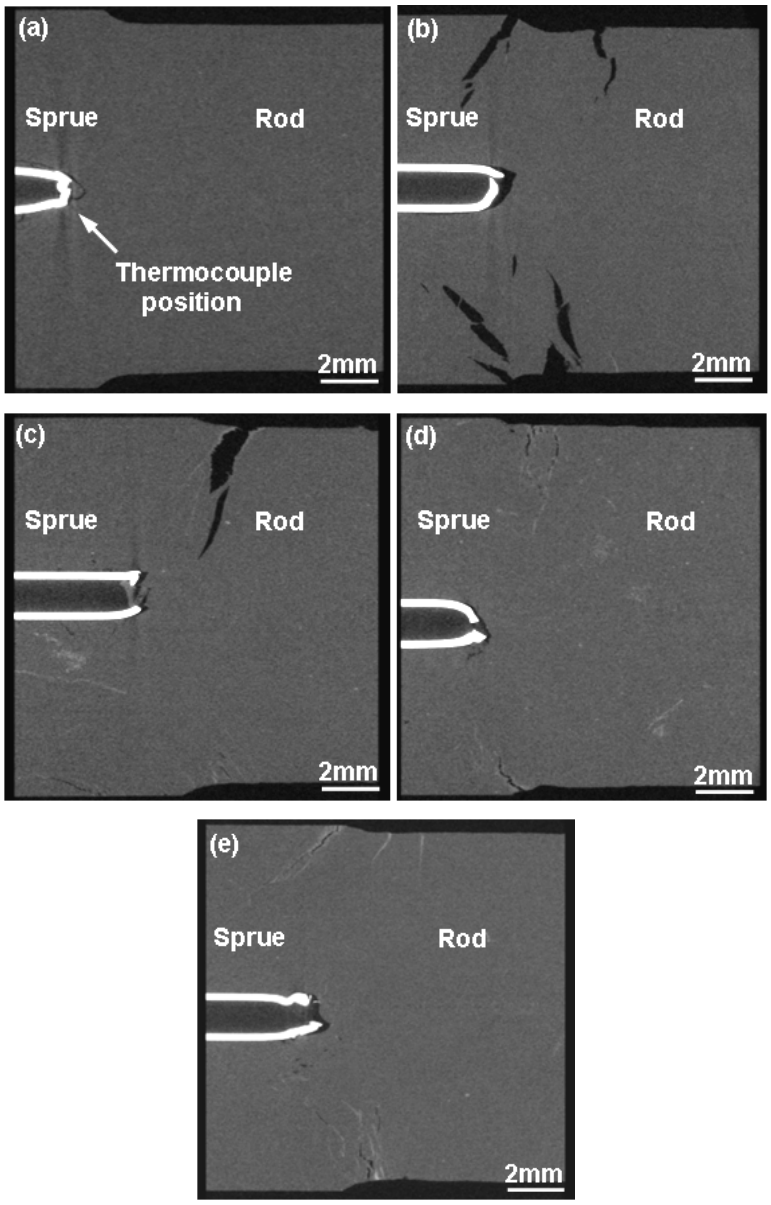

Fig. 5.14 X-ray radiographs of Mg-Y alloys showing crack morphologies at a mould temperature of 250 °C: (a) Mg-0.2Y, (b) Mg-0.9Y, (c) Mg-1.5Y, (d) Mg-2Y, (e) Mg-4Y.

Fig. 5.15 shows the X-ray micro-tomography radiographs of hot cracks for Mg-0.9Y and Mg-1.5Y alloys at a mould temperature of 450 °C. At the higher mould temperature very few and

small volume of cracks are observed. Compared with the results described above the increment in the initial mould temperature decreased the HTS.

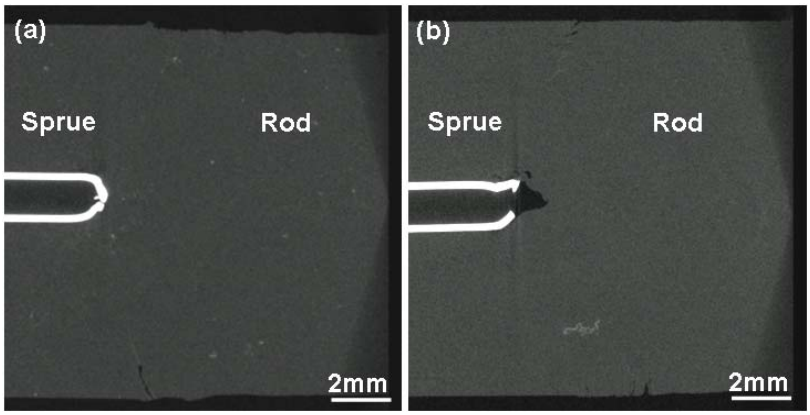

Fig. 5.15 X-ray radiographs of Mg-Y alloys showing crack morphologies at a mould temperature of 450 °C: (a) Mg-0.9Y, (b) Mg-1.5Y.

5.1.2.5 Fracture surfaces

Fig. 5.16 shows the fracture surfaces caused by hot tears in Mg-0.9Y and Mg-1.5Y alloys at a mould temperature of 250 °C. The morphology of the fracture surfaces show the typical features of hot tearing, i.e. inter-dendritic and inter-granular fractures.

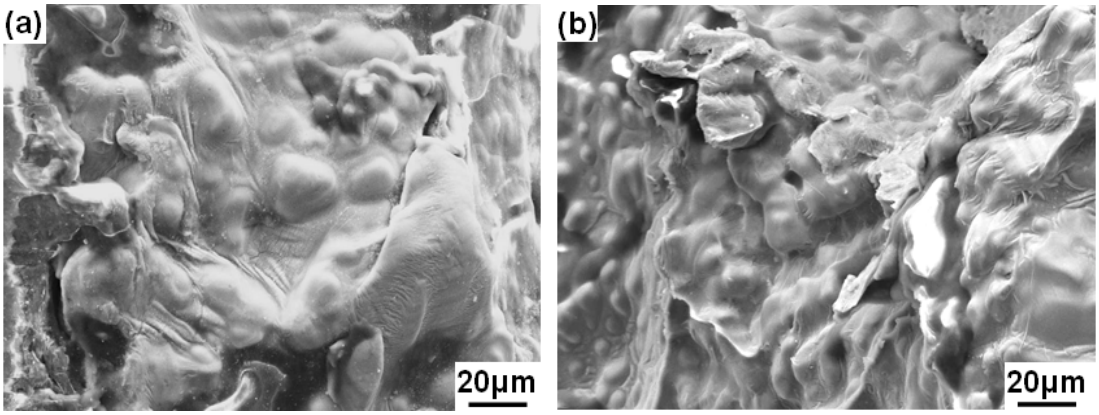

Fig. 5.16 SEM micrographs of hot tear surfaces at a mould temperature of 250 °C: (a) Mg-0.9Y, (b) Mg-1.5Y alloys.

The hot crack surfaces are smooth due to the presence of a liquid film in the inter-dendritic regions. Addition to the smooth surfaces caused by the inter-dendritic separations, the trans-granular fracture regions are also observed. The hot tearing fractures are caused during the

propagation of hot cracks that cut through connected bridges that formed before the initiation of hot tearing. Interestingly, in some areas, shown in Fig. 5.16, a thin layer is observed on the fracture surface with a fluvial pattern. The EDS analysis indicated that these layers are enrich with Y. This demonstrates that the hot tearing is due to the inter-dendritic separation, which occurs when there still exists a liquid layers enrich with solute at the dendrite boundaries.

5.1.2.6 Quantitative measurement of hot tearing

Fig. 5.17 and Fig. 5.18 show the total crack volumes measured by wax penetration and X-ray micro-tomography methods for Mg-Y alloys at two different mould temperatures. The total crack volumes depend on the Y content and the mould temperature. The crack volume increases with the increasing Y content, reaches a maximum at 0.9 wt.% Y and then reduces with further increasing the Y content at both the mould temperatures 250 °C and 450 °C. The maximum volume of hot cracks measured for Mg-0.9Y alloy is about 75.75 mm^3 by the wax penetration method (Fig. 5.17). The results show that the volumes of hot cracks decrease with increase in the initial mould temperature. Compared with the results from X-ray micro-tomography method, the crack volume measured by wax penetration method is larger. The reason for this is that the complete removal of the unwanted wax on the surface is difficult. Although the wax penetration is not as accurate, the results show that the tendency of the HTS with Y content is similar to that observed with X-ray micro-tomography.

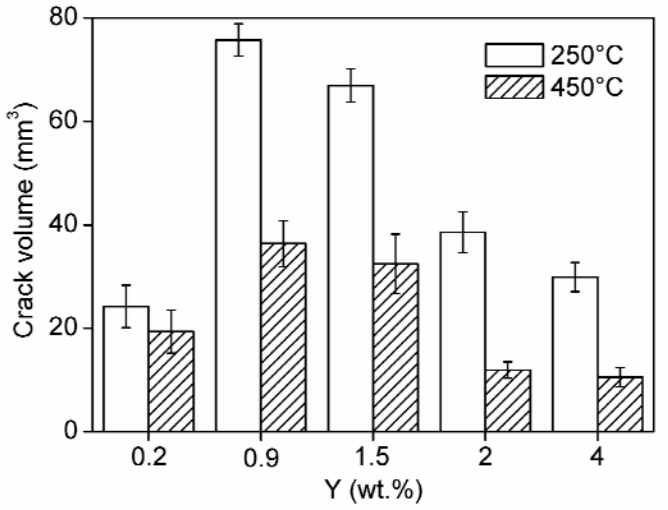

Fig. 5.17 Total crack volumes measured by wax penetration method for binary Mg-Y alloys at different mould temperatures.

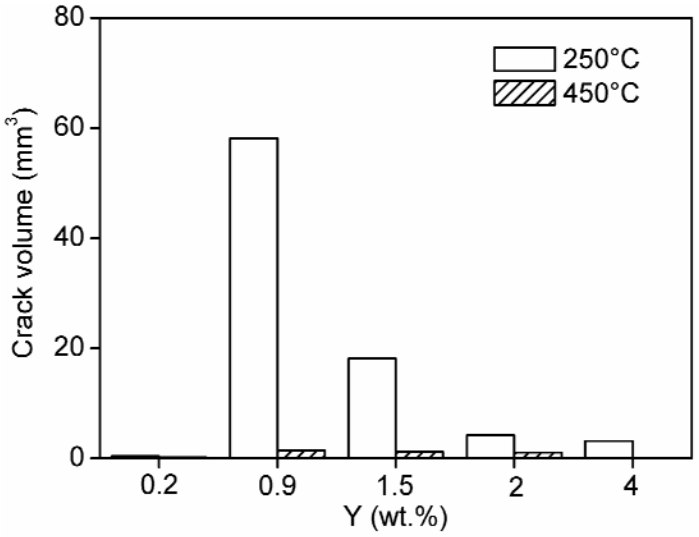

Fig. 5.18 Total crack volumes measured by X-ray micro-tomography method for binary Mg-Y alloys at different mould temperatures.

5.1.3 Numerical simulation of HTS

5.1.3.1 Temperature and solid fraction fields

Fig. 5.19 shows the predicted temperature and solid fraction fields for Mg-1.5Y alloy with an initial mould temperature of 250 °C. The viewed section is a mid-plane slice from the casting in the X-direction. Results are shown: (a) immediately after filling, (b) at a total solid fraction of 0.6, (c) at a total solid fraction of 1, and (d) at the end of the simulation. These results show that over time the casting cools and the solid fraction increases until it reaches to 1. The temperature continues to decrease until the end of the simulation. A relatively large temperature gradient is observed in the casting near the junction between the sprue and the horizontal rod. The temperature at the sprue and the rod are isothermal, but the sprue temperature is consistently higher than that of the rod temperature. These different temperatures at junction between the sprue and rod lead to large thermal contraction forces and the formation of hot tears. Similar results are shown for the Mg-4Y alloy in Fig. 5.20. Due to the shorter freezing range, the Mg-4Y alloy solidifies faster than the Mg-1.5Y alloy. This can be seen clearly by comparing Fig. 5.19 (a) and Fig. 5.20 (a). These figures show that immediately after filling, the rod in the Mg-4Y casting is almost completely solid, while the rod in the Mg-1.5Y casting contains a significant amount of liquid.

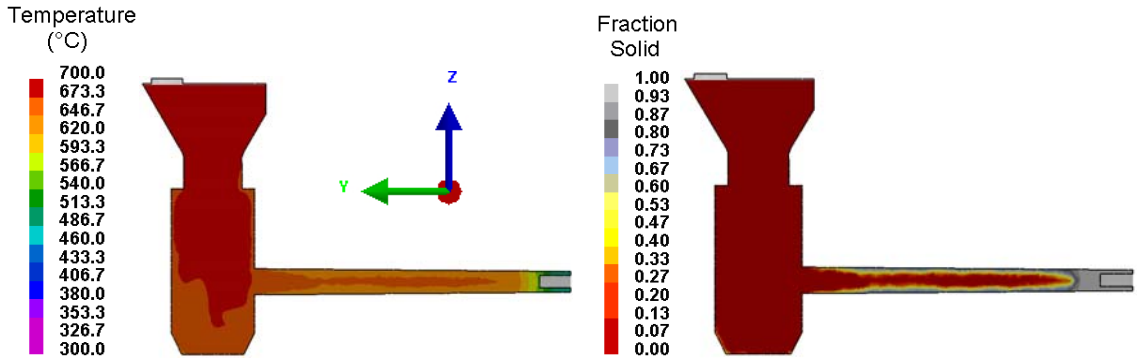

(a) Immediately after filling

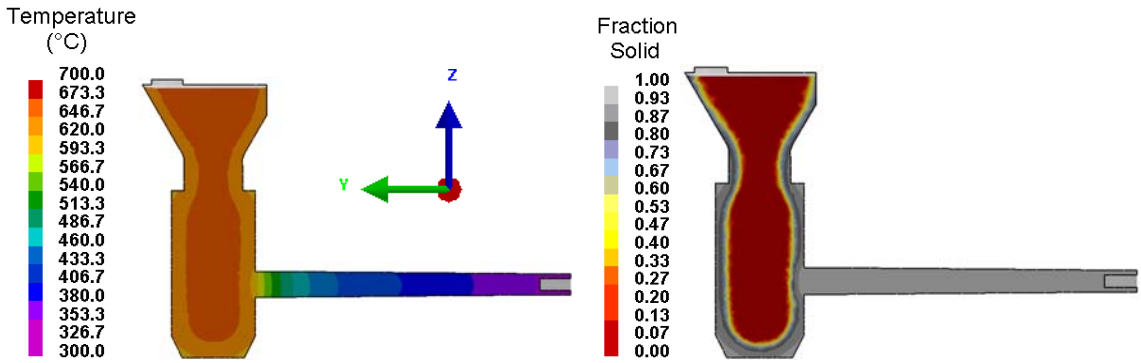

(b) At a total solid fraction of 0.6

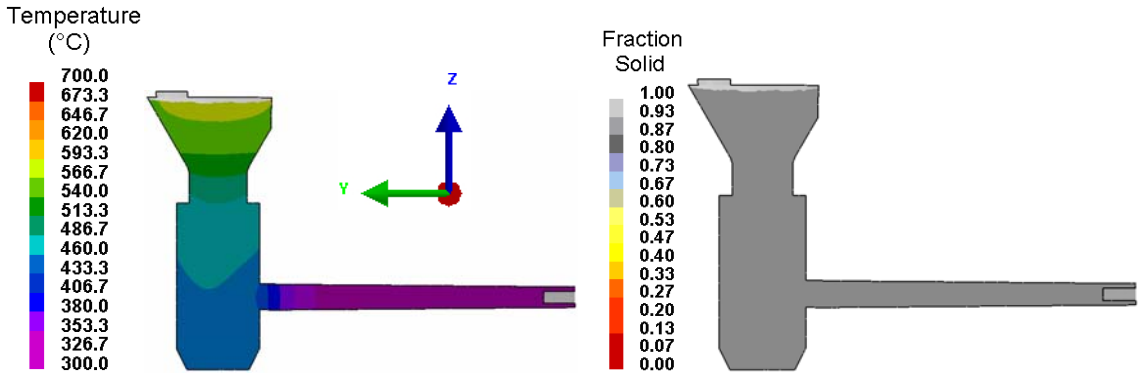

(c) At a total solid fraction of 1

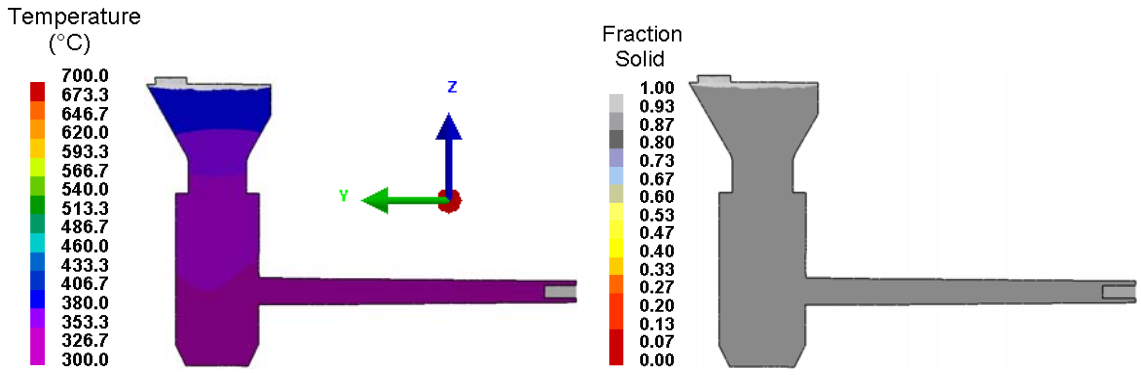

(d) At the end of the simulation

Fig. 5.19 Predicted temperature and solid fraction fields for the Mg-1.5Y alloy with an initial mould temperature of 250 °C.

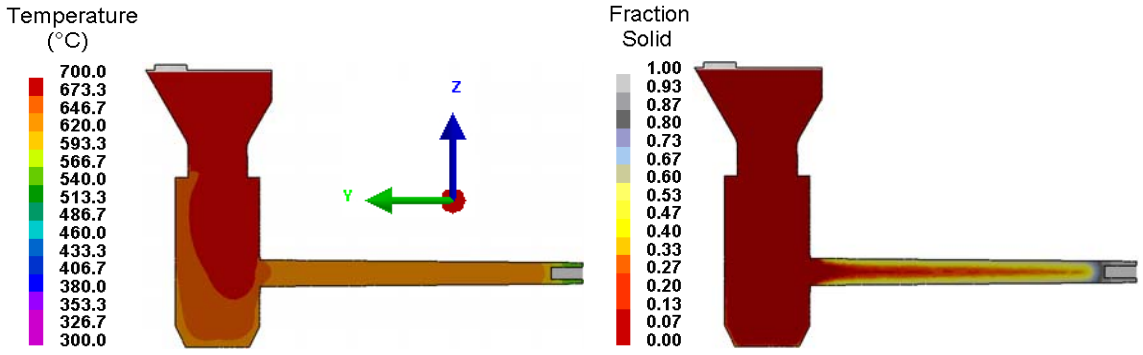

(a) Immediately after filling

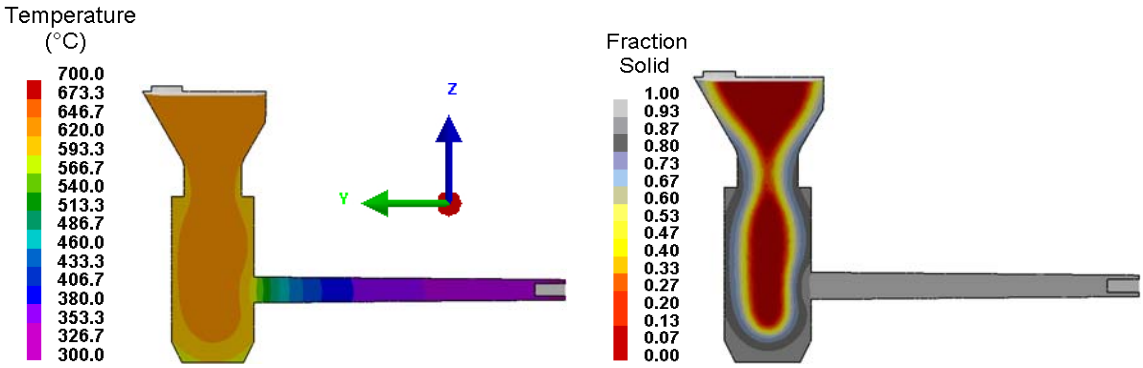

(b) At a total solid fraction of 0.6

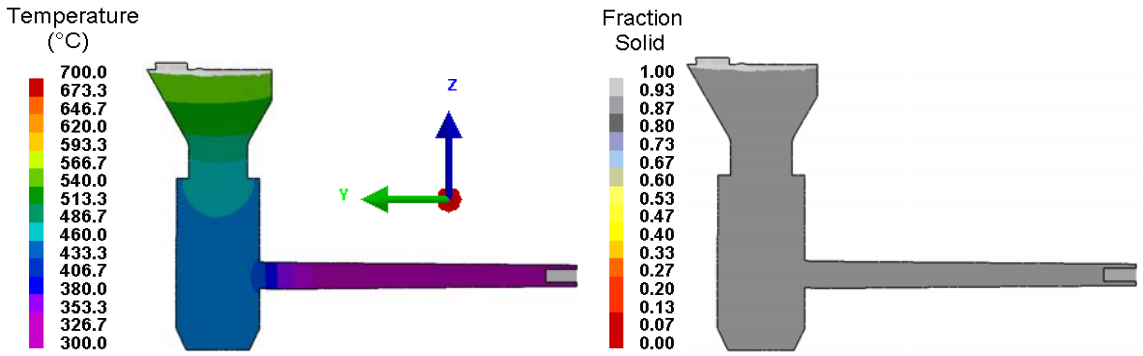

(c) At a total solid fraction of 1

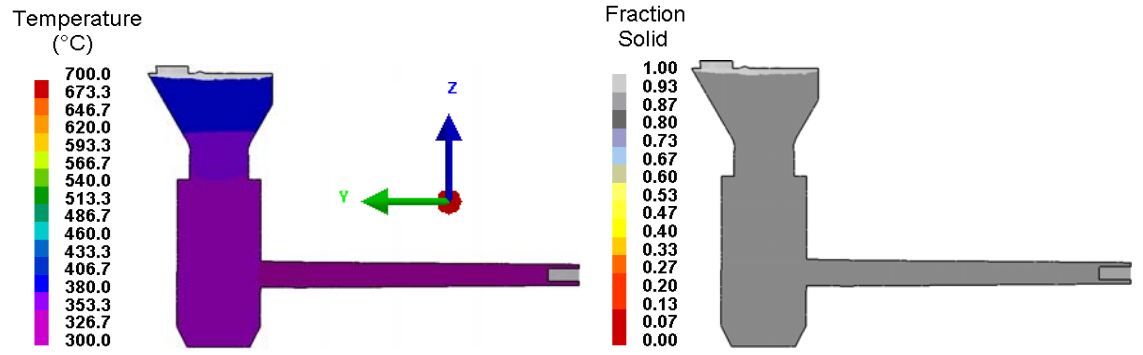

(d) At the end of the simulation

Fig. 5.20 Predicted temperature and solid fraction fields for the Mg-4Y alloy with an initial mould temperature of 250 °C.

5.1.3.2 Hot tearing indicator

Fig. 5.21 shows the comparison between the predicted HTI and experimentally observed cracks on the surfaces of Mg-Y alloys with a mould temperature of 250 °C. The simulations show mid-plane slices of the casting in the X-direction. The observations of cracks indicate that the hot tearing normally occurs at the junction between the sprue and the rod. The predictions HTI exhibit cracks at similar locations to where the hot tears are experimentally observed. The value of HTI at similar locations increases when the Y content increases from 0.2 to 1.5, and then decreases with the further increases in the Y content. The hot tear simulations do not predict the actual crack size or shape. They are simply an indicator for HTS. From the point of view of HTS, the predicted results are in good agreement with the experimental results.

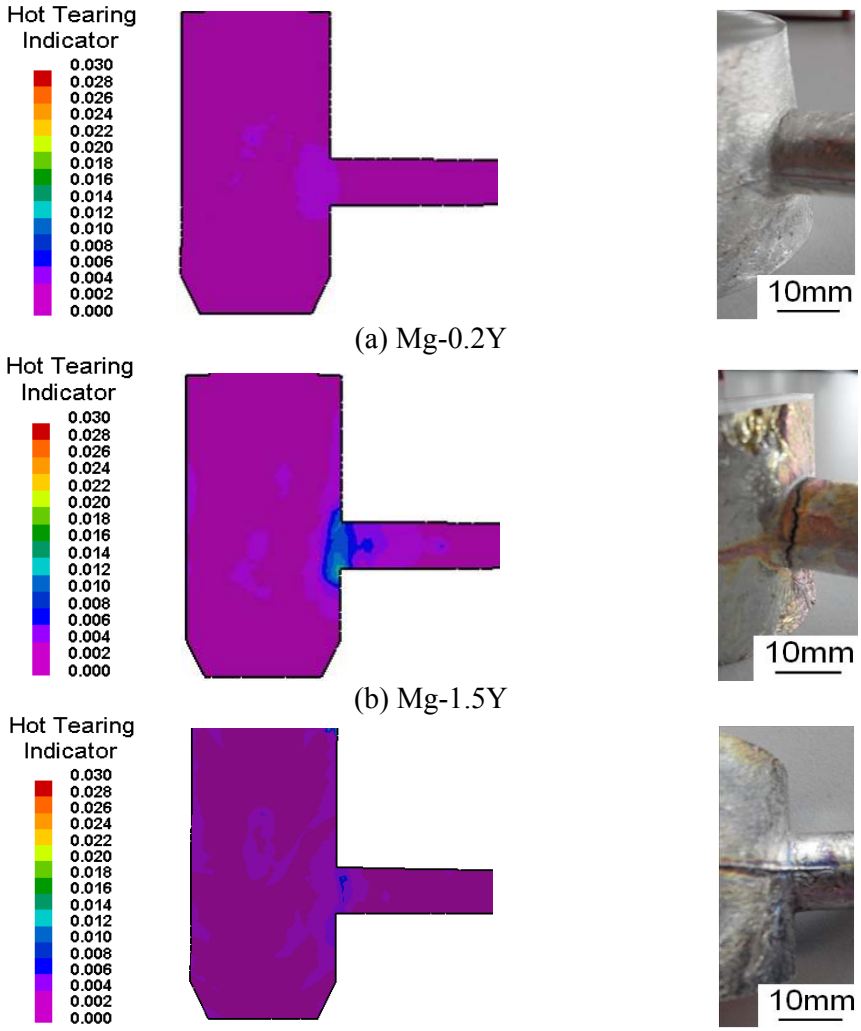

(a) Mg-0.2Y

(b) Mg-1.5Y

(c) Mg-4Y

Fig. 5.21 Comparison between the simulated HTI and experimentally observed cracks on the surfaces of Mg-Y alloys at a mould temperature of 250 °C.

Numerical simulations of hot tearing in Mg-Y castings with an initial mould temperature of 450 °C are shown in Fig. 5.22. Compared with Fig. 5.21, the values of HTI decrease for all castings, indicating that the HTS reduces when the mould temperature increases. Similarly, the simulated HTS values are in agreement with the experimental results.

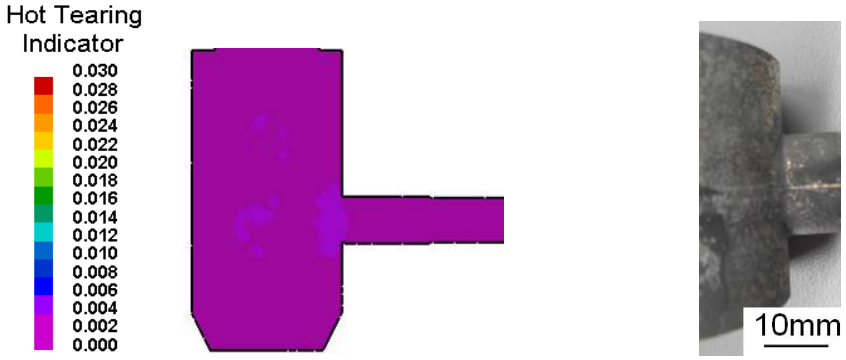

(a) Mg-0.2Y

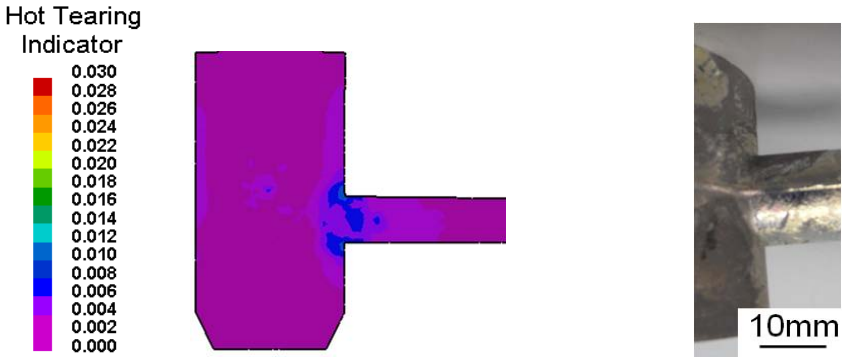

(b) Mg-1.5Y

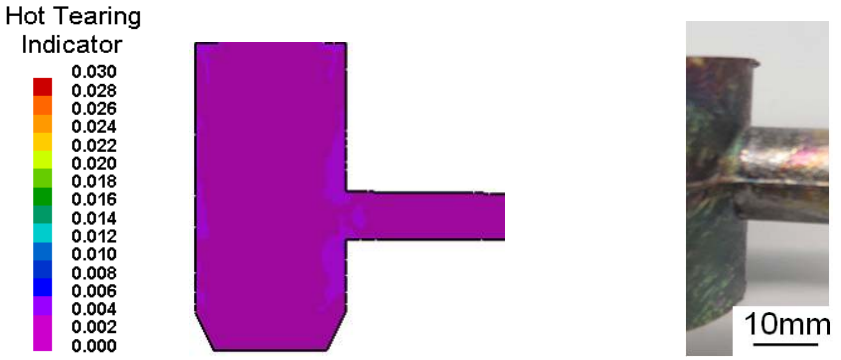

(c) Mg-4Y

Fig. 5.22 Comparison between the HTI and experimentally observed cracks on the surfaces of Mg-Y alloys at a mould temperature of 450 °C.

5.2 Hot tearing behaviour of ternary Mg-4.5Zn-xY alloys

5.2.1 Experiment of hot tearing tendency

5.2.1.1 Chemical compositions

Table 5-3 lists the actual compositions of Mg-4.5Zn-xY alloys. The actual compositions of these alloys are close to their nominal contents.

Table 5-3 Actual chemical compositions of experimental alloys (wt.%)

Alloy	Zn	Y	Zr	Mn	Si	Fe	Mg
Mg-4.5Zn	4.48	—	—	0.012	0.010	0.001	Bal.
Mg-4.5Zn-0.4Y	4.60	0.32	—	0.017	0.001	0.001	Bal.
Mg-4.5Zn-0.9Y	4.65	0.90	—	0.022	0.001	0.001	Bal.
Mg-4.5Zn-2Y	4.56	1.98	—	0.020	0.006	0.002	Bal.
Mg-4.5Zn-0.4Y-0.5Zr	4.52	0.50	0.23	0.019	0.003	0.002	Bal.

5.2.1.2 Hot tearing curves

Fig. 5.23 shows the experimental hot tearing curves of Mg-4.5Zn-xY alloys with different Y contents at a mould temperature of 250 °C. The contraction force curve of Mg-4.5Zn alloy has two peaks (Fig. 5.23 (a)). The first hot tearing initiates at a temperature of 572 °C, which corresponds to a solid fraction of 0.839. The second initiates at 473 °C, which corresponds to a solid fraction of 0.928. On both the hot tearing curves of Mg-4.5Zn-0.4Y and Mg-4.5Zn-0.9Y alloys, the contraction forces drop very sharply once the hot cracks form. For Mg-4.5Zn-0.4Y alloy (Fig. 5.23 (b)), the hot cracks initiate at 606 °C, which corresponds to a solid fraction of 0.706. After the formation of hot tearing the force monotonously reduces until the end of solidification, indicating that the casting fractured completely during the solidification. When the Y content increase to 0.9 wt.%, the hot tearing occurs at a temperature of 618 °C (Fig. 5.23 (c)), which corresponds to a solid fraction of 0.568. A large amount of liquid remains and the formed dendritic network is not in dense contact with each other. The liquid still has a chance to flow into the cracks and repair them. However, the force drops significantly, but becomes stable at the later stages of solidification. These phenomena demonstrate that casting is also fractured completely. When the Y content reaches to 2 wt.%, two peaks are again observed on the force curve. The force drop is relatively small after the

initiation of hot tearing and subsequently increases. The hot cracks initiate at 576 and 489 °C which correspond to solid fractions of 0.928 and 0.956, respectively.

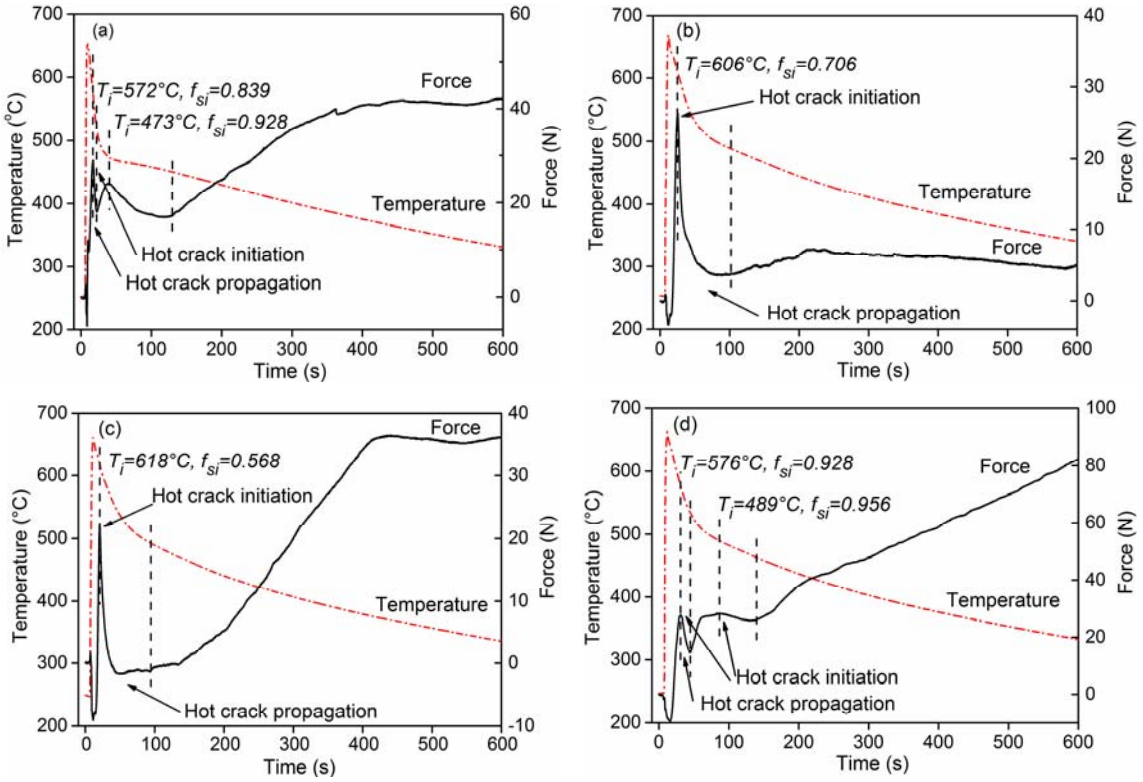

Fig. 5.23 Contraction force and temperature as a function of time for Mg-4.5Zn-xY alloys at a mould temperature of 250 °C: (a) x=0, (b) x=0.4, (c) x=0.9, (d) x=2.

The contraction force curves of Mg-4.5Zn-xY alloys recorded at a mould temperature of 450°C are shown in Fig. 5.24. Compared with Fig. 5.23, the force drops are not so apparent indicating that at the high mould temperature the alloys have a lower susceptibility to hot crack. The curves of Mg-4.5Zn and Mg-4.5Zn-2Y alloys show no drop in the contraction force meaning no crack initiation (Fig. 5.24 (a) and (d)). In contrast, Mg-4.5Zn-0.4Y and Mg-4.5Zn-0.9Y alloys have a small drop in force, indicating that some small cracks may form (Fig. 5.24 (b) and (c)). On both the hot tearing curves of both Mg-4.5Zn-0.4Y and Mg-4.5Zn-0.9Y alloys, the hot cracks initiate at relatively high temperatures, which correspond to low solid fractions of 0.413 and 0.372, respectively. The hot cracks are occurring at a little distance from the sprue-rod junction. As indicated in Fig. 2.7(c), the thermocouple locates at the centre line of the sprue-rod junction. Thus, the measured temperature is not the exact temperature at the location where the hot tearing initiates. Correspondingly, the calculated

solid fractions are not the critical value at which the hot tearing occurs, but an indication of approximate solid fraction.

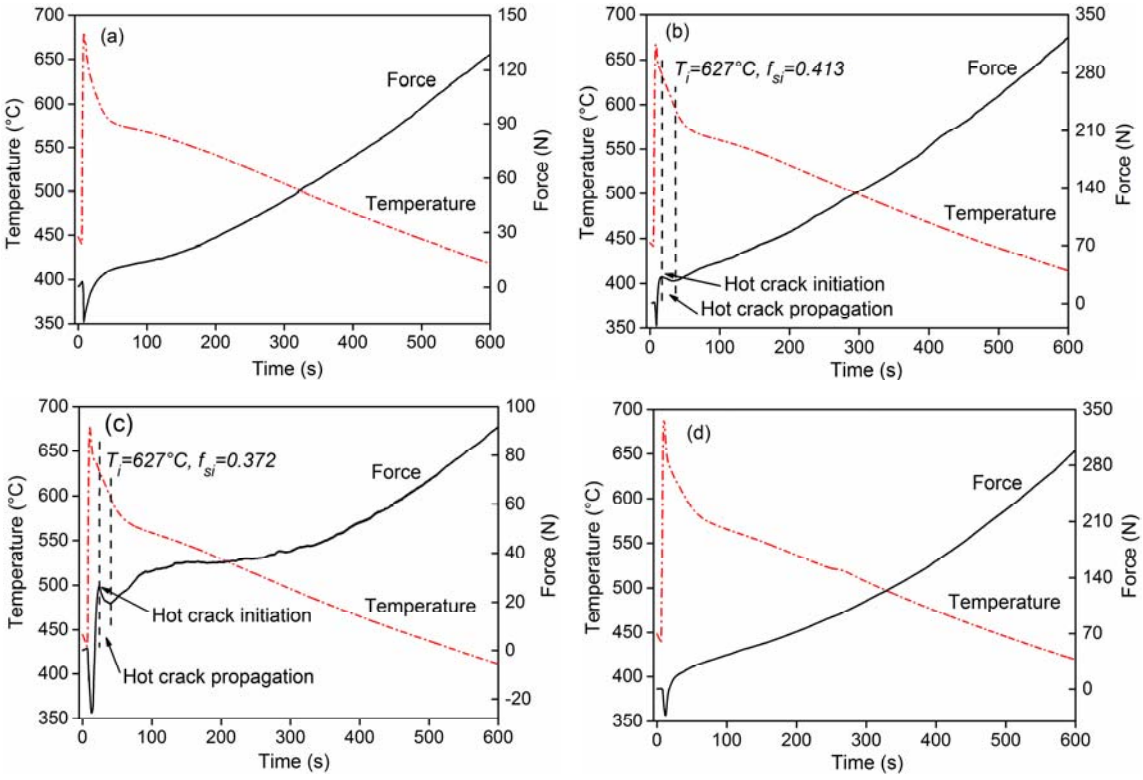

Fig. 5.24 Contraction force and temperature as a function of time for Mg-4.5Zn-xY alloys at a mould temperature of 450 ^{o}C: (a) x=0, (b) x=0.4, (c) x=0.9, (d) x=2.

In addition to the information on hot tearing initiation, information on the propagation of hot cracks can also be obtained by analyzing the experimental curves. The stage during force drop is regarded as the propagation of hot cracks. It is marked in Fig. 5.23 and Fig. 5.24 with two dashed lines. Information on the initiation and propagation of hot tearing in Mg-4.5Zn-xY alloys at different initial mould temperatures is summarized in Table 5-4. Information such as the force release (F_r) and the force release rate (V_p) can be determined. Both the initiation and propagation of hot cracks are closely related to the contraction force. The investigations on the force release rate are therefore important.

For Mg-4.5Zn-0.4Y and Mg-4.5Zn-0.9Y alloys at a mould temperature of 250 °C, the force release rates are 0.50 and 0.86 N/s, respectively. Due to the complete nature of cracks, the force drop is very large (Fig. 5.23 (b) and (c)). For Mg-4.5Zn and Mg-4.5Zn-2Y alloys at a mould temperature of 250 °C, the second hot crack propagation is chosen to calculate the

force release rate. The values are 0.21 and 0.05 N/s for Mg-4.5Zn and Mg-4.5Zn-2Y alloys, respectively. When increasing the mould temperature to 450 °C, Mg-4.5Zn and Mg-4.5Zn-2Y alloys have no apparent hot cracks. At the higher mould temperature, Mg-4.5Zn-0.4Y and Mg-4.5Zn-0.9Y alloys show very small hot crack force release rates (only 0.17 and 0.43 N/s) than that at the lower mould temperature. Generally, the higher force release rate leads to more serious cracking.

Table 5-4 Information about hot tearing initiation and propagation for Mg-4.5Zn-xY alloys at different mould temperatures.

Alloys (wt.%)	Hot crack initiation		Termination of hot crack propagation		Hot crack propagation		
	T_i (°C)	f_{si}	T_f (°C)	f_{sf}	F_r (N)	t_p (s)	V_p (N/s)
Mg-4.5Zn (250°C)	572	0.839	451	0.935	4.9	23.1	0.21
Mg-4.5Zn (450°C)	No crack						
Mg-4.5Zn-0.4Y (250°C)	606	0.706	488	0.940	22.4	45.2	0.50
Mg-4.5Zn-0.4Y (450°C)	627	0.431	589	0.804	4.4	25.2	0.17
Mg-4.5Zn-0.9Y (250°C)	618	0.568	492	0.955	24.0	28.0	0.86
Mg-4.5Zn-0.9Y (450°C)	627	0.372	596	0.749	7.0	16.3	0.43
Mg-4.5Zn-2Y (250°C)	576	0.928	463	0.980	2.3	45.3	0.05
Mg-4.5Zn-2Y (450°C)	No crack						

T_i : crack initiation temperature, f_{si} : solid fraction at which the cracks initiate, T_f : temperature at which the crack does not propagate any more, f_{sf} : solid fraction at which the propagation of cracks stops, F_r : force release, t_p : propagation time, V_p : force release rate, which is proportional to the crack propagation rate.

5.2.1.3 Macro-structural observations

The macrostructures of hot cracks for Mg-4.5Zn-xY alloy castings are shown in Table 5-5. The alloy compositions and mould temperatures have significant effect on the HTS. At a mould temperature of 250 °C, the regions near the junctions of Mg-4.5Zn-0.4Y and Mg-4.5Zn-0.9Y alloys fracture completely. In contrast, Mg-4.5Zn and Mg-4.5Zn-2Y alloys have a relative smaller crack. When increasing the mould temperature, the size and amount of macro-cracks reduce. As aforementioned, due to the different cooling rates and heat transfer conditions, the hot cracks occur at little distance from the sprue-rod junction at a mould temperature of 450 °C.

Table 5-5 Macro-graphs of hot cracks for Mg-4.5Zn-xY alloys at different mould temperatures

Mould temperature	Mg-4.5Zn	Mg-4.5Zn-0.4Y	Mg-4.5Zn-0.9Y	Mg-4.5Zn-2Y
250 °C				
450 °C		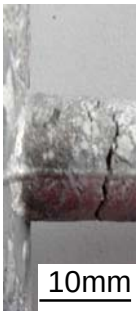		

5.2.1.4 Microstructual observations

Two main factors that influence the formation of hot tearing are the grain size and the grain morphology [62]. Fig. 5.25 and Fig. 5.26 show the polarized optical micrographs of the regions near the sprue-rod junction of the investigated alloys at a mould temperature of 250°C and 450 °C, respectively.

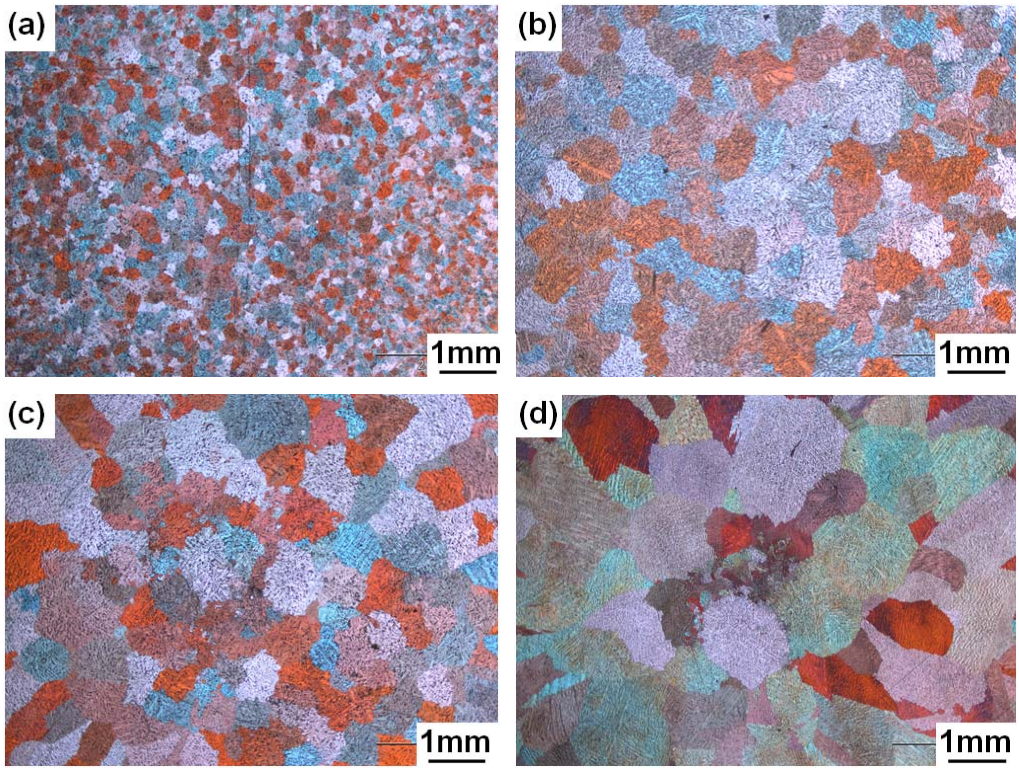

Fig. 5.25 Optical microstructures of Mg-4.5Zn-xY alloys at a mould temperature of 250 °C: (a) x=0, (b) x=0.4, (c) x=0.9, (d) x=2.

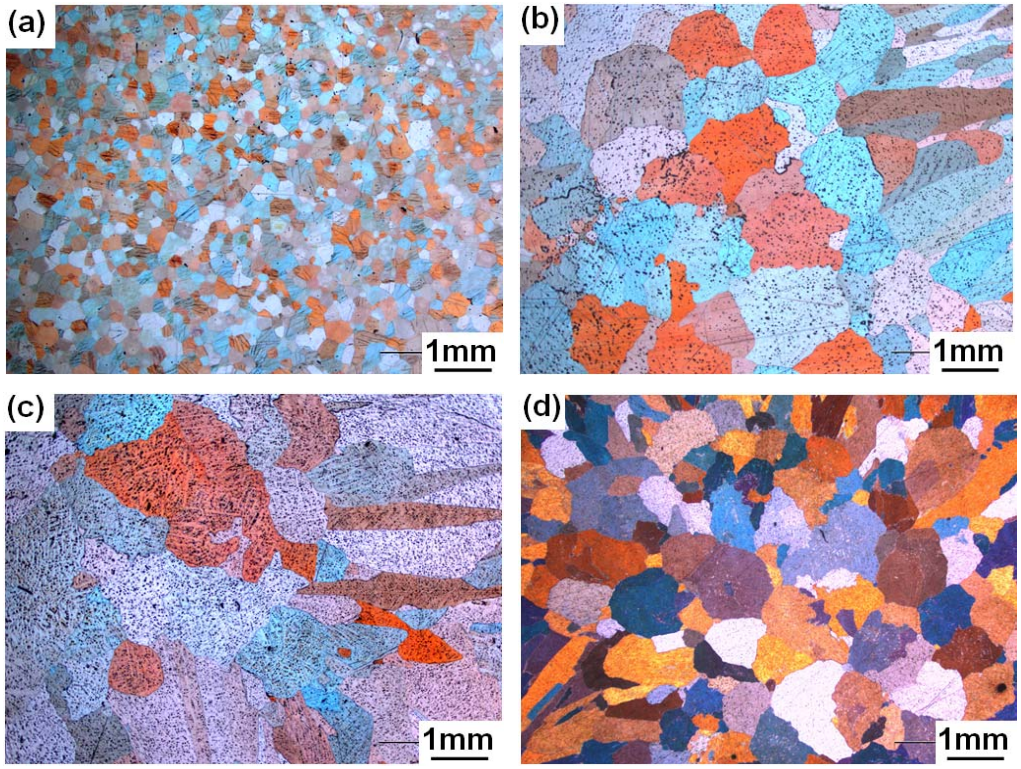

Fig. 5.26 Optical microstructures of Mg-4.5Zn-xY alloys at a mould temperature of 450 °C: (a) x=0, (b) x=0.4, (c) x=0.9, (d) x=2.

The Mg-4.5Zn alloy has smallest grain size among all investigated alloys at both the mould temperatures of 250 and 450 °C. With the addition of Y the grain size increases and continues to increase with increased Y content. At a mould temperature of 250 °C, the equiaxed grains dominate in the Mg-4.5Zn-xY alloys. This may be caused by the higher cooling rate. At a mould temperature of 450 °C, the microstructures of Mg-4.5Zn-0.4Y and Mg-4.5Zn-0.9Y alloys contain some coarse elongated columnar grains as the cooling rate decreases. The grain size of Mg-4.5Zn and Mg-4.5Zn-2Y alloys do not change at high mould temperature if compared with that a mould temperature of 250 °C.

Fig. 5.27 shows SEM microstructures of hot cracks in the regions near the sprue-rod junctions on the longitudinal surfaces at a mould temperature of 250 °C. The top of the image shows the fracture surface of hot tears. On the longitudinal sections, the regions with white contrast can be seen in Fig. 5.27 (b). These white river patterns are arrays of second phases. It is interesting to notice that many particles present around and in front of these patterns. These white patterns are evidence that the pre-existing cracks were refilled by the remaining liquid. The remains liquid in the later stage of solidification contains high content of solute. As a result, after solidification the regions where the hot cracks were refilled had a large amount of particles. In fact, this phenomenon demonstrates that the previously formed hot cracks can be healed by the inter-granular feeding at the later stages of solidification. With increasing the Y content the amount of white river pattern like structure increases.

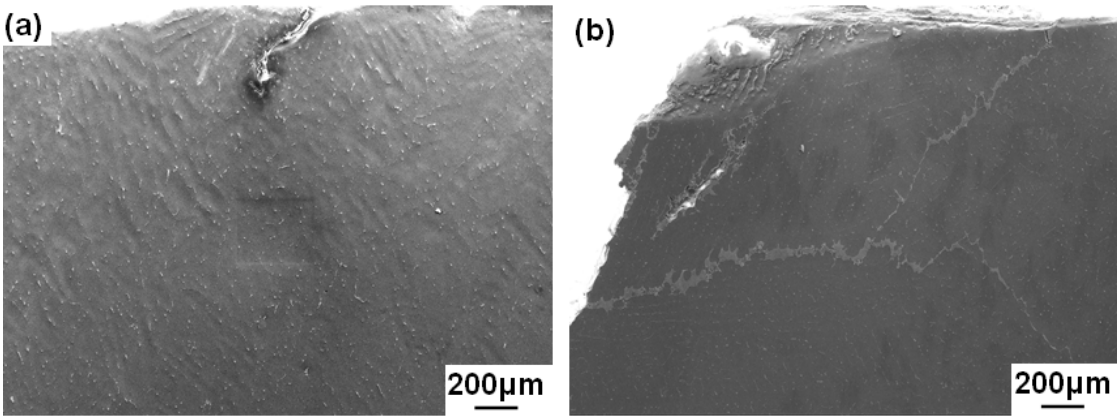

Fig. 5.27 SEM micrographs showing the cracks in the regions near the sprue-rod junction at a mould temperature of 250 °C: (a) Mg-4.5Zn-0.9Y, (b) Mg-4.5Zn-2Y.

5.2.1.5 Fracture surfaces of hot tearing

Fig. 5.28 shows the fracture surfaces of hot crack regions for Mg-4.5Zn-0.4Y and Mg-4.5Zn-0.9Y alloys at different mould temperatures. There are differences in the hot crack morphologies between at low and high mould temperatures. At the low mould temperature 250 °C, the surface of the hot crack is quite smooth, with dendrite-like bumps on the fracture surface. These characteristics of fracture surface indicate that the formation of hot tears was caused by an inter-dendritic separation within the mushy zone. With the increase in the mould temperature, the fracture surface is smooth and flattened, and the dendrite-like surface bumps disappear. As shown in Fig. 5.16, some tearing ridges were also observed on this fracture surface, indicating that a number of inter-dendritic bridging connections existed before the crack propagation. These connections improve the resistance to hot tearing.

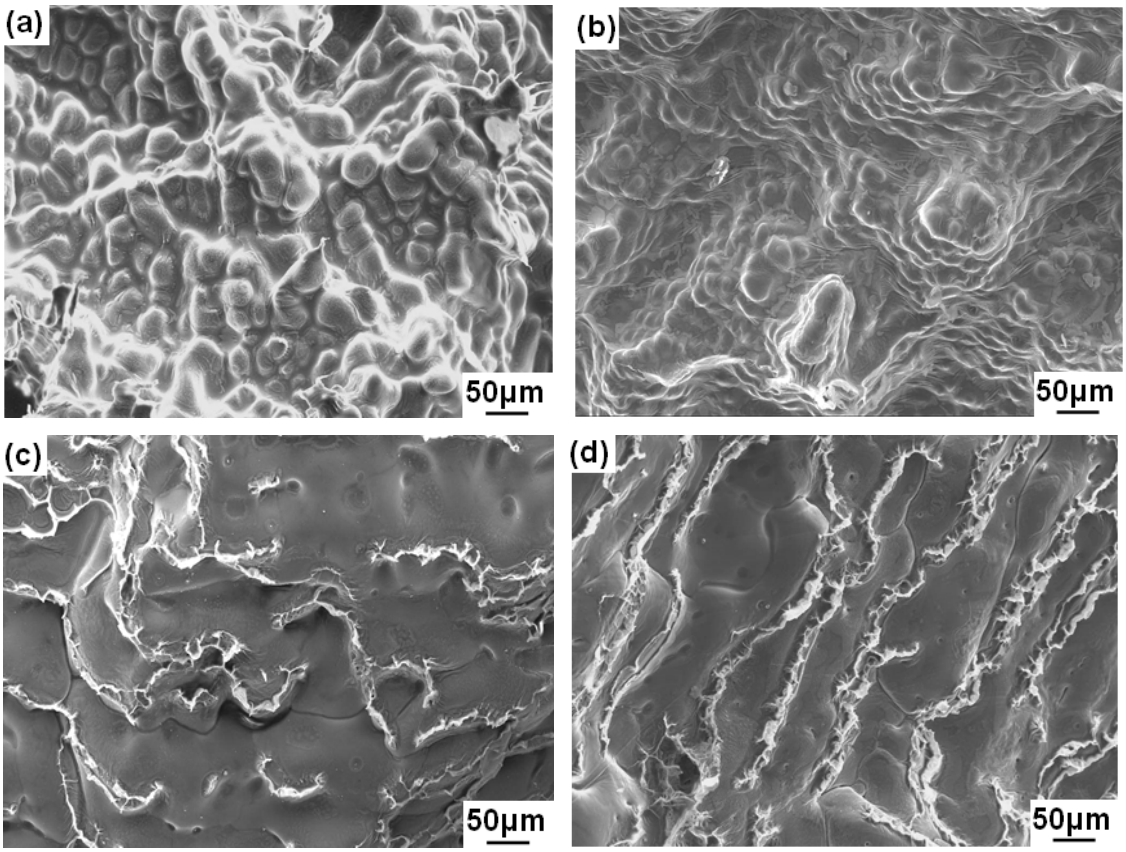

Fig. 5.28 Fracture surfaces of hot tearing for Mg-4.5Zn-xY alloys at different mould temperatures: (a) Mg-4.5Zn-0.4Y, T_{mould}=250 °C, (b) Mg-4.5Zn-0.9Y, T_{mould}=250 °C, (c) Mg-4.5Zn-0.4Y, T_{mould}=450 °C, (d) Mg-4.5Zn-0.9Y, T_{mould}=450 °C.

5.2.1.6 Quantitative measurement of hot tearing

Fig. 5.29 shows the influence of different Y content on the total crack volume of Mg-4.5Zn-xY alloys at different initial mould temperatures determined with wax penetration method. The total crack volume depends on the Y content and the initial mould temperature. The crack volume increased with the increased Y content, such as Mg-4.5Zn-0.4Y and Mg-4.5Zn-0.9Y alloys. After the Y content is above 0.9 wt.%, the crack volume decreases at both mould temperatures. At the lower mould temperature of 250 °C, the crack volume of Mg-4.5Zn alloy is 182.5mm^3. The castings of 0.4 and 0.9 wt.% Y containing alloys fracture completely. So, the top of the histogram is indicated by a dashed line. Mg-4.5Zn-2Y alloy has the lowest crack volume from alloys investigated. With increase in the mould temperature from 250 to 450 °C, the hot tearing resistances improve.

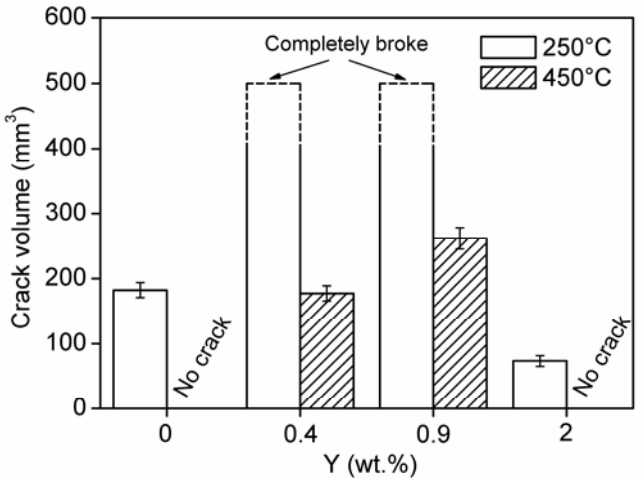

Fig. 5.29 Total crack volumes measured with wax penetration method for Mg-4.5Zn-xY alloys at different mould temperatures.

5.2.1.7 Influence of Zr addition on HTS

Fig. 5.30 shows the microstructures and macrostructures of Mg-4.5Zn-0.4Y and Mg-4.5Zn-0.4Y-0.5Zr at a mould temperature of 450 °C. The grain size decreases significantly with the addition Zr. In the Zr-containing alloy, equiaxed grains are dominant. The grain size measured using the linear intercept method and shown a reduction from 433 to 68 µm between Zr free and Zr containing Mg-4.5Zn-0.4Y alloys, respectively.

At an initial mould temperature of 450 °C, no cracks were observed on the surface of Zr-containing alloy. In contrast, some cracks were detected on the surface of Mg-4.5Zn-0.4Y

alloy. Based on all these results, the addition of Zr improves the resistance to hot tearing through microstructural refinement. It is easier an alloy with finer grain size to accommodate local strains without formation of defects. Grain size affects the mode of eutectic phase distribution. When alloy has a finer grain size, the eutectic is present at the grain boundaries permits free movement of the grains to accommodate the contractions during solidification. Consequently, HTS is reduced.

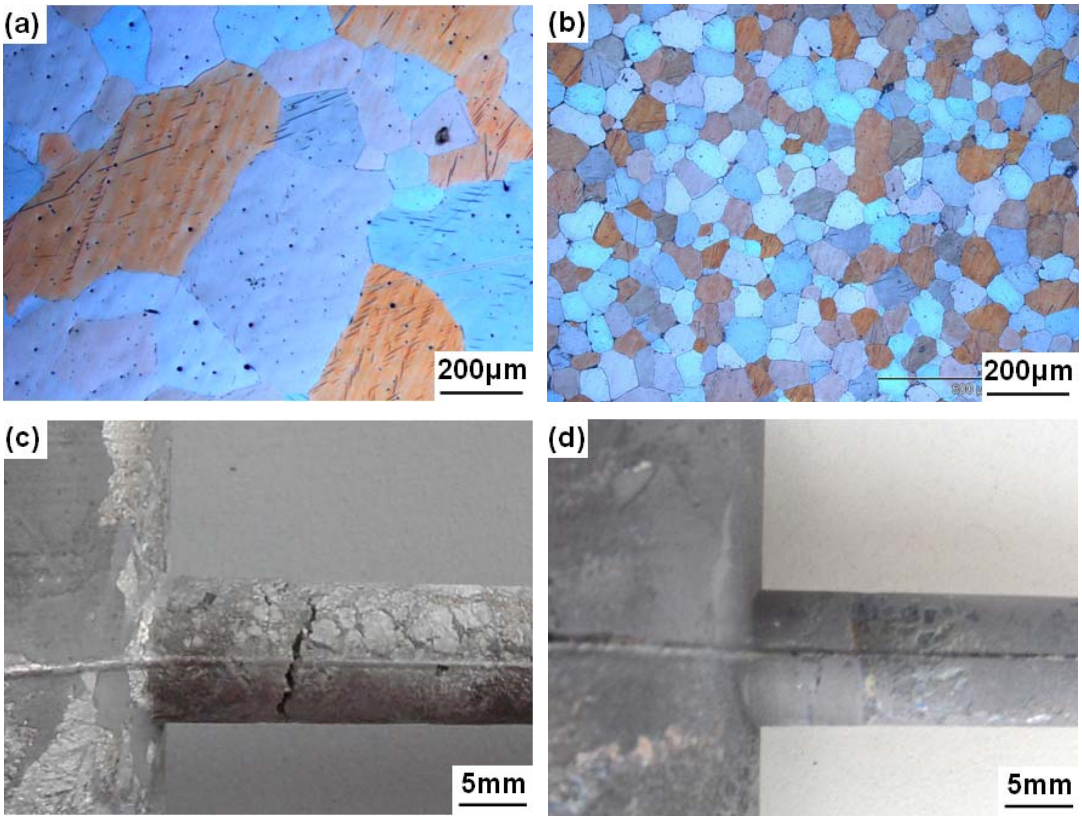

Fig. 5.30 Optical micrographs and macrographs of Mg-4.5Zn-0.4Y and Mg-4.5Zn-0.4Y-0.5Zr alloys at a mould temperature of 450 °C: (a) Mg-4.5Zn-0.4Y (OM), (b) Mg-4.5Zn-0.4Y-0.5Zr (OM), (c) Mg-4.5Zn-0.4Y (macrograph), (d) Mg-4.5Zn-0.4Y-0.5Zr (macrograph).

5.2.2 Numerical simulation of HTS

The HTI of the ternary alloys were simulated with the ProCAST software (Fig. 5.31). The HTI simulations are compared with the experimental results for Mg-4.5Zn-xY alloys at a mould temperature of 250 °C. HTI simulations agree with the experimental results. The maximum value of HTI increases with the Y content, and reaches a maximum at 0.9 wt.% Y, and then it decreases with further increase in the Y content.

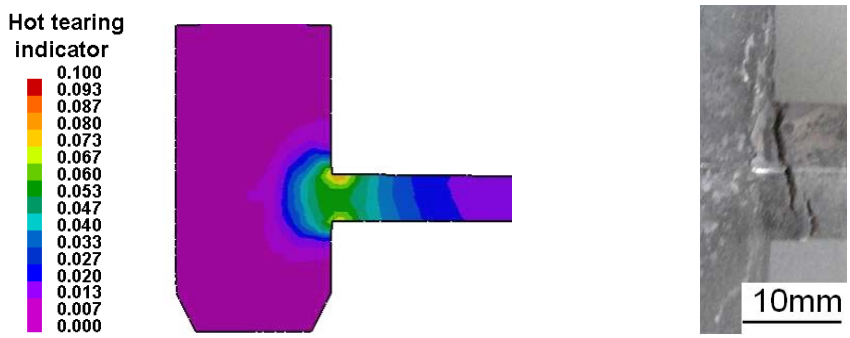

(a) Mg-4.5Zn alloy

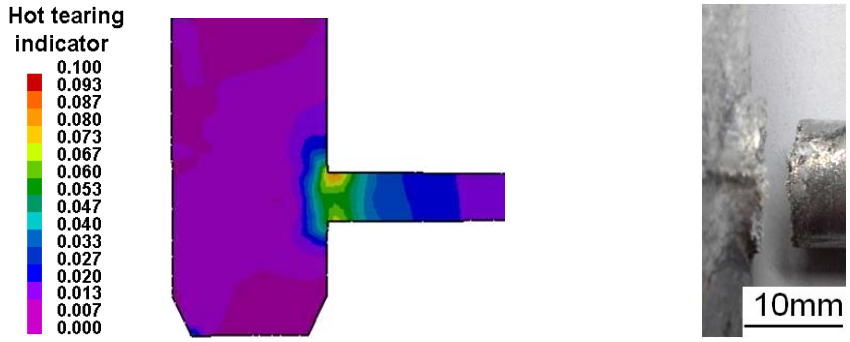

(b) Mg-4.5Zn-0.4Y alloy

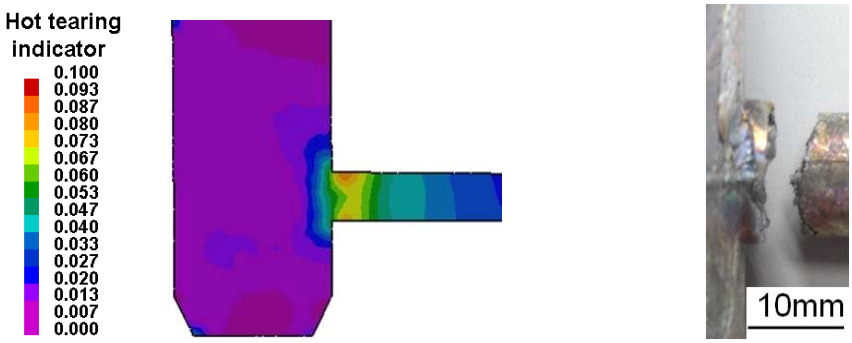

(c) Mg-4.5Zn-0.9Y alloy

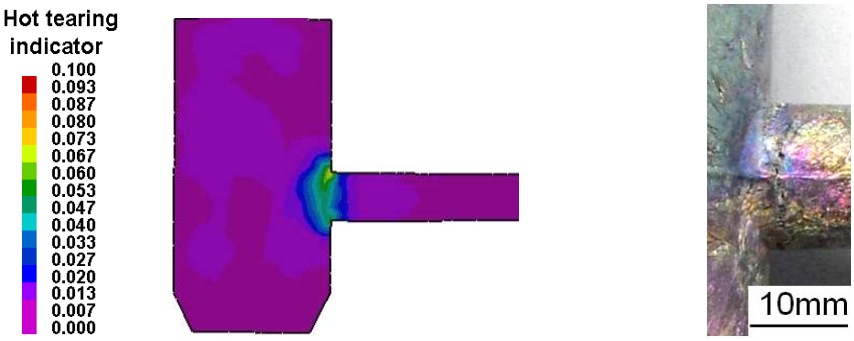

(d) Mg-4.5Zn-2Y alloy

Fig. 5.31 Comparison between the results of HTI and experimental observations for Mg-4.5Zn-xY alloys at a mould temperature of 250 °C.

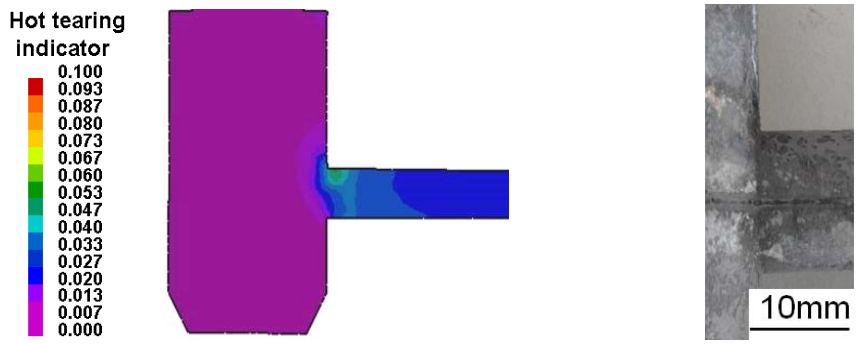

(a) Mg-4.5Zn alloy

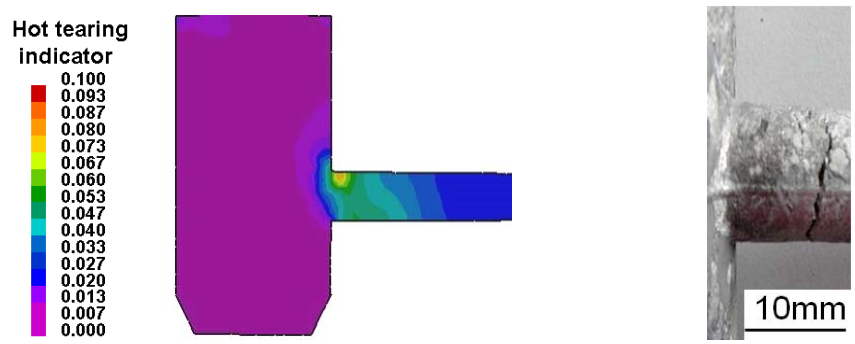

(b) Mg-4.5Zn-0.4Y alloy

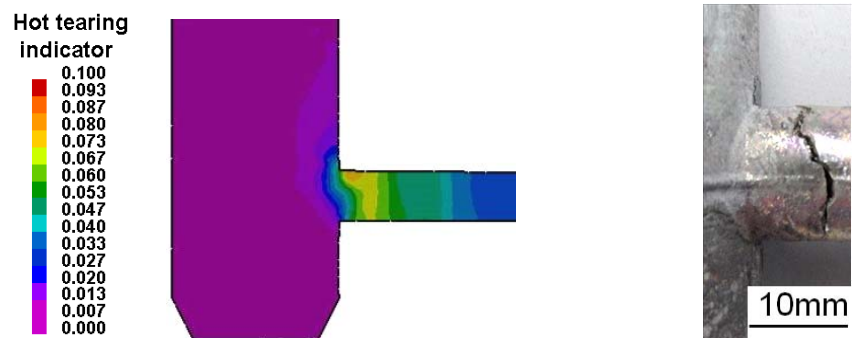

(c) Mg-4.5Zn-0.9Y alloy

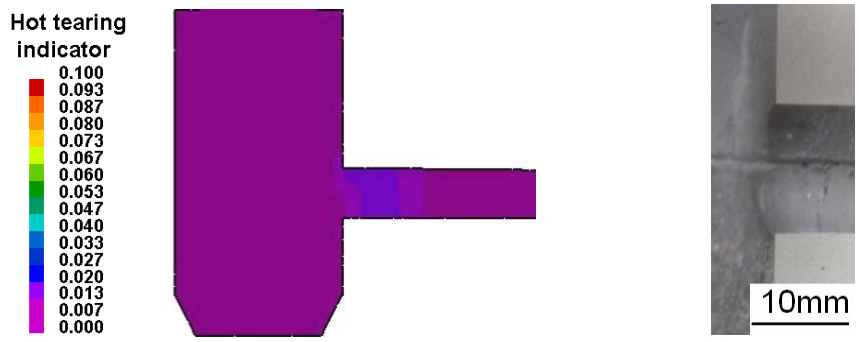

(d) Mg-4.5Zn-2Y alloy

Fig. 5.32 Comparison between the results of HTI and experimental observations for Mg-4.5Zn-xY alloys at a mould temperature of 450 °C.

Comparison between the HTI simulations and experimental observations for Mg-4.5Zn-xY alloys at a mould temperature of 450 °C are shown in Fig. 5.32. A good agreement is obtained between the numerical simulations and experimental results at a mould temperature of 450 °C. The value of HTI increases with the Y content, reach to a maximum at 0.9 wt.% Y and then decreases with further increase in the Y content. Compared to the HTI values determined for a lower initial mould temperature of 250 °C, the HTI values are lower at the higher mould temperature of 450 °C.

5.3 Hot tearing of other ternary Mg-Y-Zn alloys

5.3.1 Hot tearing of Mg-1.5Zn-xY alloys

5.3.1.1 Chemical compositions

Table 5-6 lists the actual compositions of Mg-1.5Zn-xY alloys. It is close to the nominal compositions.

Table 5-6 Actual chemical compositions of experimental alloys (wt.%)

Alloy	Zn	Y	Mn	Si	Fe	Mg
Mg-1.5Zn-0.2Y	1.49	0.22	0.039	0.021	0.003	Bal.
Mg-1.5Zn-2Y	1.68	1.50	0.041	0.006	0.001	Bal.
Mg-1.5Zn-3Y	1.20	2.87	0.036	0.003	0.001	Bal.

5.3.1.2 Hot tearing curves

Fig. 5.33 shows the experimental curves of Mg-1.5Zn-xY alloys with different Y contents. The hot tearing initiation temperatures are dependent on the Y content. For Mg-1.5Zn-0.2Y alloy, the hot cracks initiate at 638 °C, which corresponds to a solid fraction of 0.634 (Fig. 5.33 (a)). The hot cracks in Mg-1.5Zn-2Y alloy initiate at 618 °C, at which the solid fraction is 0.790 (Fig. 5.33 (b)). The hot tearing curves of both Mg-1.5Zn-0.2Y and Mg-1.5Zn-2Y alloys, show sharp force drops once the hot cracks. Generally, the sharper the force drop, the larger the crack size of the samples investigated. Unlike aforementioned two alloys, a sharply drop in the force curves not observed at the beginning of the solidification for Mg-1.5Zn-3Y alloy. The initiation temperature for hot tearing in this alloy is 621 °C, which corresponds to a solid fraction of 0.706.

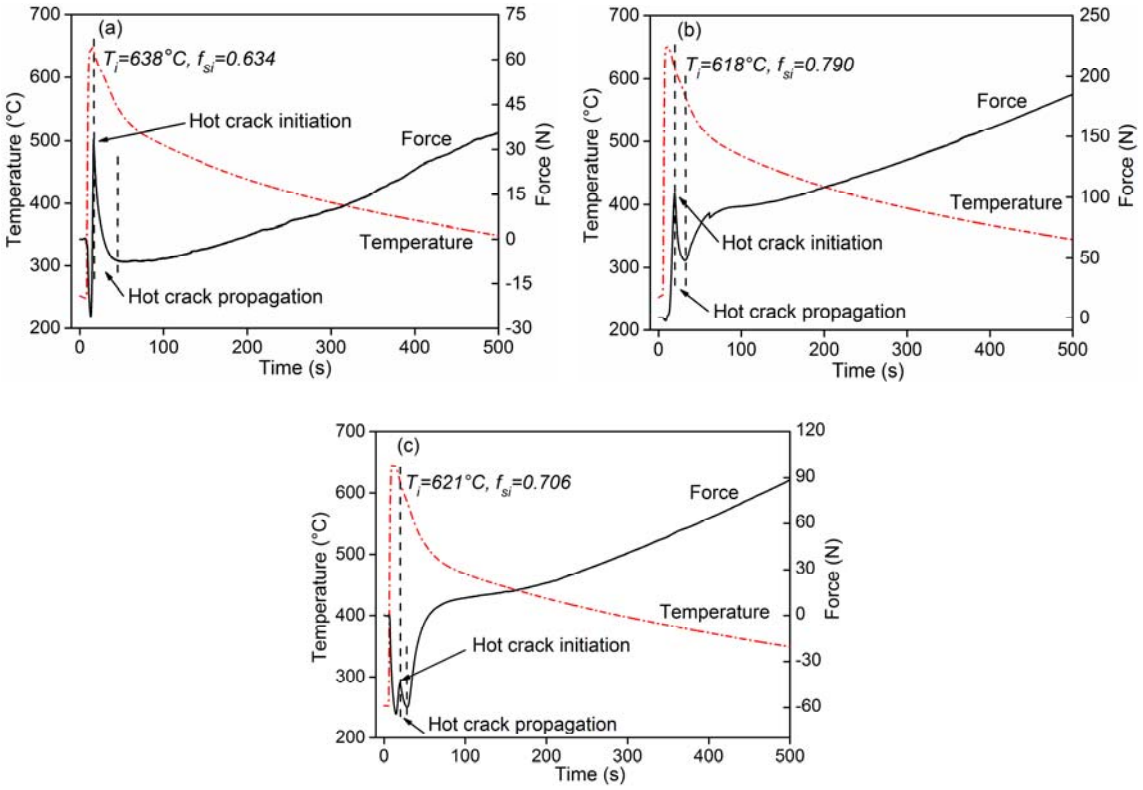

Fig. 5.33 Contraction force and temperature as a function of time for Mg-1.5Zn-xY alloys at a mould temperature of 250 ^{o}C: (a) x=0.2, (b) x=2, (c) x=3.

Table 5-7 Information about the initiation and propagation of hot tearing for Mg-1.5Zn-xY alloys at a mould temperature of 250 °C.

Alloys	Hot crack initiation		Termination of hot crack propagation		Hot crack propagation		
	T_i (°C)	f_{si}	T_f (°C)	f_{sf}	F_r (N)	t_p (s)	V_p (N/s)
Mg-1.5Zn-0.2Y	638	0.634	552	0.970	46.7	29.5	1.58
Mg-1.5Zn-2Y	618	0.790	589	0.976	50.8	22.7	2.34
Mg-1.5Zn-3Y	621	0.706	613	0.780	15.0	10.7	1.40

T_i : crack initiation temperature, f_{si} : solid fraction at which the cracks initiate, T_f : temperature at which the crack does not propagate any more, f_{sf} : solid fraction at which the propagation of cracks stops, F_r : force release, t_p : propagation time, V_p : force release rate, which is proportional to the crack propagation rate.

Information on the initiation and propagation of hot tearing for Mg-1.5Zn-xY alloys at a mould temperature of 250 °C are summarized in Table 5-7. For Mg-1.5Zn-0.2Y and Mg-1.5Zn-2Y alloys, the force release rates are 1.58 and 2.34 N/s, respectively. The contraction forces for these two alloys drop significantly (Fig. 5.33 (a) and (b)). As shown in Table 5-7, the forces drops of Mg-1.5Zn-0.2Y alloys and Mg-1.5Zn-2Y alloys are 46.7 and 50.8 N, respectively. In contrast, the force release of Mg-1.5Zn-3Y alloy is smaller, and a drop in the contraction force is 15 N, indicating that the HTS is small.

5.3.1.3 Macro-structural observations

The macroscopic structures showing hot crack in castings of Mg-1.5Zn-xY alloys are shown in Table 5-8. The macrographs show that the hot cracks are located on the surfaces of the restrained rods for Mg-1.5Zn-xY alloys. The compositions of alloys significantly influence the amount of hot cracks. No apparent macro-cracks are found near the junctions of Mg-1.5Zn-3Y alloy. In contrast, the macro-cracks are observed near the junction of Mg-1.5Zn-0.2Y and Mg-1.5Zn-2Y alloys. The cracks on the surface of the 0.2 wt.% Y containing alloy are more serious than that of the 2 wt.% Y containing alloy, indicating that Mg-1.5Zn-0.2Y alloy has the highest HTS among the three alloys investigated.

Table 5-8 Macro-graphs of crack for Mg-1.5Zn-xY alloys at a mould temperature of 250 °C

Mould temperature	Mg-1.5Zn-0.2Y	Mg-1.5Zn-2Y	Mg-1.5Zn-3Y
250 °C			

5.3.1.4 Microstructual observations

Fig. 5.34 shows the optical micrographs of ternary Mg-1.5Zn-xY alloys from the regions near the junction between the sprue and the horizontal rod. With increasing the Y content the microstructure changes from columnar grains to equiaxed grains. The Mg-1.5Zn-0.2Y alloy has the largest grain size among the Mg-1.5Zn-xY alloys. Small equiaxed grains are dominant in Mg-1.5Zn-3Y alloy. The fine microstructure supplies more paths for the remaining liquid to

flow so that the refilling is improved at the later stages of solidification. Consequently, the HTS of this alloy is lower.

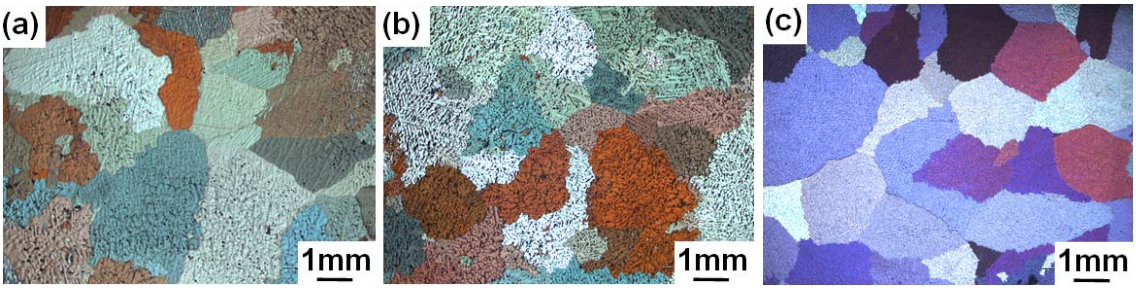

Fig. 5.34 Optical microstructures showing the grain structure of ternary Mg-1.5Zn-xY alloys at a mould temperature of 250 °C: (a) x=0.2, (b) x=2, (c) x=3.

5.3.1.5 Fracture surfaces of hot tearing

Fig. 5.35 shows the fracture surfaces of hot cracked Mg-1.5Zn-0.2Y and Mg-1.5Zn-2Y alloys. In Mg-1.5Zn-0.2Y alloy, the fracture surface is very smooth without any trans-granular tears. The dendrite-like bumps on the fracture surface are observed (Fig. 5.35 (a)). It indicates that a significant amount of inter-dendritic liquid was still present at the initiation of hot tearing. As mention previously, the liquid fraction is 0.366 when the hot cracks initiate in Mg-1.5Zn-0.2Y alloy. In Mg-1.5Zn-2Y alloy, the dendrite-like bumps are also observed on the fracture surfaces. Interestingly, the trans-granular tears are also observed, indicating that the interconnections of dendrites have happened before the initiation of hot tearing.

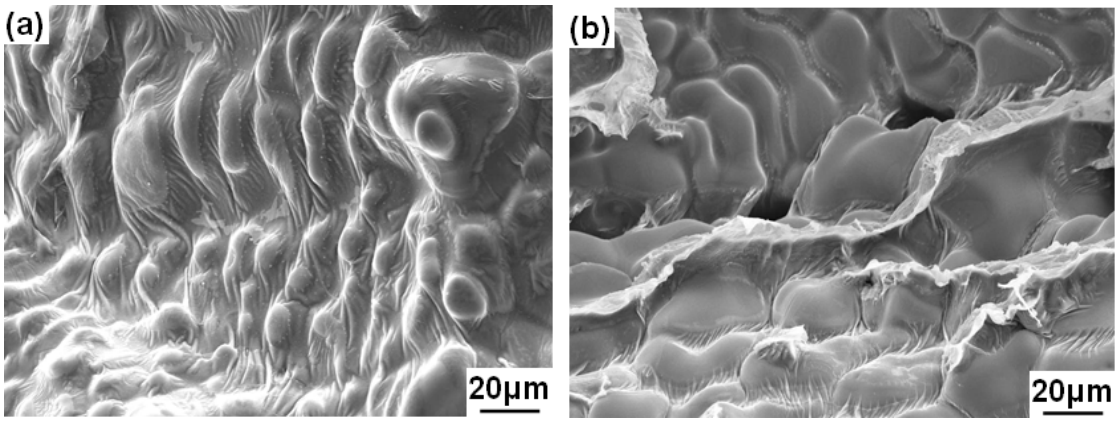

Fig. 5.35 SEM micrographs of hot tear surfaces of (a) Mg-1.5Zn-0.2Y and (b) Mg-1.5Zn-2Y alloys at a mould temperature of 250 °C.

Compared with the Mg-1.5Zn-0.2Y alloy, the liquid fraction at the initiation of hot cracks is lower with a value of about 21% for this alloy. With a smaller amount of liquid remaining, the inter-granular liquid film is thin. The formed bumps are therefore not so high as that observed in Mg-1.5Zn-0.2Y alloy (Fig. 5.35 (b)).

5.3.1.6 Quantitative measurement of hot tearing

Fig. 5.36 shows the total crack volume measured by the wax penetration method. The total crack volume depends on the Y content. The addition of Y to Mg-1.5Zn alloy has a positive effect on alleviating HTS. The hot crack volumes continuously decrease with increase in the content of Y. When the content of Y reaches to 3 wt.%, the volume of hot crack is very low with a value of only 10.5 mm^3.

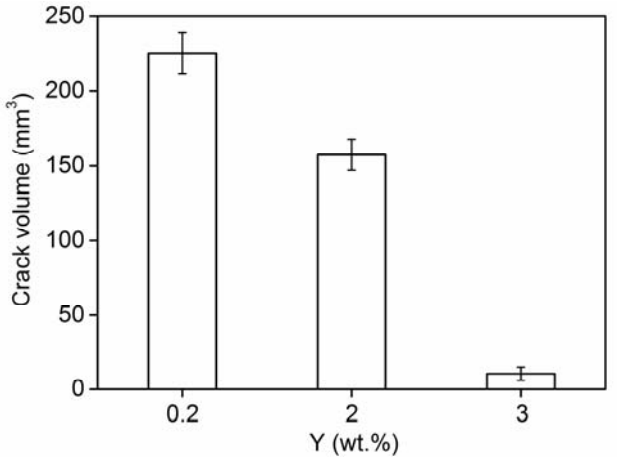

Fig. 5.36 Total crack volumes measured by wax penetration method for Mg-1.5Zn-xY alloys at a mould temperature of 250 °C.

5.3.1.7 Numerical simulation of HTS

Comparison between the results from HTI simulations and observed cracks on the surfaces of Mg-1.5Zn-xY alloys at a mould temperature of 250 °C are shown in Fig. 5.37. The numerical simulations show that the HTS decreases with increase in the Y content. When the content of Y is only 0.2 wt.%, the value of HTI is very high. The HTI value of Mg-1.5Zn-3Y alloy decreases due to the increment of Y content. As shown by macro-graphs, the HTS also reduces with the Y content increased from 0.2 to 3 wt.%. The numerical simulation results agree well with the experimental results. The susceptibility of hot tearing can be predicted accurately by ProCAST.

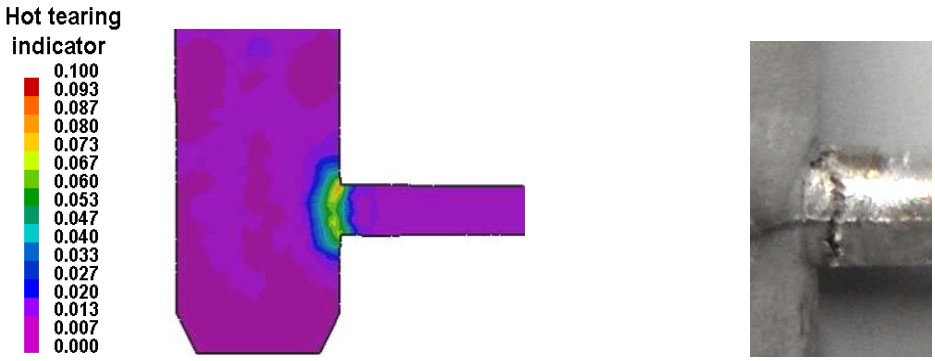

(a) Mg-1.5Zn-0.2Y alloy

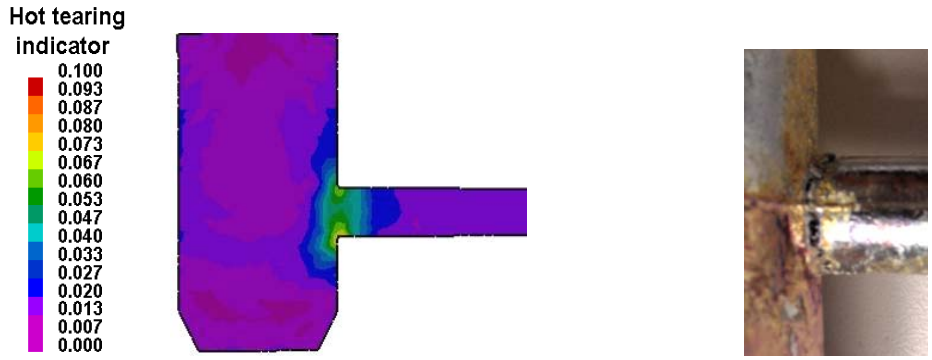

(b) Mg-1.5Zn-2Y alloy

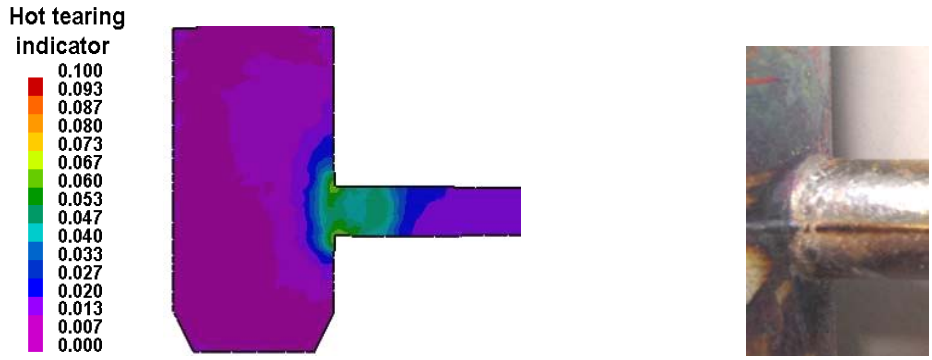

(c) Mg-1.5Zn-3Y alloy

Fig. 5.37 Comparison between the results of HTI and observed cracks on the surfaces of Mg-1.5Zn-xY alloys at a mould temperature of 250 °C.

5.3.2 Hot tearing of Mg-xZn-2Y alloys

5.3.2.1 Chemical compositions

Table 5-9 lists the actual compositions of the experimental Mg-xZn-2Y alloys, which are close to their nominal compositions.

Table 5-9 Actual chemical compositions of experimental alloys (wt.%)

Alloy	Zn	Y	Mn	Si	Fe	Mg
Mg-2Y	—	1.90	0.031	0.014	0.002	Bal.
Mg-0.5Zn-2Y	0.73	1.50	0.032	0.008	0.001	Bal.
Mg-1.5Zn-2Y	1.89	1.53	0.038	0.005	0.001	Bal.
Mg-4.5Zn-2Y	4.47	1.51	0.027	0.007	0.001	Bal.

5.3.2.2 Hot tearing curves

Fig. 5.38 shows the experimental hot tearing curves for Mg-xZn-2Y alloys at a mould temperature of 250 °C.

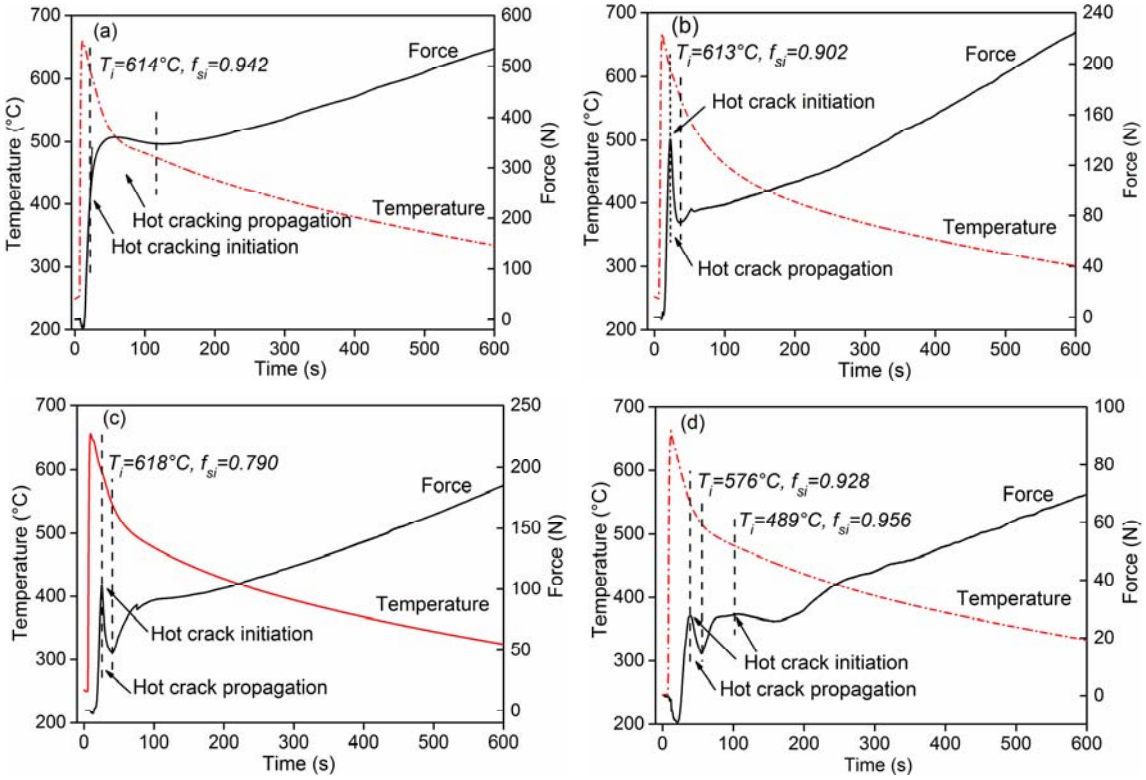

Fig. 5.38 Contraction force and temperature as a function of time for Mg-xZn-2Y alloys at a mould temperature of 250 °C: (a) x=0, (b) x=0.5, (c) x=1.5, (d) x=4.5.

In the Mg-2Y alloy, the hot tearing initiates at a temperature of 614 °C which corresponds to a solid fraction of 0.942. The hot tearing initiation of Mg-0.5Zn-2Y alloy happens at a temperature of 613 °C, which corresponds to a solid fraction of 0.902 (Fig. 5.38 (b)). When increasing the content of Zn to 1.5 wt.%, the hot tearing initiates at 618 °C, which corresponds to a solid fraction of 0.79 (Fig. 5.38 (c)). When there is a large amount of liquid remained, the

liquid still had a chance to flow into the cracks and possibly repair them. However, there is a large force drops, indicating that this alloy is cracked seriously. When the content of Zn reaches to 4.5 wt.%, two peaks are observed on the curve. Corresponding to each peak, there is small drops in force. The hot tearing initiates 576 and 489 °C for this alloy, which correspond to solid fractions of 0.928 and 0.956, respectively.

Information on the initiation and propagation of hot tearing for Mg-xZn-2Y alloys at an initial mould temperature of 250 °C are summarized in Table 5-10. For Mg-0.5Zn-2Y and Mg-1.5Zn-2Y alloys, the force release rates are 2.29 and 2.34 N/s, respectively. In these two alloys, there are very large decrease in force (Fig. 5.38 (b) and (c)). Both Mg-2Y and Mg-4.5Zn-2Y alloys have lower force release rate than other alloys. Normally, the high force release rate shows a low resistance to hot tearing.

Table 5-10 Information on the initiation and propagation of hot tearing for Mg-xZn-2Y alloys at an initial mould temperature of 250 °C

Alloys	Hot crack initiation		Termination of hot crack propagation		Hot crack propagation		
	T_i (°C)	f_{si}	T_f (°C)	f_{sf}	F_r (N)	t_p (s)	V_p (N/s)
Mg-2Y	614	0.942	475	1.000	13.1	58.9	0.22
Mg-0.5Zn-2Y	613	0.902	564	0.998	58.7	25.6	2.29
Mg-1.5Zn-2Y	618	0.790	589	0.976	50.8	22.7	2.34
Mg-4.5Zn-2Y	576	0.928	463	0.980	2.3	45.3	0.05

T_i : crack initiation temperature, f_{si} : solid fraction at which the cracks initiate, T_f : temperature at which the crack does not propagate any more, f_{sf} : solid fraction at which the propagation of cracks stops, F_r : force release, t_p : propagation time, V_p : force release rate, which is proportional to the crack propagation rate.

5.3.2.3 Macro-structural observations

The macrographs of hot crack for the castings of Mg-xZn-2Y alloys are shown in Table 5-11. Based on the macro-structural observations of the cracks on the surface of castings, it is demonstrated that the compositions of alloys significantly influence the HTS. Near the junctions of Mg-4.5Zn-2Y alloy, small macro-cracks are observed. In contrast, the macro-

cracks are clearly observed near the junctions of Mg-0.5Zn-2Y and Mg-1.5Zn-2Y alloys. The later alloy has a larger open crack on the surface of its casting than Mg-0.5Zn-2Y alloy, indicating that Mg-1.5Zn-2Y alloy has the largest HTS among all alloys in Mg-xZn-2Y system.

Table 5-11 Macro-graphs of hot crack for Mg-xZn-2Y alloys at a mould temperature of 250°C

Mould temperature	Mg-2Y	Mg-0.5Zn-2Y	Mg-1.5Zn-2Y	Mg-4.5Zn-2Y
250 °C				

5.3.2.4 Fracture surfaces of hot tearing

Fig. 5.39 shows SEM images of the fracture surfaces caused by hot tearing for Mg-0.5Zn-2Y and Mg-1.5Zn-2Y alloys. In Mg-0.5Zn-2Y alloy, the morphology of the fracture surface shows typical inter-dendritic separations. The fracture surfaces are dominated by smooth dendritic bumps, and there are no trans-granular tears on the fracture surface. In Mg-1.5Zn-2Y alloy, the dendrite bumps are still observed on the fracture surfaces, but additionally trans-granular tears are also observed (Fig. 5.39 (b)).

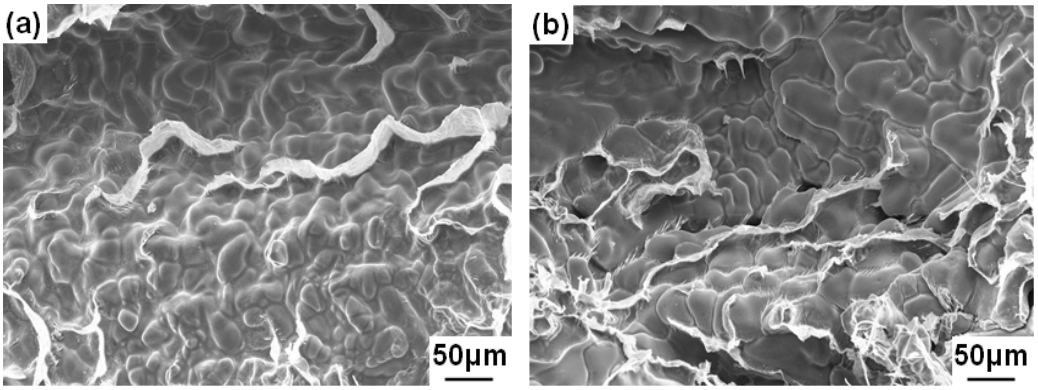

Fig. 5.39 SEM micrographs of hot tear surfaces of (a) Mg-0.5Zn-2Y and (b) Mg-1.5Zn-2Y alloys.

5.3.2.5 Microstructual observations

Fig. 5.40 shows the optical micrographs of ternary Mg-xZn-2Y alloys taken from the regions near the junction of the sprue and horizontal rod. The grain sizes and morphology are almost identical for all alloys. With increase in the Zn content, the amount of particles at the dendritic boundaries increases.

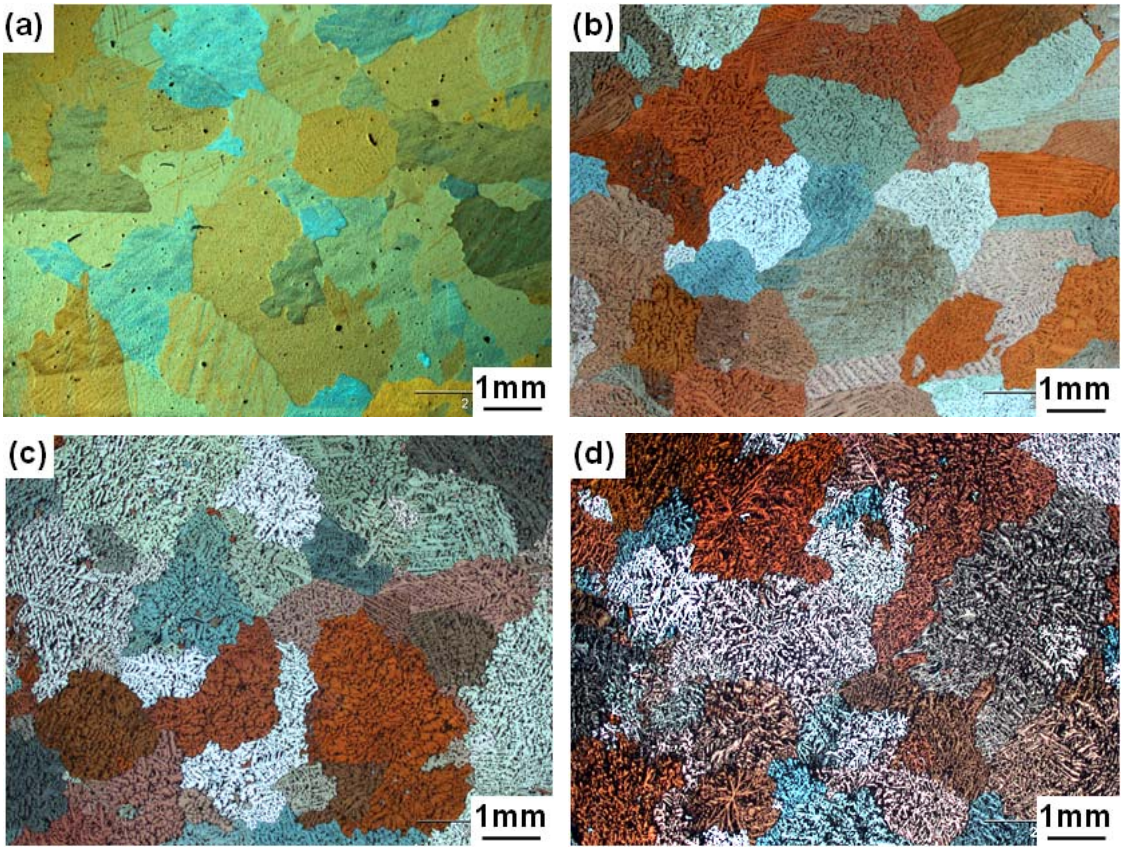

Fig. 5.40 Optical microstructures of Mg-xZn-2Y alloys at a mould temperature of 250 °C: (a) x=0, (b) x=0.5, (c) x=1.5, (d) x=4.5.

5.3.2.6 Quantitative measurement of hot tearing

Fig. 5.41 shows the total crack volume of Mg-xZn-2Y alloys measured with wax penetration method. The total crack volume depends on the content of Zn. The volume of hot cracks increases with increase in the content of Zn, reaches the maximum at 1.5 wt.% Zn, and then decrease with further increase in the content of Zn.

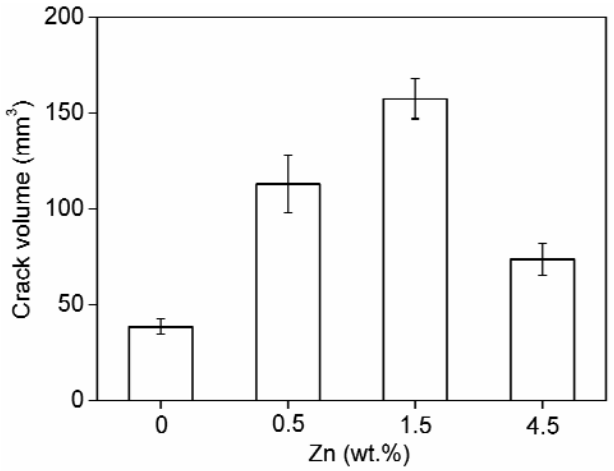

Fig. 5.41 Total crack volumes measured by wax penetration method for Mg-xZn-2Y alloys at a mould temperature of 250 °C.

5.3.2.7 Numerical simulation of HTS

Fig. 5.42 shows the calculated HTIs and experimental observations of hot tearing at the sprue and rod junction for Mg-xZn-2Y alloys. For Mg-xZn-2Y alloys, the calculated HTI first increases with the content of Zn, reaches the maximum at 1.5 wt.% Zn, and then decreases with further increment in the content of Zn. The susceptibility of hot tearing predicted by numerical simulation is in agreement with the experimental observations.

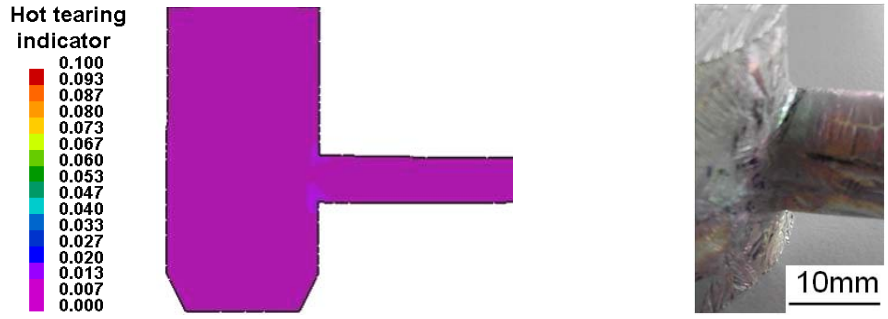

(a) Mg-2Y alloy

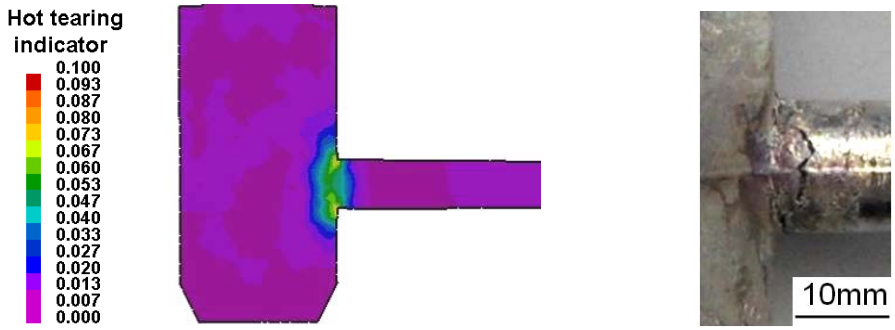

(b) Mg-0.5Zn-2Y alloy

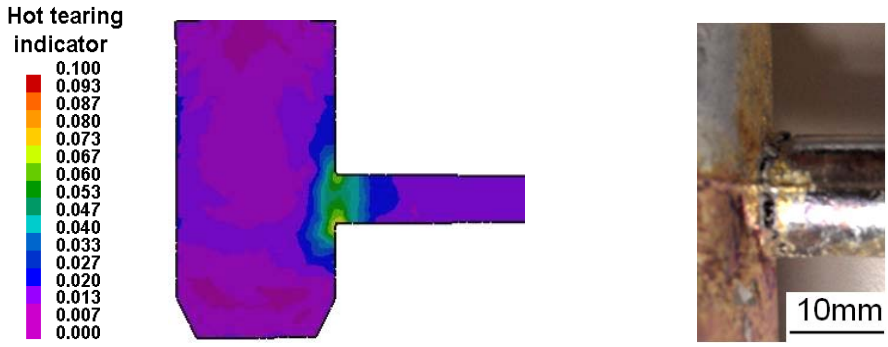

(c) Mg-1.5Zn-2Y alloy

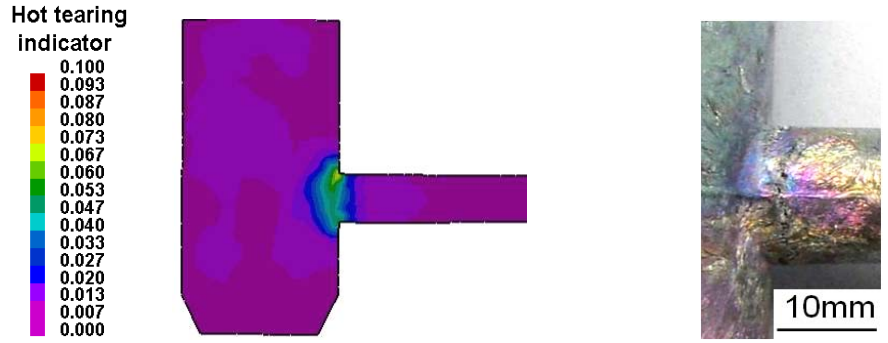

(d) Mg-4.5Zn-2Y alloy

Fig. 5.42 Comparison between the results of HTI and observed cracks on the surfaces of Mg-xZn-2Y alloys at a mould temperature of 250 °C.

6 DISCUSSION

6.1 Hot tearing of binary Mg-Y alloys

6.1.1 Comparisons of thermodynamic calculations with experimental results

Comparison between predicted CSC and experimental HTS for actual chemical compositions of binary Mg-Y alloys with B-Spline fitting the curve are shown in Fig. 6.1. The results from thermodynamic calculations are in agreement with that obtained experimentally. Both indicate that the HTS changes with Y content even though the parameters used to evaluate the HTS in both cases are different. The HTS for most binary alloy systems, with respect to the alloy compositions, follows the so-called "λ" curve [22, 59].

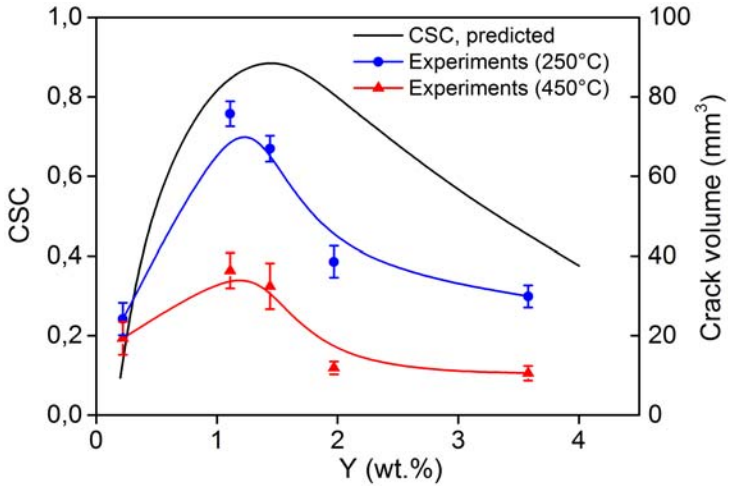

Fig. 6.1 Comparison of predicted CSC and experimental HTS for actual chemical compositions of binary Mg-Y alloys.

Theoretically, pure metal and the alloys with their compositions near the eutectic point have a high resistance to hot tearing, whereas at intermediate solute compositions with a large freezing range is very susceptible to hot tearing, as the alloy is in the vulnerable region of solidification in which thin film of liquid exist for a long time [5, 34]. When the solute in added to a pure metal, HTS increases rapidly to a maximum. The maximum point shown in Fig. 6.1 is normally associated with the appearance of eutectic liquid in the alloy [15]. With the increment in the content of alloying element the amount of eutectic liquid also increases. This increment in the amount of eutectic liquid results in the improvement of healing ability [67-68]. Consequently, the inter-dendritic gaps have more possibilities to be filled. The pre-existing cracks could partially or completely heal. Thus, with further increase in the content of

alloying elements, the HTS reduces significantly due to the increment in the amount of eutectic liquid.

According to the Zhou [23] and Cao's [54] investigations, Clyne and Davies' theory is one of the most accurate and simple model to evaluate the influence of composition on the HTS [22, 54]. During thermodynamic calculations, the parameter "CSC" (see Equation 2-21) defined by Clyne and Davies was used to estimate the HTS. During the experiments the parameter "crack volume" was directly used to evaluate the HTS. Indeed, these two parameters have no direct relationship. However, they are useful to evaluate how the composition of primary alloying element influences the HTS of alloys. Especially for the parameters used in thermodynamic calculations, it would be quite useful during alloy design when the experimental measurements of HTS become difficult. Based on the present results, it is concluded that it is reasonable to use the Clyne and Davies' model to evaluate the influence of compositions on the HTS.

Although Fig. 6.1 shows similar shapes of the HTS curves and indicates almost the same peak position (at 1 to 1.5 wt.% Y) for the thermodynamic calculations and experimental measurements, there is a discrepancy between them. After the peak position, the crack volume measured by experimental tests reduces more sharply than that of the calculated CSC value. This discrepancy is caused by the limitations of Clyne and Davies' model. In their model, the definition of the vulnerable period during which the hot tearing occurs easily is not always accurate. They defined this period ($0.9 < f_s < 0.99$) based only on the previous experimental results. In some cases, the hot tearing can happen with a liquid fraction of more than 0.1 which is not in their defined range [34, 66, 69]. In addition, Clyne and Davies' model used a fixed equation to estimate the cooling rate which was simplified based on the situation of heat flow [34]. They did not incorporate the influence of mould temperature into their equation. Even so, Clyne and Davies' model is still useful to evaluate the influence of the alloy compositions on the HTS of an alloy.

6.1.2 Influences of Y on HTS

The HTS of Mg-Y alloy is mainly influenced by the Y content in two ways: the solidification range and the microstructure. Normally, the HTS is proportional to the solidification range, especially temperature range for the vulnerable solidification region from the solid fraction 0.90 to 0.99. For Mg-Y alloys, the thermodynamic calculations reveal that an increase in the

content of Y changes the latent heat of the alloys, from 8.46 (0.2 wt.% Y) to 8.30 kJ/mol (4 wt.% Y). In addition, the cooling curves of all alloys are more or less identical for the solid fraction between 0 and 0.90. Since the heat release dQ/dt can be assumed to be same. Equation (5-9) can be modified to [32]:

$$CSC = \frac{A(T_{0.9} - T_{0.99})}{t_{0.9} - t_{0.4}} \tag{6-1}$$

with A is the conversion factor. In addition, the denominator $(t_{0.9} - t_{0.4})$ in equation (2-21) can be assumed to be constant, and then equation (6-1) is rewritten as:

$$CSC^* = T_{0.9} - T_{0.99} = \Delta T \tag{6-2}$$

where ΔT is the temperature difference between the temperature at a solid fraction of 0.9 ($T_{0.9}$) and that at 0.99 ($T_{0.99}$). The large value of ΔT can lead to a large HTS. Table 6-1 lists the ΔT values obtained by thermodynamics calculations. As shown in Fig. 6.2 and Table 6-1, the vulnerable solidification region depends on the nominal compositions of Mg-Y alloys. The ΔT increases with the content of Y to 1.5 wt.%, and then decreases with further increasing the content of Y. Mg-0.9Y, Mg-1.5Y and Mg-2Y three alloys have wider freezing ranges than Mg-0.2Y and Mg-4Y alloys. The alloy spends long time in the vulnerable solidification zone, demonstrating the possibility of hot cracking initiation may be large. However, as shown in Fig. 5.10, although Mg-2Y alloy has a larger freezing range than Mg-0.9Y alloy, it has a small grain size and contain rich eutectic phase. Its positive microstructural characterization results in the reduction of HTS.

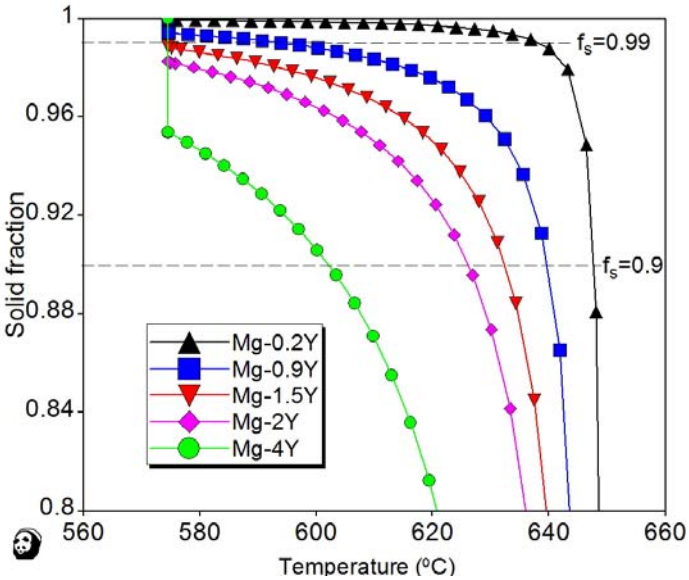

Fig. 6.2 Solidification temperature changes with solid fraction in vulnerable region.

Table 6-1 Characteristic temperatures and ΔT for nominal compositions of Mg-Y alloys

Composition (wt.%)	$T_{0.9}$ (°C)	$T_{0.99}$ (°C)	ΔT (°C)
Mg-0.2Y	644	638	6
Mg-0.9Y	640	594	46
Mg-1.5Y	632	574	58
Mg-2Y	626	574	52
Mg-4Y	602	574	28

The critical solid fraction at which the hot tearing initiates depends on the Y content (Fig. 5.8). It decreases from 0.997 to 0.918 with the increase in the Y content from 0.2 to 4. As shown in Fig. 6.2, the solid fraction increases sharply at the beginning of solidification, and slows down near the solidus temperature. For the alloys with low contents of Y, like Mg-0.2Y alloy, the solid fraction increases rapidly below its liquidus temperature. In that case, the strains due to thermal contraction will build up and impose on the casting at high solid fractions. When the accumulated strain is larger than a critical value, the cracking is induced. In contrast, the solid fraction of high Y content alloy increases very slowly. The solid fraction at which the hot tearing initiates is well known with a value below 1 (0.918 for Mg-4Y alloy).

The addition of Y to Mg affects the grain morphology, which was considered as one of the most important factors that influence the initiation of hot tearing [62, 103]. The large grains and columnar structure normally easily promote the initiation and propagation of hot cracks. As shown in Fig. 5.10 (b), the grain size of Mg-0.9Y alloy is the largest, and therefore this alloy shows a higher HTS. In contrast, a fine grain and equiaxed structure help to avoid the initiation of hot tearing. The fine microstructure is not only beneficial in accommodating the local deformation but also allow the melt to flow due to the increased amount of grain boundary. Thus, it is possible to refill the fresh hot tears by the liquid remaining. As a consequence, some of pre-existing hot tearing is possibly healed. As shown in Fig. 5.10 (e), the grain of Mg-4Y alloy has a fine equiaxed structure, and therefore this alloy shows a lower HTS.

As shown in Fig. 5.12 and Fig. 5.13, in front of the main cracks, the second phases with different contrasts are observed. At high magnification (Fig. 6.3 (a)), these can be clarified as

second phases. EDS analysis indicates that these regions are Y rich (Fig. 6.3). In Mg-4Y alloy, the content of Y in the white region reaches to 32.43 wt.%. With the increase in the content of Y the amount of white river patterns increases. These river patterns can be seen clearly in Fig. 6.3, which contains eutectic phases and regards as feeding traces.

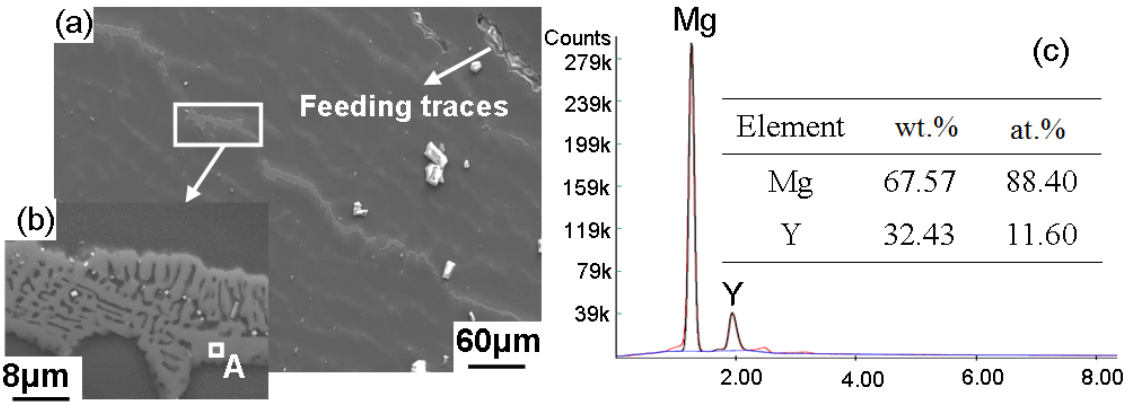

Fig. 6.3 As-cast microstructure of Mg-4Y alloy and EDS analysis result of point A: (a) SEM image, (b) magnified view of second phase, (c) EDS result of point A.

The amount of eutectic liquid is also regarded as one of the most important factors that influence the initiation of hot tearing, especially for the binary alloys [5-6, 104]. In Mg-Y binary alloys, the amount of eutectic liquid depends on the content of Y. Generally, the fluidity of melt increases with the amount of low melting point eutectic liquid [6]. In the Mg-Y binary alloys with a high content of Y, the HTS is lower due to the large amount of eutectic liquid that remaining in the final stage of solidification. The eutectic liquid heals the cracks that previously formed due to the high fluidity. Experimental results show that the hot tearing almost disappear when the content of Y is more than 2 wt.% (Fig. 6.1).

Finally, the second phase particles that form from the liquid above the solidus may act as nuclei for the initiation of hot tearing. For the present Mg-Y alloys, the influence of second phases on the initiation of hot tearing may be neglected. The microstructural observations confirm that there are only few second phase particles in binary Mg-Y alloys (Fig. 5.12). In addition, for Mg-0.9Y and Mg-4Y alloys, their solidification paths calculated using Scheil model indicate that the fraction of second phase are almost zero (Fig. 6.4). Even in Mg-4Y alloy, only 2 mol% $Mg_{24}Y_5$ phase is expected to form after complete solidification. As shown in Fig. 5.8, for the Mg-Y binary alloys investigated, the temperatures at which the hot tears initiate are normally more than 590 °C. Above the temperature 590 °C, the second phase

$Mg_{24}Y_5$ does not yet start to form even for Mg-4Y alloys. At that time the amount of second phases should be zero. The initiations of hot tears were not caused by the precipitation of second phases.

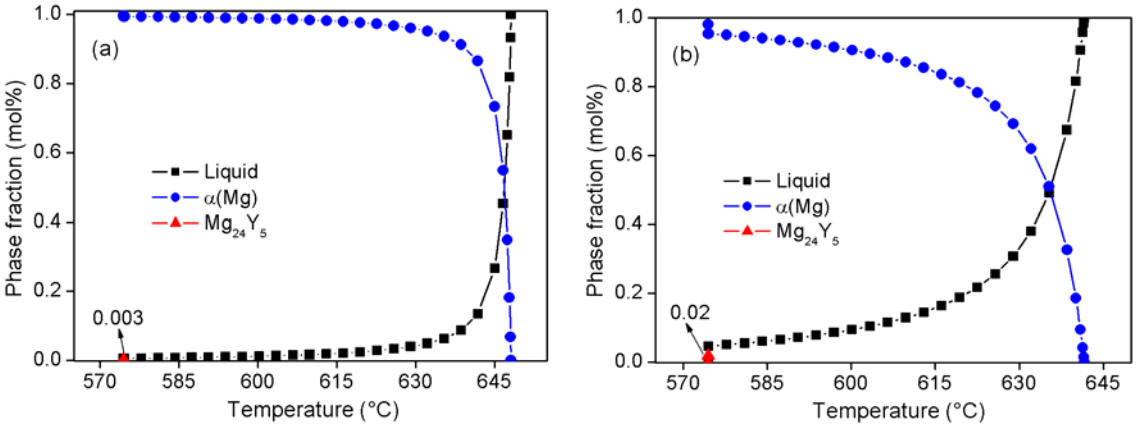

Fig. 6.4 Solidification processes of (a) Mg-0.9 Y and (b) Mg-4Y, which are calculated by thermodynamic calculations using Scheil model.

6.1.3 Influences of mould temperatures on HTS

The HTS of Mg-Y alloy is influenced by the initial mould temperature. Table 5-2 shows that HTS decreases with the increase in the mould temperature from 250 to 450 °C. This reduction may be attributed to the low mould temperature that leads to a larger thermal gradient and a high contraction stress imposed on the solidifying casting. Based on the strain theory proposed by Pellini [47-48], the initiation of hot tearing depends on the strain rate developed in the liquid film regions. Generally, hot tearing resistance decreases with the increase in the strain contraction rate [49]. Thus, the elevated mould temperature reduced the HTS by lowering the strain contraction rate. The lower strain rate provides an opportunity for the casting to recover from such a strain through microscopic movements of the dendrite cells or liquid metal; however, this kind of compensation may not be possible at such a high strain rate.

Fig. 6.5 shows the experimental cooling curves of Mg-0.9Y and Mg-1.5Y alloys at different mould temperatures. The cooling rate was calculated using the whole temperature change in the solidification range divided by the corresponding solidification time. Faster solidification leads to a larger thermal gradient at the sprue-rod junction, which is considered to be one important criterion for the initiation of hot tearing.

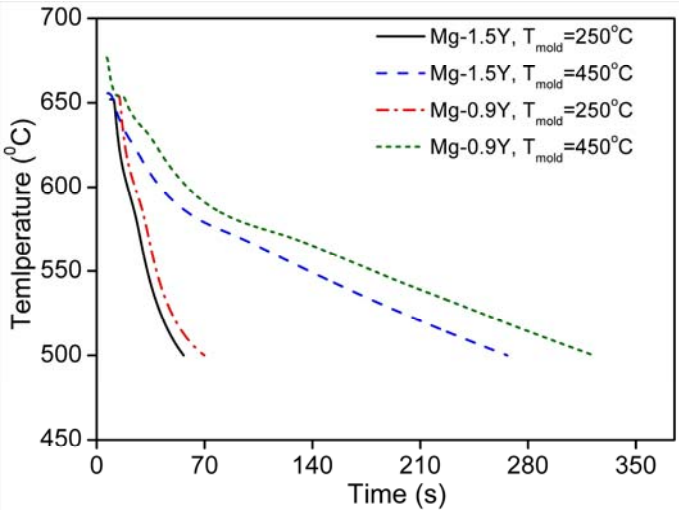

Fig. 6.5 Experimental cooling curves of Mg-0.9Y and Mg-1.5Y alloys with different mould temperatures.

According to the cooling curves, the cooling rates of Mg-1.5Y alloy were 4.24 °C/s at a mould temperature of 250 °C and 0.81 °C/s at a mould temperature of 450 °C. For Mg-0.9Y alloy, the cooling rates were 4.07 °C/s at a mould temperature of 250 °C and 0.73 °C/s at a mould temperature of 450 °C. The temperature differences between various parts of the casting can cause internal contraction stress. In addition, the temperature differences between the mould and casting can increase the thermal gradient and stress. The elevated mould temperature can effectively reduce the temperature difference between the casting and mould. In this case, the distribution of solute and the solidification are close to equilibrium state. The contraction stress is reduced. Therefore, an elevated initial mould temperature can decrease the HTS of alloys by reducing the cooling rate.

On the other hand, increase in the mould temperature not only significantly reduces the cooling rate but also influences the grain size. The changes in the microstructure affect the hot tearing behaviour. Comparing Fig. 5.10 with Fig. 5.11, with increasing the mould temperature, the grain sizes decrease and the cracks are eliminated.

6.2 Ternary Mg-Y-Zn alloys

6.2.1 Influences of Y on HTS

Clyne and Davies' thermodynamic model correlated the HTS with the composition only for binary systems. They predicted HTS based on presence of a critical time periods during the solidification when the microstructure is most vulnerable to cracking. In order to have an

internal-consistent CSC for the multi-component system, a simplified version of Clyne and Davies' model (ΔT) was proposed (equation 6-2). Aforementioned, that in Clyne and Davies' model, the t_V corresponding to the period of inter-dendritic separation during which the liquid phase becomes fragmented and the feeding ceases. For the present ternary Mg-4.5Zn-xY and Mg-1.5Zn-xY alloys, it was suggested that the time period with the solid fraction between 0.90 and 0.98 as the vulnerable period. In contrast to Clyne and Davies' model, the solid fraction 0.98 rather than 0.99 was chosen, because according to Table 5-4 and Table 5-7, the hot tearing propagation finishes when the solid fraction is above 0.98 for all alloys investigated. In addition, this value is assumed to be more relevant than 0.99 because at the solid fraction $f_s \geq 0.98$ the structure develops considerable strength and solid-state creep can compensate the strain caused by thermal contraction [105].

Fig. 6.6 shows the last stage of the "solid fraction vs. temperature" f_s (T) curve in the range of 0.8< f_s <1 for nominal compositions of Mg-4.5Zn-xY alloys, calculated using Scheil model.

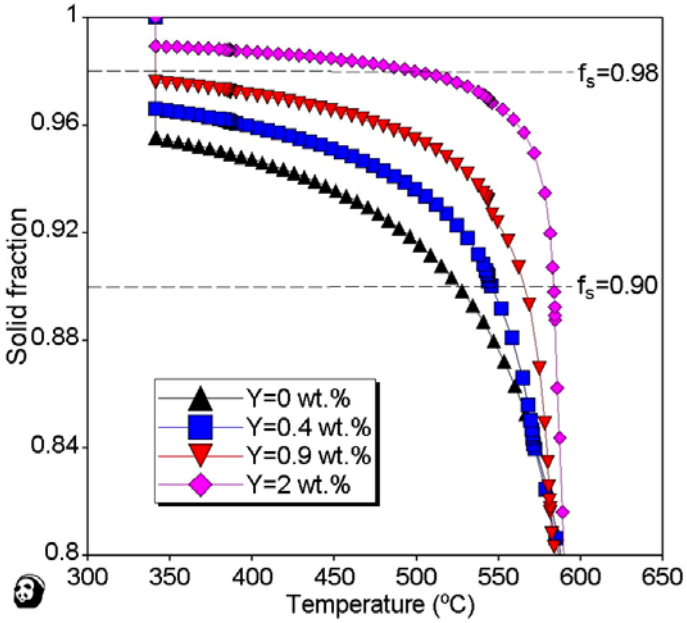

Fig. 6.6 Solid fraction vs. temperature curves for nominal compositions of Mg-4.5Zn-xY alloys calculated using Scheil model.

The Mg-4.5Zn-0.4Y and Mg-4.5Zn-0.9Y alloys have a larger ΔT value than other alloys. The alloy with a wide crystallization range promotes hot tearing because as the alloy remains for a

longer time in the vulnerable zone in which the thin liquid films exist between the dendrites. According to the prediction of ΔT, the hot tearing tendencies of Mg-4.5Zn-xY alloys correlate very well with the experimental results (Fig. 6.7). Therefore an alloy with a large ΔT value is considered to be more prone to hot tearing.

Table 6-2 Characteristic temperatures and ΔT for nominal compositions of Mg-4.5Zn-xY alloys

Composition (wt.%)	$T_{0.9}$ (°C)	$T_{0.98}$ (°C)	ΔT (°C)
Mg-4.5Zn	524	341	183
Mg-0.4Y-4.5Zn	545	341	204
Mg-0.9Y-4.5Zn	565	341	224
Mg-2Y-4.5Zn	583	489	94

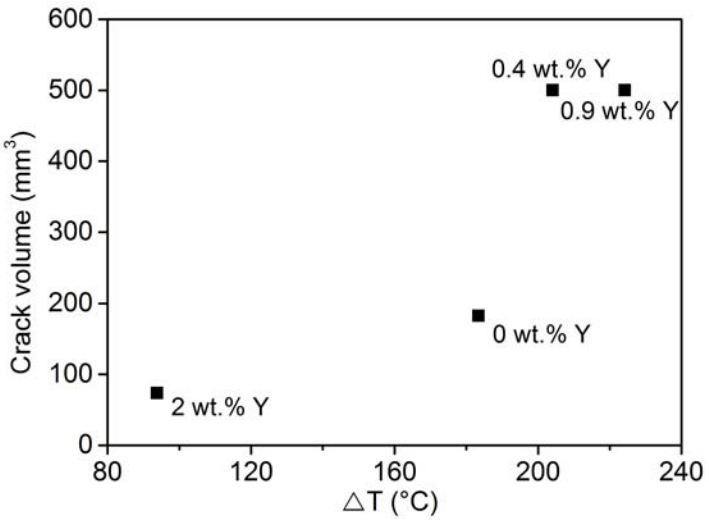

Fig. 6.7 Hot crack volume at a mould temperature of 250 °C represented as a function of ΔT.

Fig. 6.8 shows the last stage of the "solid fraction vs. temperature" f_s(T) curve in the range of 0.8< f_s <1 for nominal compositions of Mg-1.5Zn-xY alloys, calculated using Scheil model. Mg-1.5Zn-0.2Y alloy has the highest ΔT value among these alloys, and it exhibits a poor resistance to hot tearing. The ΔT value decreases with increased Y the content. According to the experiments results, the hot tearing resistances of Mg-1.5Zn-xY alloys improve with the increased Y content.

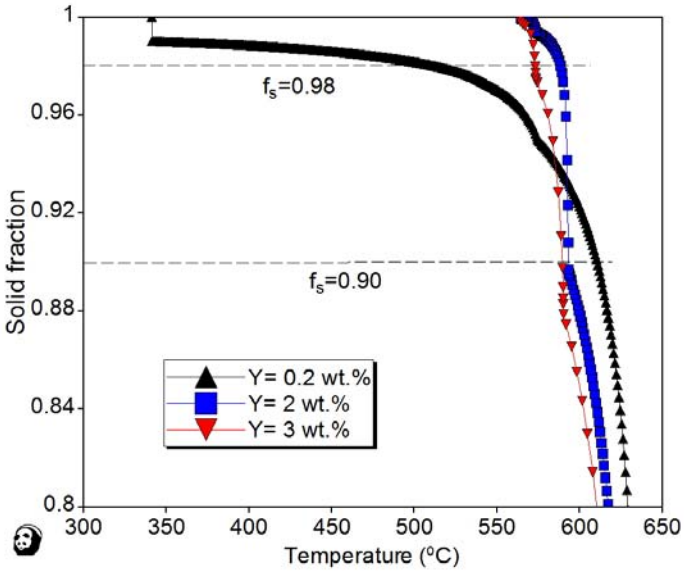

Fig. 6.8 Solid fraction vs. temperature curve for nominal compositions of Mg-1.5Zn-xY alloys calculated using Scheil model.

Table 6-3 Characteristic temperatures and ΔT for nominal compositions of Mg-1.5Zn-xY alloys

Composition (wt.%)	$T_{0.9}$ (°C)	$T_{0.98}$ (°C)	ΔT (°C)
Mg-0.2Y-1.5Zn	610	512	98
Mg-2Y-1.5Zn	593	587	6
Mg-3Y-1.5Zn	589	573	16

According to Clyne's investigation, the second phases may play an important role in influencing the initiation of hot tearing [34].

- The second phases with low melting point may decrease the solidus temperature of the alloy, thereby prolonging the liquid film stage where hot tearing is likely to occur.
- The brittle second phases with higher melting point may contribute to the fracture of the interconnected coherent solid network in the critical temperature range.
- The presence of second phases may also influence the properties of the inter-dendritic liquid that is present in the hot tear region, (i.e., wettability).

Fig. 6.9 shows SEM images of Mg-4.5Zn-xY alloys with low and high magnifications. The fraction of second phases increases with the increased the content of Y from 0.4 to 2 wt.%.

The microstructure consists of primary α-Mg dendrites and one or two types of second phases, I-phase (Mg_3Zn_6Y) and/or W-phase ($Mg_3Zn_3Y_2$) in the inter-dendritic areas. W-phase distributes as a divorce eutectic structure, but I-phase has a lamella eutectic structure. These phases were identified by X-ray diffraction (Fig. 6.10). The intensities of diffraction peak for both W-phase and I-phases increase with the increment of Y content.

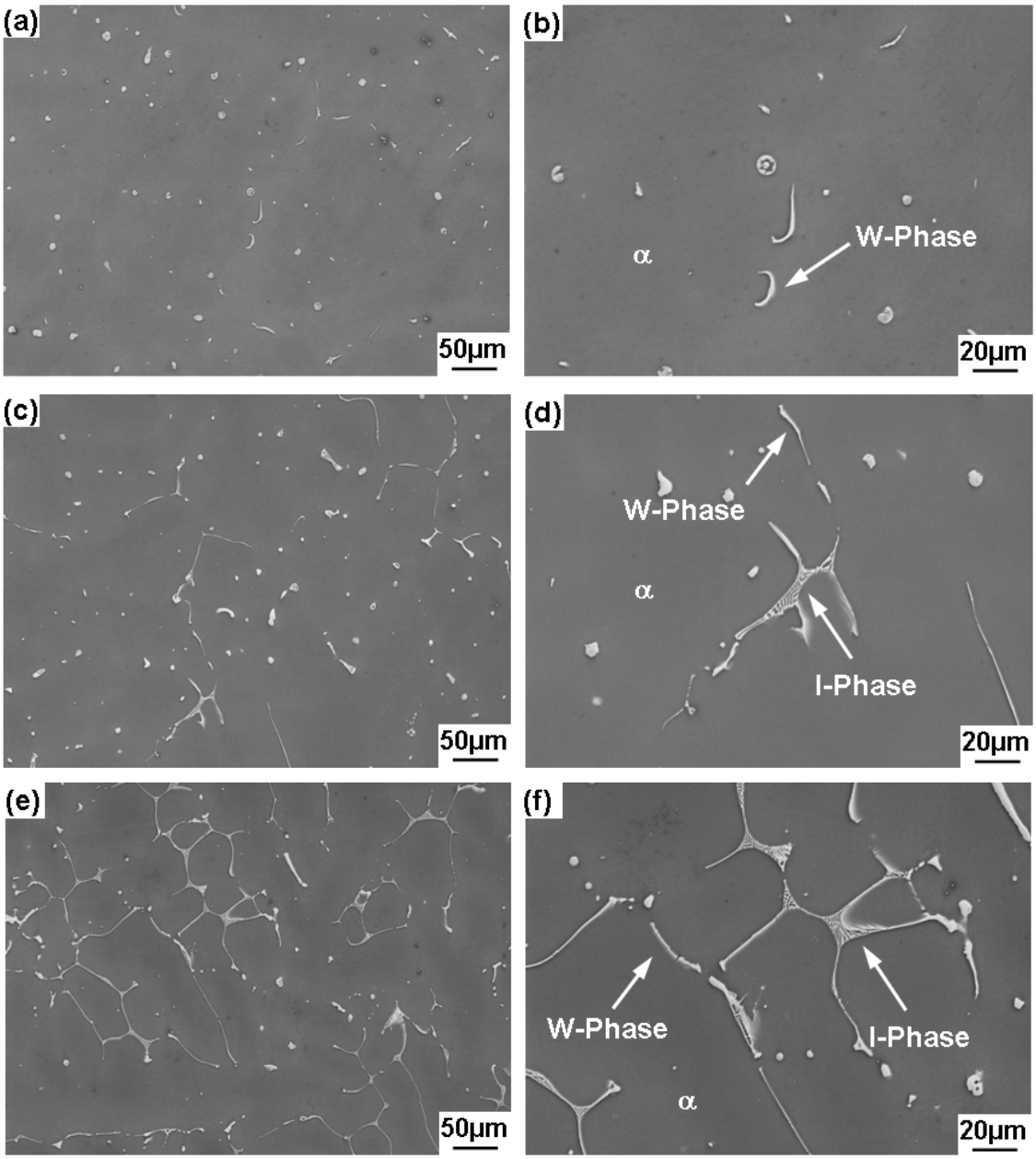

Fig. 6.9 SEM images of ternary Mg-Y-Zn alloys at a mould temperature of 250 °C: (a) and (b) Mg-4.5Zn-0.4Y, (c) and (d) Mg-4.5Zn-0.9Y, (e) and (f) Mg-4.5Zn-2Y.

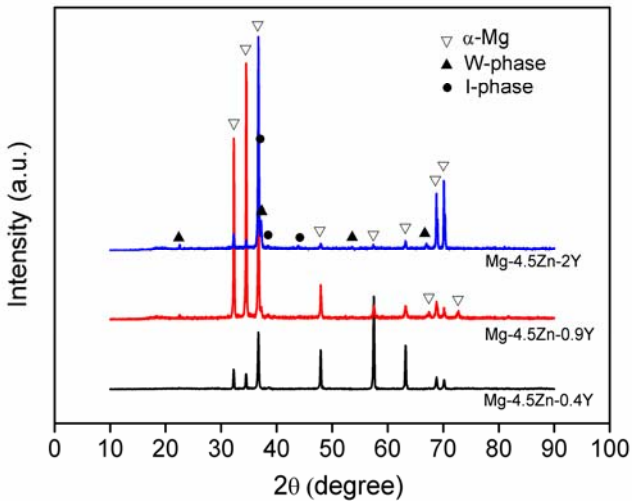

Fig. 6.10 XRD patterns of the as-cast Mg-4.5Zn-xY alloys.

Fig. 6.11 shows the calculated liquidus projection of the magnesium-rich corner of the ternary Mg-Y-Zn system. It was calculated using Pandat software [106] and the PanMg8.0 database [107]. The calculated solidification paths calculated based on the Scheil solidification model, for the three alloys investigated are superimposed on the liquidus projection.

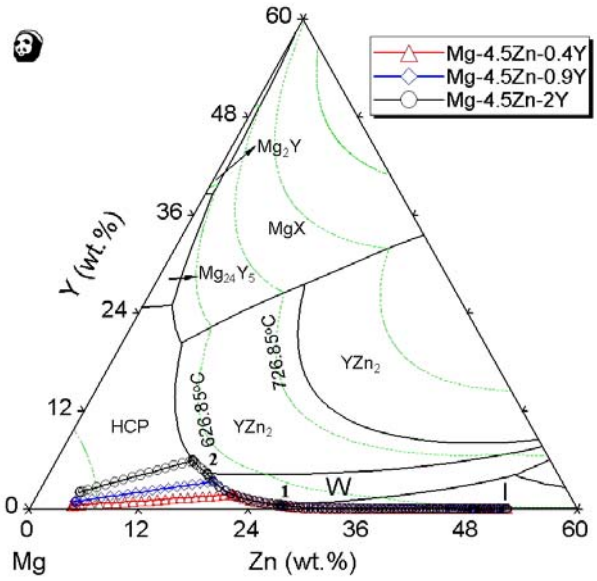

Fig. 6.11 Liquidus projection of Mg-Y-Zn alloys calculated in weight percent using Pandat.

The solidification paths of Mg-4.5Zn-0.4Y, Mg-4.5Zn-0.9Y and Mg-4.5Zn-2Y alloys in Fig. 6.11 show that α-Mg solidifies from the liquid first (primary solidification phase). For Mg-4.5Zn-0.4Y and Mg-4.5Zn-0.9Y alloys, upon reaching the W-phase valley, the W-phase

begins to form from the liquid, and then on reaching point 1, the part of remaining liquid begins to form I-phase. For Mg-4.5Zn-2Y alloy, upon reaching the α-YZn_2 valley, YZn_2 begins to form from the liquid, then reaching point 2, W-phase begins to form from the remaining liquid. When the point 1 is reached, the remaining liquid begins to form I-phase. Based on the above solidification path, the solidification always ends with the formation of the I-phase. The final amounts of I-phase increase as the content of Y increases from 0.4 to 2 wt.% (Fig. 6.9). The fluidity of the melt increases with the amount of low melting point phase increasing. Hence, it is possible to refill the fresh hot tears by the remaining liquid. For the alloy with high content of Y, the HTS is low due to the large amount of liquid present at the final stage of solidification, which transforms into I-phase.

6.2.2 Influence of mould temperatures on HTS

The HTS of ternary Mg-4.5Zn-xY alloys is influenced by the initial mould temperatures. Table 5-5 suggests that the HTS decreases with the increment in the mould temperature. The lower mould temperature leads to a larger thermal gradient and higher strain rate imposed on the solidifying casting. Table 5-4 shows that the force release rates in Mg-4.5Zn-0.4Y alloys drops from 0.50 N/s to 0.17 N/s with the increase in mould temperature from 250 to 450 °C. For Mg-4.5Zn-0.9Y alloy, the force release rate also decreases from 0.86 N/s to 0.43 N/s with the increase in the initial mould temperature.

The increment in the mould temperature not only reduced the force release rate but also increases the amount of low melting phase at the last stage of solidification. The feeding ability could therefore improve the cracks healing. Fig. 6.12 shows SEM microstructures and EDS analysis on the crack surface of Mg-4.5Zn-0.9Y alloy at a mould temperature of 450 °C. Compared with the crack surface at a mould temperature of 250 °C (Fig. 5.28 (b)), large second phases on the surface of Mg-4.5Zn-0.9Y alloy are observed with a mould temperature of 450 °C. They are mainly eutectic phases. EDS analysis indicates that these are low melting phases enrich with Y and Zn and that there is some remaining liquid when the hot crack initiated. The amount of liquid is sufficient to refill the cracks that form and heal them. Furthermore, the slower the force release rate, the longer the time available for the liquid to refill the crack. The Mg-4.5Zn-0.9Y alloy has a good hot tearing resistance at the high mould temperature due to the presence of low melting temperature phases and sufficiently long time to heal the cracks.

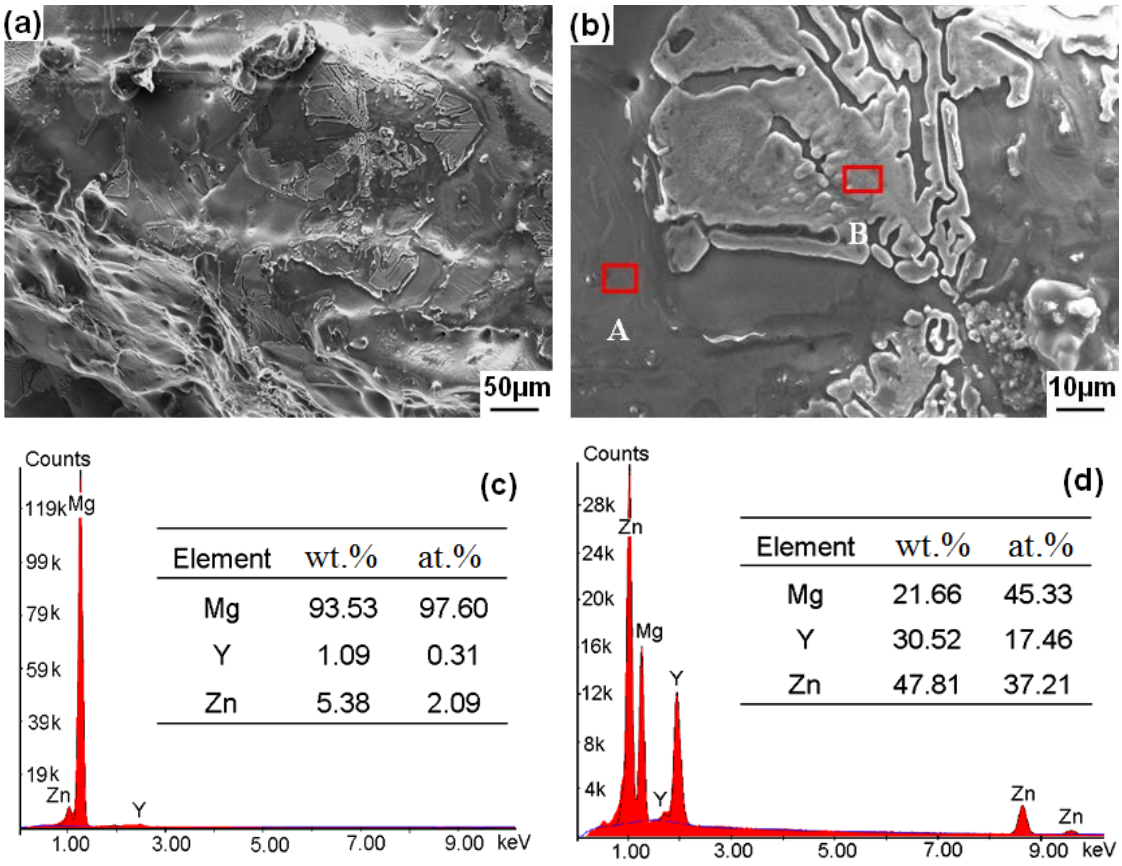

Fig. 6.12 Morphology and EDS analysis results of hot crack fracture surface for Mg-4.5Zn-0.9Y alloy at a mould temperature of 450 °C: (a) and (b) SEM images; (c) A point; (d) B point.

6.2.3 Influence of grain size on HTS

Zirconium can be added to pure Mg or Mg alloys containing Zn, Ag, Y, or Th for grain refinement [108]. One of the major benefits derived from the zirconium addition is the superior efficiency of grain refinement compared with other methods. The peritectic mechanism is usually accepted for grain refinement mechanism promoted by Zr additions, i.e., Zr particles precipitate first as Zr-rich particles, which promote nucleation of primary magnesium grains [109]. Zr has the same *hcp* crystal structure as Mg, and the lattice parameters of Zr (a=0.323 nm, and c=0.514 nm) are very close to those of Mg (a=0.320 nm, and c=0.520). It is believed that elemental Zr, particles or intermetallic, are a powerful nucleant in Mg because of the similarities in the lattice parameters.

As shown in Fig. 5.30, the grain refinement significantly reduces the HTS. It has been shown the hot tearing occur at the mushy zone where the dendrites begin to interlock. For the alloy

without grain refinement, the growth tips of the coarse dendrites meet each other at an earlier stage of solidification. This reduces the duration of the mass feeding and therefore increases the HTS. However, for the alloys with grain refinement, the small equiaxed grains form, and the number of paths for the liquid to flow increase, which can increase the refilling capacity and possible healing of the cracks that formed previously. In addition, this microstructure is more beneficial for the accommodation of deformation caused by the thermal contraction. As a result, the hot crack resistance is improved.

6.3 Prediction of critical liquid fraction

By the measuring of hot tearing curve, the temperature at which the hot tearing initiate can be recorded. Based on this temperature, the corresponding solid fraction or liquid fraction can be calculated using thermodynamic software. The parameter "critical liquid fraction" is important for understanding the hot tearing mechanisms [23]. Critical liquid fraction means the fraction of remaining liquid which cannot flow into the cracks formed previously to heal them. The remaining liquid is blocked by the interconnected dendrites. The previous investigations indicate that the parameter value is in the range from 0.78 to 0.95 [5, 112].

The critical liquid fraction can be estimated based on the morphology of grains [110]. Due to the different cooling rates and under-cooling conditions, two main grain structures form: columnar grains and equiaxed grains [110]. Indeed, the present microstructural observations indicate that the columnar or equiaxed grains are dominant in Mg-Y and Mg-Y-Zn alloys (Fig. 5.10, Fig. 5.11, Fig. 5.25, Fig. 5.26, Fig. 5.30, Fig. 5.34 and Fig. 5.40). Following will be used to calculate the critical liquid fraction based on these two types of grain morphology.

6.3.1 Critical liquid fraction for columnar grain

The columnar grain structures are idealized as equal diameter of cylinder. The solidification enters uncompensated stage when the columnar grains touch with each other. The radius of columnar grains with a cylindrical shape is assumed to be R=1 (Fig. 6.13 (a)) [110]:
The area of inter-dendritic spaces surrounding by points A'B'C' is:

$$S_{A'B'C'} = S_{\Delta ABC} - \frac{1}{2}\pi R^2 = \sqrt{3} - \frac{\pi}{2} \tag{6-3}$$

The liquid volume fraction f_{L1} is calculated as follows:

$$f_{L1} = \frac{S_{A'B'C'}}{S_{\Delta ABC}} = \frac{\sqrt{3} - \frac{\pi}{2}}{\sqrt{3}} = 0.093 \tag{6-4}$$

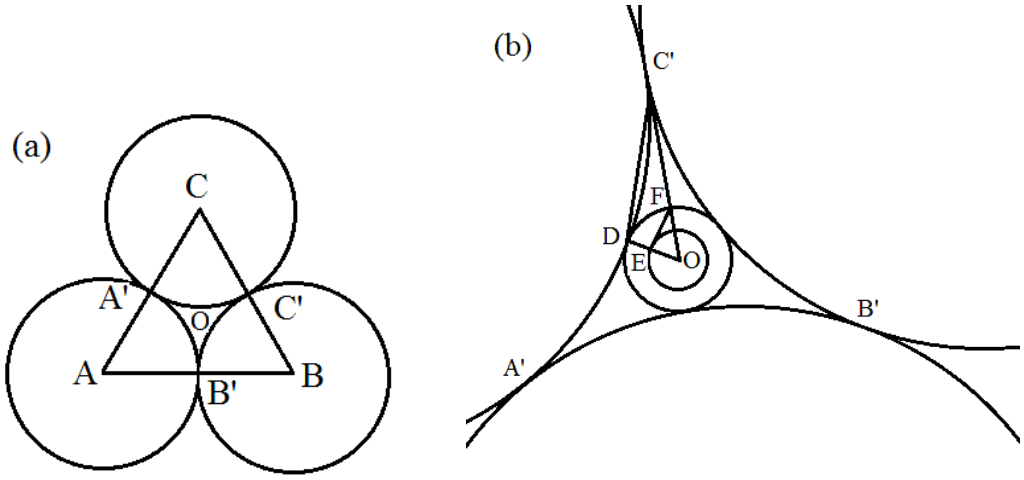

Fig. 6.13 Schematic of calculating the critical liquid fraction for columnar grains: (a) Structure of columnar grains, (b) geometrical relationship [110].

Inter-dendritic separation occurs only below a certain liquid fraction since it requires the liquid to be distributed as an inter-dendritic film. At late stages of solidification, the integrity of the inter-dendritic film becomes impaired and regions of solid cohesion are established between the adjacent dendrites. Under ideal conditions, the liquid remaining between the dendrities solidifies to the centre point O when its shape is similar to a small cylinder ($OE = r$). At that time, the solidification stage enters the inter-dendritic bridging. As show in Fig. 6.13 (b), the liquid volume fraction f_{L2} is calculated as follows:

$$OD = OF = OA - 1 = \frac{2\sqrt{3}}{3} - 1 \tag{6-5}$$

According to the triangle similarity, we can get relationship:

$$\frac{r}{OF} = \frac{OD}{OC'} \tag{6-6}$$

where $OC' = \frac{\sqrt{3}}{3}$. Substituting equation (6-5) into equation (6-6) the following equation is obtained,

$$r = \frac{7\sqrt{3} - 12}{3} \tag{6-7}$$

The liquid volume fraction f_{L2} is then calculated:

$$f_{L2} = \frac{\pi r^2}{\sqrt{3}} = 0.0031 \tag{6-8}$$

Conclusion is that the uncompensated stage and bridging, occurs when the liquid fraction is in the range from 0.0031 to 0.093 for the alloys with columnar grains.

6.3.2 Critical liquid fraction for equiaxed grain

It is assumed that the equiaxed grains are idealized as equal diameter balls. The solidification enters uncompensated stage after the equiaxed grains touch with each other. The ball radius is assumed to be 1 (Fig. 6.14 (a)), then the length of tetrahedral edge: $a = 2$ [111]. The volume of tetrahedron V_{ABCD} is:

$$V_{ABCD} = \frac{1}{3} S_{ABD} h = \frac{\sqrt{2}}{12} a^3 = \frac{2\sqrt{2}}{3} \tag{6-9}$$

where S_{ABD} is the area of triangle, h is the height of the tetrahedron.

The liquid volume fraction f_{L1} is calculated to be:

$$f_{L1} = \frac{\frac{2\sqrt{2}}{3} - 4 \times \frac{\sqrt{2}}{12} - \frac{4\pi}{3}\left[3 - (1 - \frac{\sqrt{3}}{2})\right](1 - \frac{\sqrt{3}}{2})^2}{\frac{2\sqrt{2}}{3}} = 0.26 \tag{6-10}$$

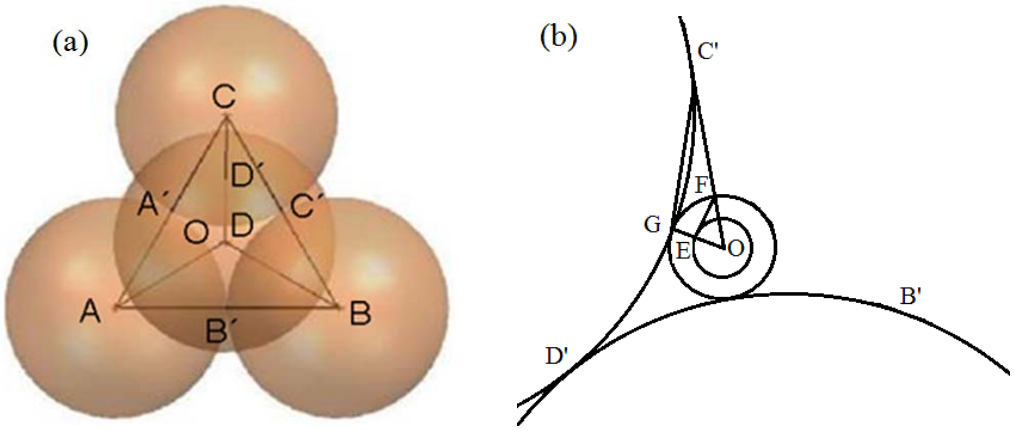

Fig. 6.14 Schematic of calculating the critical liquid fraction for equiaxed grains: (a) structure of equiaxed grains, (b) geometrical relationship [111].

At the last stages of the solidification, the inter-dendritic bridging occurs, and then regions of solid cohesions are established between the adjacent dendrites. Under ideal conditions, the liquid remaining between the dendrities solidifies to the centre point O when its shape is similar to small ball ($OE = r$). At that time, it can be regarded that the solidification stage

enters inter-granular bridging. As show in Fig. 6.14 (b), the liquid volume fraction f_{L2} is calculated to be:

$$OF = OG = OA - 1 = \frac{\sqrt{6}-2}{2} \tag{6-11}$$

According to the similarity in triangle, we can get relation to be:

$$\frac{r}{OG} = \frac{OF}{OC'} \tag{6-12}$$

where is $OC' = \frac{\sqrt{2}}{2}$. Substituting equation (6-11) into equation (6-12) the following equation can then be obtained,

$$r = \frac{5\sqrt{2}}{2} - 2\sqrt{3} \tag{6-13}$$

The liquid volume fraction f_{L2} is calculated to be:

$$f_{L2} = \frac{\frac{4}{3}\pi r^3}{\frac{2\sqrt{2}}{3}} = 0.0016 \tag{6-14}$$

It is concluded that the uncompensated stage and bridging, occurs when the liquid fraction is in the range from 0.0016 to 0.26 for the alloy with equiaxed grains.

Most of the previous investigations illustrate that the hot tearing normally initiates at a solid fraction of about 0.95. However, improving theoretical models and experimental techniques, this value is considered to be changeable. The present results have confirmed that this value depends on the Y content (Fig. 5.8). It changes from 0.918 to 0.997. Fig. 5.23, Fig. 5.33 and Fig. 5.38 show the hot tearing of ternary Mg-Y-Zn alloys at a mould temperature of 250 °C initiate at a solid fraction ranging from 0.568 to 0.942. For Mg-Y and Mg-Y-Zn alloys, the microstructures contained either columnar or equiaxed grains. By analyzing experimental results, it is found that the initiation of hot cracks occurs mostly in the critical fraction range calculated based on these two types of grain morphology. In a recent review [5], Eskin indicated that the critical solid fraction is in the range from 0.85 to 0.95. Interestingly, Cao's investigations showed that the hot tears can initiate even at a lower remained solid fraction of 0.78 [112]. The initiation of hot tearing is affected by many factors: composition, freezing range, grain size and morphology, eutectic phase and mould temperature. In addition, even if the onset temperature is determined, the solid fraction corresponding to this temperature is

normally calculated using thermodynamic calculations. The solidification models i.e. equilibrium model or Scheil model used to calculate the solid fractions are different from the real situation during solidification. Therefore, it is very difficult to determine this value accurately.

6.4 Mechanisms of hot tearing

Over the years, much work has been devoted to understand the mechanism of hot tearing. In general, it is accepted that hot tearing occurs due to solidification shrinkage and thermal deformation that developed during solidification. However, the mechanisms of hot tearing are still not very clear. Up to now, several mechanisms have been proposed: liquid film theory, feeding theory and inter-dendritic bridging theory.

This section discusses the microstructures, hot tearing fracture surfaces and solidification characteristics of Mg-Y-(Zn) alloys, to understand the hot tearing mechanism of Mg-Y-(Zn) alloys at different mould temperatures.

6.4.1 Liquid film theory

Pellini et.al. firstly introduced the liquid film concept in their investigations [47]. They found that the tears start at the time when the metal temperature is above the solidus. At this stage, there is a thin continuous liquid film remaining between the solidified dendrites. It is suggested that the mechanism of hot tearing was the separation of the film at the solidification stage when the solidus is approaching and a minimal amount of liquid remains. The illustration of hot tearing formation based on the liquid film theory is shown in Fig. 6.15 [6]. The linear contraction of volume, deformation of the solid metallic matrix, and the surface tension at that liquid film were investigated for this theory. For simplification, it is assumed that the grains are simplified as shown in Fig. 6.15 and the force is perpendicular to the liquid film layer. Highly concentrated forces can build up in the liquid film region. When the contraction stress is high enough to reach the deformation limit, the hot cracks occur along one of the liquid films. The extension rate of the liquid film region undergoing contraction may vary widely due to a number of factors, including cooling rate and width of the hot spot. If the casting has a fast cooling rate and narrow hot spot, which contribute to a high strain rate, it may result in high HTS. A casting may have a high strain rate, but if the casting has a very short time to maintain its liquid film stage it may exhibit low HTS.

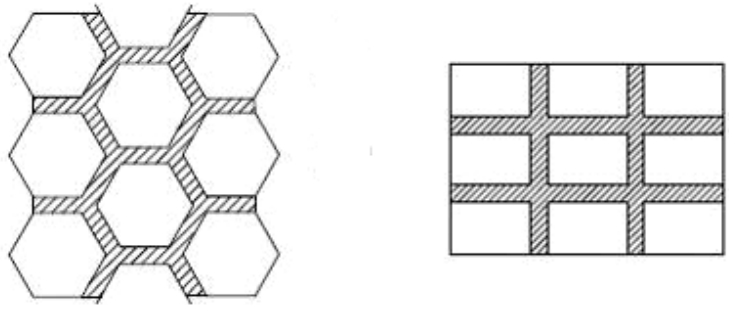

Stage 1: liquid film between grains

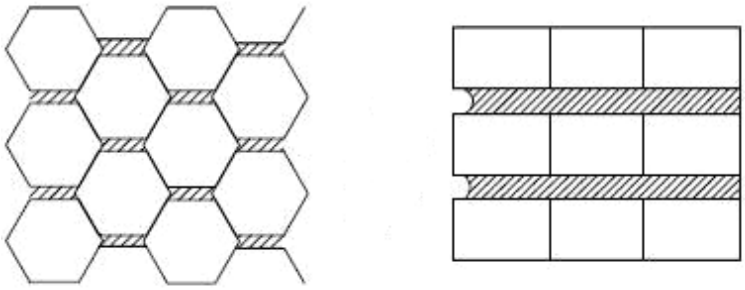

Stage 2: solidification contraction stress causes dendritic separation

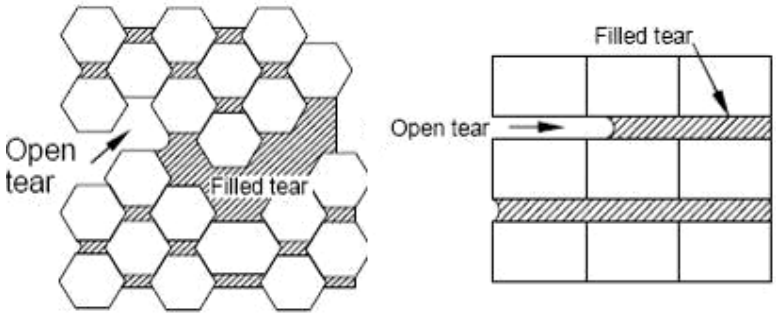

Stage 3: formation of hot tearing

Fig. 6.15 A simple model of hot tearing formation based on liquid film theory [6].

Fig. 6.16 shows the high magnification fracture surfaces of hot cracks in Mg-4.5Zn-xY alloys at a mould temperature of 250 °C. The fracture surfaces are clean and smooth, and dendrite-like bumps on the fracture surfaces are observed. This indicates that a significant amount of inter-dendritic liquid is still present at the initiation of hot tearing. The liquid film region undergoing contraction may cause the dendritic separation, and consequently, the hot tearing forms. The inter-dendritic eutectic liquid increases with the increased in the Y content. In Mg-4.5Zn-2Y alloy, higher volume fraction of low-melting temperature phases form between the dendrite-like bumps due to higher amount of inter-dendritic eutectic liquid present in the final stage of solidification.

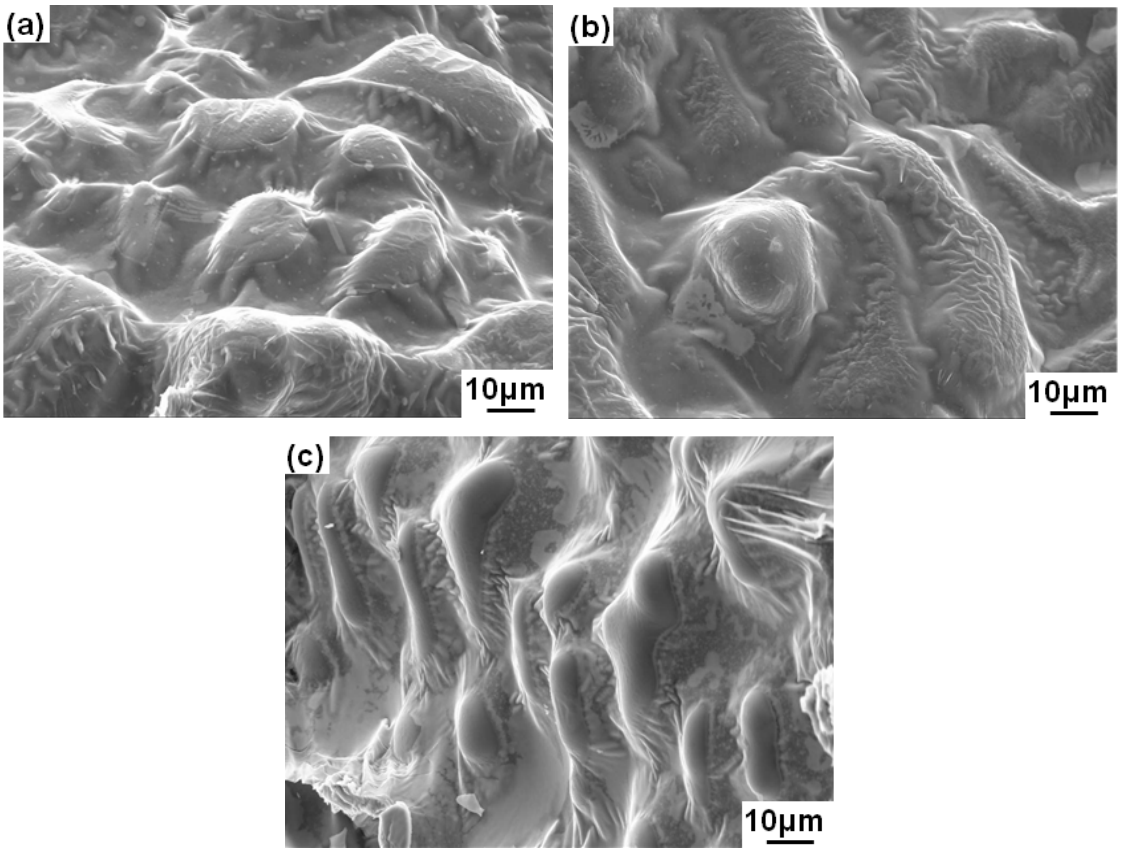

Fig. 6.16 Morphologies of hot tearing surfaces of Mg-4.5Zn-xY alloys at a mould temperature of 250 °C: (a) Mg-4.5Zn-0.4Y, (b) Mg-4.5Zn-0.9Y, (c) Mg-4.5Zn-2Y.

Fig. 6.17 shows the morphological observations of dendrite and tearing ridges for Mg-Y-Zn alloys at a mould temperature of 250 °C. In Mg-0.4Y-4.5Zn-0.5Zr alloy, the dendrites and tearing ridges are observed on the fracture surfaces due to the liquid film undergoing contraction force at the last solidification stage. Interestingly, some elongated liquid films appear on the dendritic surface. The dendrite and tearing ridges are also observed on the fracture surfaces of hot tears in Mg-0.2Y-1.5Zn and Mg-2Y-0.5Zn alloys. However, the dendritic-like bumps are not so apparent on the fracture surface of Mg-2Y-0.5Zn alloy. In addition, many white fracture surfaces are observed after formation of hot tearing due to high contraction stress building up on the liquid film region.

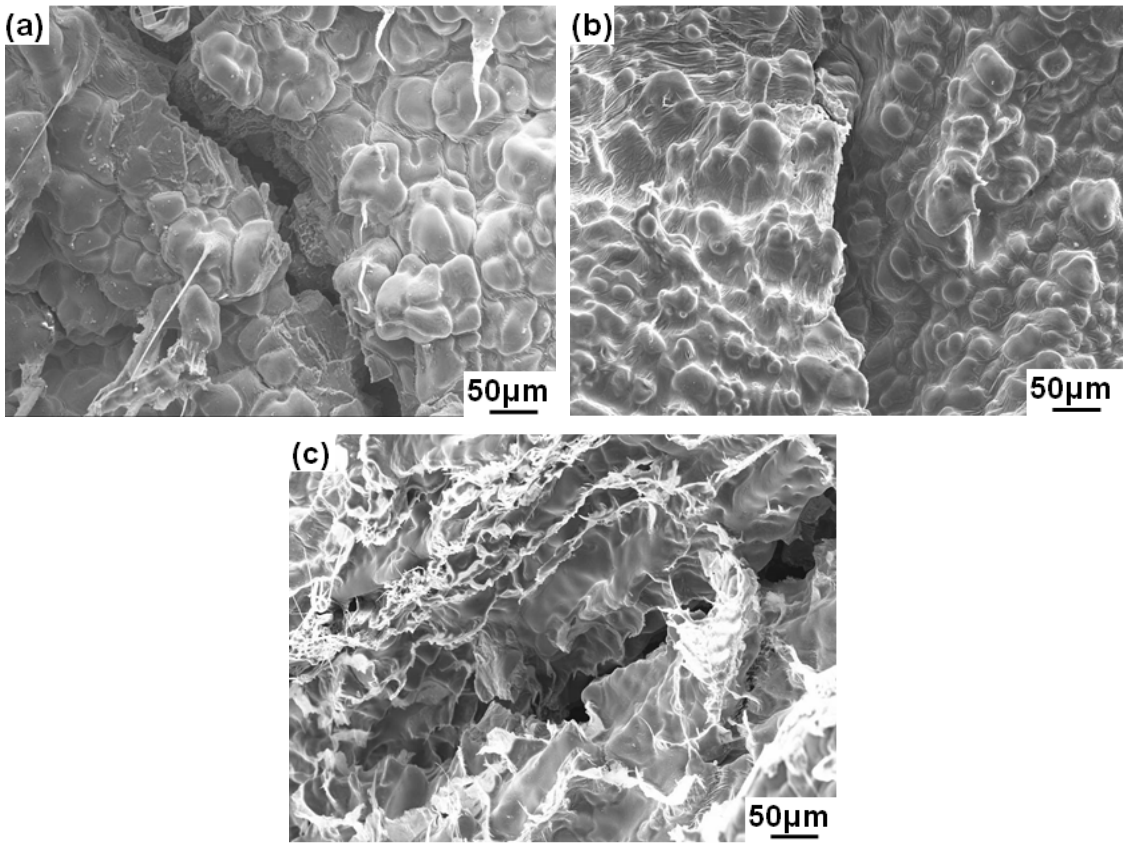

Fig. 6.17 Morphological observations of dendrite and tearing ridges for Mg-Y-Zn alloy: (a) Mg-0.4Y-4.5Zn-0.5Zr, (b) Mg-0.2Y-1.5Zn, (c) Mg-2Y-0.5Zn.

Fig. 5.28 (a) and (c) show the fracture surfaces of Mg-4.5Zn-0.4Y alloy at different mould temperatures. At a lower mould temperature, the fracture surfaces show dendritic fracture. However, with the increase in the mould temperature, the dendrite-like surface morphology disappears. Instead, many fracture surfaces are observed. In industrial practice, most materials used for casting are not pure metal. Low temperature melting phases, and second phases, etc. are always concentrated at grain boundaries under non-equilibrium freezing conditions. The EDS analysis on different positions as shown in Fig. 6.18, it can be found that Y is enriched in these tear ridges with bright contrast that forms at the end of solidification. These tear ridges increase the hot tearing resistance of alloys at a higher mould temperature.

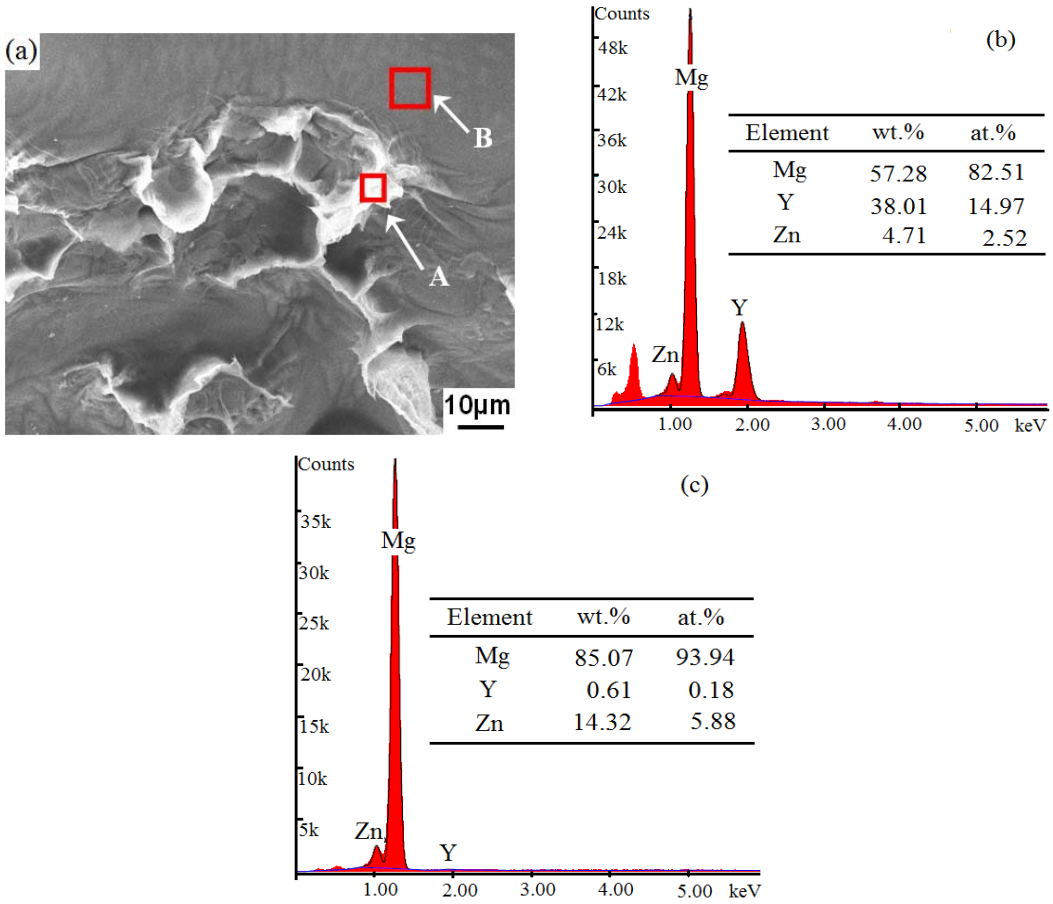

Fig. 6.18 Morphology and EDS analysis results of hot crack fracture surface for Mg-4.5Zn-0.4Y at a mould temperature of 450 °C: (a) SEM image, (b) EDS result of point A, (c) EDS result of point B.

The free dendrites can be observed on the tear surface of the Mg-Y-(Zn) alloys, which are shown in Fig. 5.16, Fig. 5.28, Fig. 5.35 and Fig. 5.39. They indicate that a significant amount of dendritic liquid is still present at the initiation of hot tearing. The liquid film region undergoing contraction mainly causes the dendritic separation and the formation of hot tearing. Some fracture surfaces exhibit tearing ridges at a higher mould temperature.

6.4.2 Feeding theory

It is well known that hot tearing initiate above the solidus temperature at the last stage of solidification with small amount of liquid phase remaining. As the metal approach the end of solidification, the film became thinner and thinner, and the deformation tended to concentrate on the few remaining hot zones, which would lead to hot cracks. It is suggested that the mechanism of hot tearing is the separation of the film at the final solidification stage [113].

However, hot tearing would not occur while there is sufficient feeding during the solidification [68].

According to Eskin et al.'s [5] investigations, four stages of solidification characterize the permeability of the solid network: (1) mass feeding, in which both the liquid and solid can freely move; (2) inter-dendritic feeding, in which the dendrites start to form a solid skeleton and the liquid must flow through the dendritic network; (3) inter-dendritic separation, in which the liquid network becomes fragmented, and pores form or hot tearing may occur; and (4) inter-dendritic bridging, in which the ingot has developed a considerable strength and solid-state creep compensates further contraction. The last two stages are important for hot tearing. With the increase in the solid fraction, the permeability of the solid network becomes very low. The liquid feeding ceases when the solid fraction increases to a critical value. Meanwhile, it is considered that the hindered feeding of the solid phase by the liquid is the main cause of hot tearing. Fig. 6.19 shows a simple model of hot tearing formation based on solidification shrinkage feeding [111]. Based on this theory, the hot tear will not occur as long as there is feeding during solidification. If there is more remaining liquid when the hot crack initiates, the amount of liquid available to refill the crack is more abundant. Furthermore, the slower the crack propagates, the longer is the time available for the liquid to refill the crack.

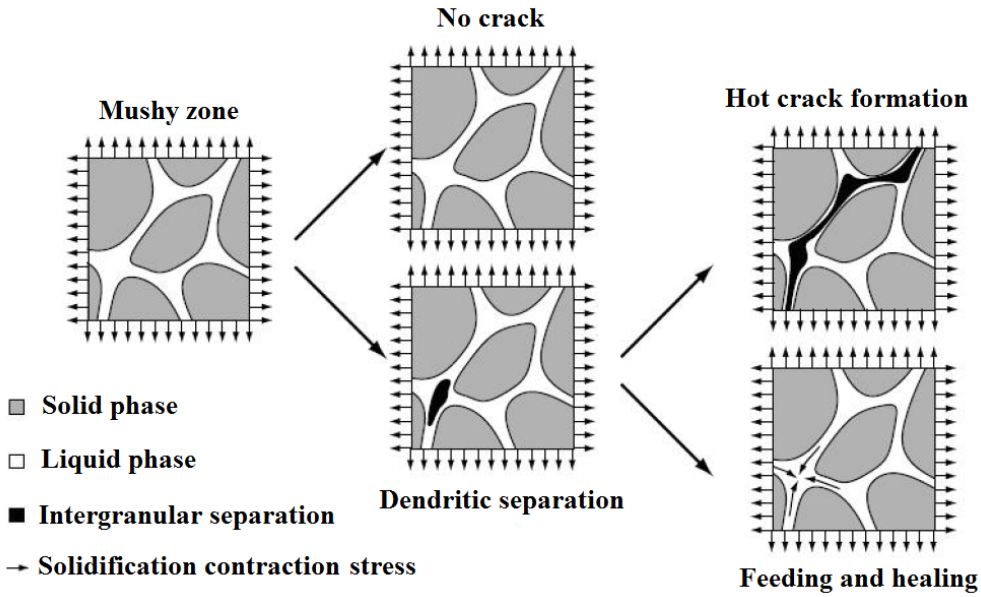

Fig. 6.19 Schematic representation of the conditions required for the hot tearing formation based on solidification shrinkage feeding [111].

As shown in Fig. 5.12 and Fig. 5.14, the refilling of hot cracks by the remaining liquid can be traced. After the hot cracks form, the regions near them have a negative pressure [66, 114]. This negative pressure causes the sucking back the liquid, and refilling of hot cracks to occur. The remaining liquid is enriched with Y, and so it density is much higher than the average density of the alloy. These regions with Y enrichment are seen with white contrast in SEM and in X-ray micro-tomography.

Refilling of hot cracks can be observed in the alloys with high Y content (Fig. 5.12 (e) and Fig. 5.13 (e)). High density of white river-like patterns has been observed in Mg-4Y alloy. In the alloys with higher content of Y, there is a higher volume fraction of low melting point eutectic phases present. The remaining liquid has a higher fluidity. This is reason for the hot cracks that form in these alloys having a higher possibility of healing. Moreover, due to the easy refilling and healing of hot cracks, no apparent drop in load was observed on the hot tearing curve of Mg-4Y alloy.

Fig. 6.20 shows the optical microstructures of hot cracks on the longitudinal sections for Mg-4.5Zn-0.4Y alloy at different mould temperatures. At a mould temperature of 450 °C, the crack feeding is clearly traced through the presence of the second phase particles along the crack path. The elevated mould temperature is beneficial for improving the feeding ability at the last stages of solidification.

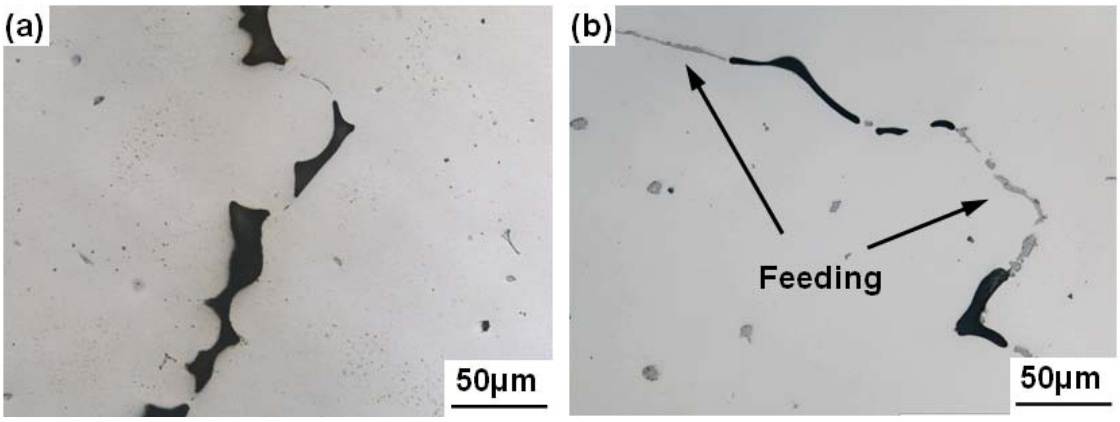

Fig. 6.20 Optical microstructures showing the cracks near the sprue-rod junction of Mg-4.5Zn-0.4Y alloy at different mould temperatures: (a) 250 °C, (b) 450 °C.

Both the low and high magnification optical microstructures of Mg-1.5Zn-xY alloy at a mould temperature of 250 ° C are shown in Fig. 6.21. The increased hot tearing resistance

displayed by the Mg-1.5Zn-xY alloy may be attributed to an increase in the volume fraction of eutectic phase resulting from the higher Y content, which in turn enhances the crack healing. Such an improvement, caused by the higher eutectic liquid fraction, is illustrated by the microstructures shown in Fig. 6.21.

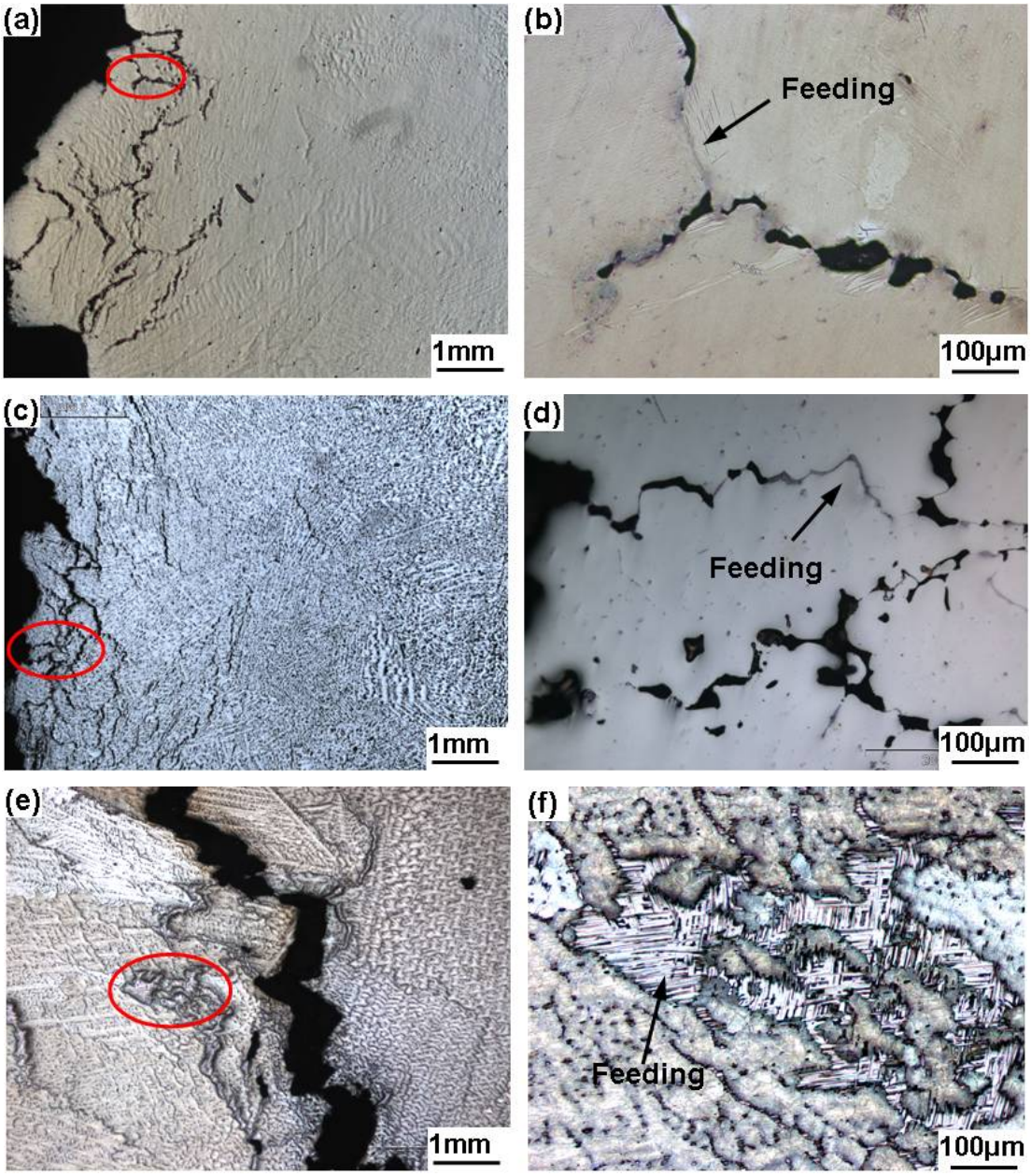

Fig. 6.21 Hot crack region in Mg-1.5Zn-xY at a mould temperature of 250 °C: (a) and (b) Mg-1.5Zn-0.2Y, (c) and (d) Mg-1.5Zn-2Y, (e) and (f) Mg-1.5Zn-3Y.

In the alloys with a higher content of Y (Fig. 6.21 (e)), the HTS is lower due to the large amount of eutectic liquid present at the final stages of solidification which heals the cracks

due to the high fluidity. For example, in Mg-3Y-1.5Zn alloy, there is a coarse river-like structure connecting with a peripheral skeleton-like structure (see the mark in Fig. 6.21 (f)). This is typical characteristic where a hot tearing separation is refilled by the remaining liquid at the last stages of solidification. This liquid, being rich in solute elements, presents itself as regions with higher amounts of eutectic phases after solidification.

6.4.3 Inter-dendritic bridging theory

Hot tearing is defined as failure occurring in the mushy zone of a freezing alloy, i.e. at solid fraction f_s<1. As aforementioned, at the first stage of solidification, the coherent network does not form and hot tears would not occur. As the dendrites grow and come into contact, a coherent network forms. At this time there is a thin continuous liquid film remain between the solidified dendrites. If the remaining eutectic liquid is sufficient, it would feed and "heal" the incipient tears. As the metal approaches the end of solidification, the film becomes thinner and thinner. The deformation tends to concentrate on the few remaining hot zones, which would result in the hot crack. At later stages of the solidification, the integrity of the inter-dendritic film becomes impaired. The regions of solid cohesion are established between the adjacent dendrites. If this can occur to a sufficient extent, then the strength of the casting is greater than that required for preventing the inter-dendritic separation. Evidence of bridging was not frequently observed in microstructure (because the efficient bridges eliminates inter-dendritic separation), but optical observations show that the inter-dendritic bridges exist in the alloys prepared at a mould temperature of 250 °C (Fig. 6.22 and Fig. 6.23).

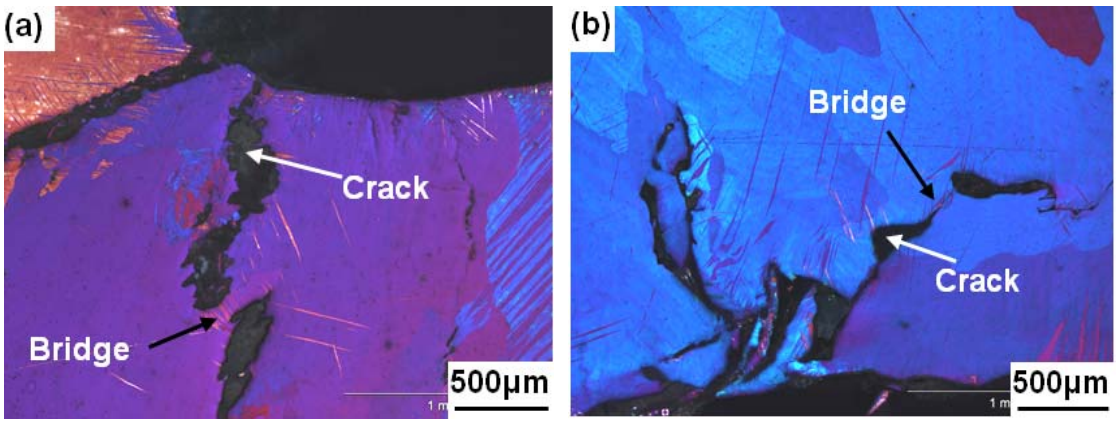

Fig. 6.22 Bridging of hot cracks at a mould temperature of 250 °C: (a) Mg-0.9Y, (b) Mg-1.5Y.

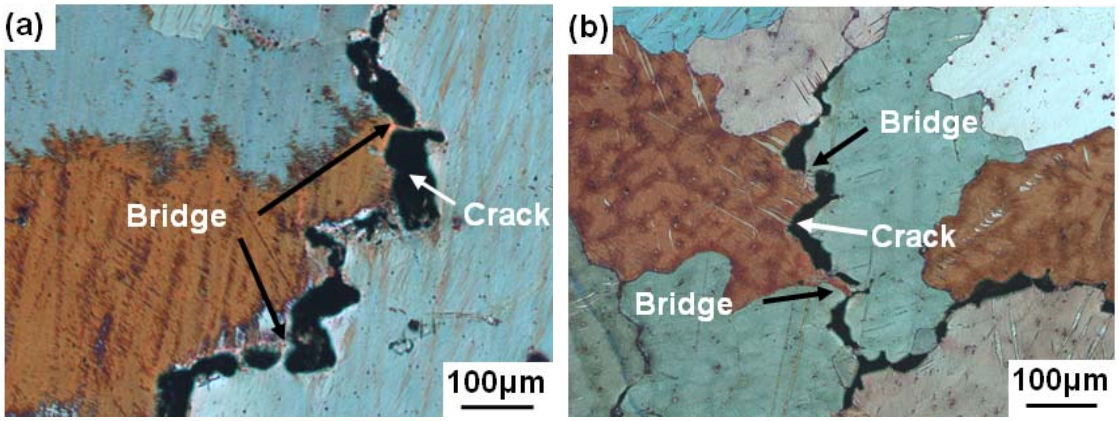

Fig. 6.23 Bridging of hot cracks at a mould temperature of 250 °C: (a) Mg-0.2Y-1.5Zn, (b) Mg-2Y-1.5Y.

After the hot tears initiate, they propagate along the dendrite and grain boundaries with the assistance of thermal stress that occur during solidification (Fig. 6.22, and Fig. 6.23). The thermal stress is released, leading to the further drop in the load (Fig. 5.8), which is clearly reflected on the hot tearing curves. As indicated by Fig. 5.16, the propagation of hot cracks in Mg-0.9Y alloy is easy and proceeds by the inter-dendritic separations. On the fracture surface, a bumpy surface covered with a smooth layer is observed, which shows a typical traces of solidified remaining eutectic liquid film. A similar situation is seen in Mg-1.5Y alloy. In this alloy, the hot crack propagates through inter-dendritic separations. Compared with Mg-0.9Y alloy, the difference is that the amount of tears of interconnected dendrites increases in Mg-1.5Y alloy (Fig. 6.22). This means that in this alloy the propagations of hot cracks are blocked by the interconnected regions. This can also explain why this alloy has slightly lower HTS compared with the Mg-0.9Y alloy. As shown in Fig. 6.23, there are also some small bridges in the regions of hot cracks for Mg-0.2Y-1.5Zn and Mg-2Y-1.5Zn alloys.

The micrographs of inter-dendritic bridging among the hot cracks in Mg-4.5Zn-0.4Y and Mg-4.5Zn-0.4Y-0.5Zr alloys are shown in Fig. 6.24. The inter-dendritic bridging could be broken as shown at point A, but some bridging connects two grains (at point B in Fig. 6.24 (a)). The inter-dendritic separation occurs due to the contraction stress set up during solidification, and then bridging is broken as shown point A. However, for point B, the two adjacent dendrite separation distances is shorter under contraction stress set up, so the bridge is just stretch without being broken, the bridge remains in the crack surface. Fig. 6.24 (b) shows the inter-dendritic bridge at the grain boundaries (such as point A).

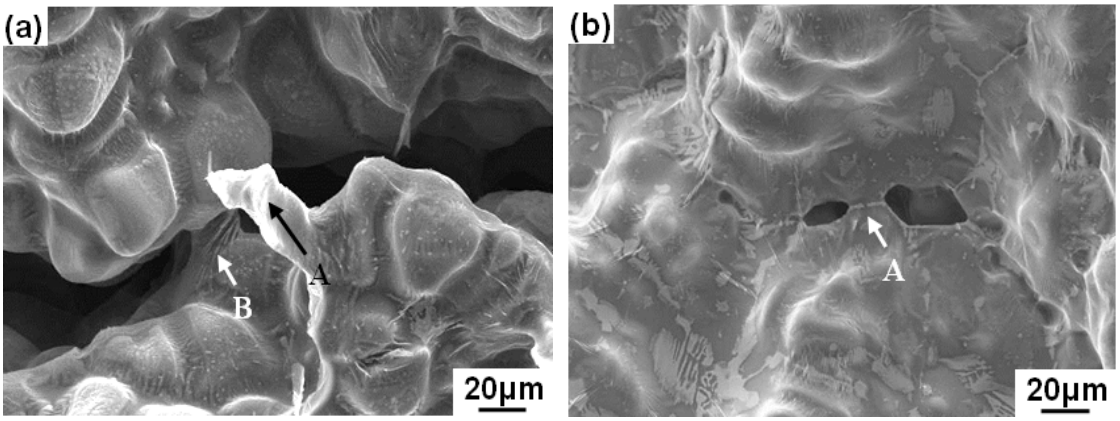

Fig. 6.24 Interdendritic bridging among the hot cracks in Mg-4.5Zn-0.4Y and Mg-4.5Zn-0.4Y-0.5Zr alloys at a mould temperature of 250 °C.

Based on the above discussion, the liquid film theory is applicable for the most binary Mg-Y and ternary Mg-Y-Zn alloys. The inter-dendritic bridges were frequently observed when the alloys show serious HTS. At the last stages of solidification, the inter-dendritic bridging can be broke easily. The hot cracks that form when the bridges are not sufficiently strong to withstand the contraction stress. The feeding theory is dominant mechanism in the alloys with high contents of Y and Zn when the mould temperature is high. Generally, the fluidity of melt increases with the amount of low melting point eutectic liquid. In the alloys with a high content of Y and Zn, the HTS is lower due to the large amount of eutectic liquid present at the final stages of solidification, which heals the cracks.

7 SUMMARY

The hot tearing characteristics of Mg-Y alloy and Mg-Y-Zn alloy castings were investigated with an instrumented CRC mould apparatus. The HTS of alloys was indexed by total volume of hot tears using wax penetration and X-ray micro-tomography methods. Meanwhile, in order to predict the hot tearing behaviour on shape of castings, ProCAST software was used to simulate the HTS of alloys at different compositions and initial mould temperatures. The following summary is drawn.

(1) The influence of Y content on HTS of binary Mg-Y alloys is accurately predicted using thermodynamic calculations based on Clyne and Davies' model. The results show that the curve of HTS as a function of Y content follows a typical "λ" shape. The CSC first increases with increment in Y content, reaches the maximum between 1~2 wt.% Y and then decreases with further increasing the Y content. A simplified version of Clyne and Davies' model was successfully used to illustrate the influence of the solidification range ΔT on HTS of Mg-Y and Mg-Y-Zn alloys.

(2) The CRC method is successfully used to evaluate the HTS of binary Mg-Y and ternary Mg-Y-Zn alloys. When hot tearing initiates, a drop in force is observed on hot tearing curves. For binary Mg-Y alloys, the hot cracks initiate at a critical solid fraction between 0.918 and 0.990. It decreases with the increased content of Y. For ternary Mg-Y-Zn alloys, the hot cracks initiate at large range of solid fractions from 0.372 to 0.942, and depend on the alloy composition and mould temperature.

(3) The initiation and propagation of hot tearing are influenced by alloy composition, grain morphology and size, solidification range and amount of eutectic phases. When the alloy contains large columnar grains, wide solidification range and small amount of second phase it possesses serious HTS, e.g. Mg-0.9Y and Mg-4.5Zn-0.4Y alloys. When the grain sizes decrease with Zr addition, the HTS reduces.

(4) The increment in mould temperature from 250 to 450 °C significantly reduces the HTS of binary Mg-Y alloys and ternary Mg-Y-Zn alloys. High mould temperature reduces the cooling rate resulting in a small thermal gradient and low strain rate imposed on the solidifying casting.

(5) There are three main mechanisms leading to the initiation of hot tearing: liquid film theory, feeding theory and inter-dendritic bridging theory.

- The liquid film theory is applicable for binary Mg-Y and ternary Mg-Y-Zn alloys.
- The feeding theory is dominated mechanism the when alloys have a high content of Y and Zn or were cast at a high mould temperature.
- The inter-dendritic bridges are more observed on microstructures when the alloys have serious HTS.

(6) The predictions of HTS for binary Mg-Y alloys and ternary Mg-Y-Zn alloys using HTI based on the accumulated plastic strain at the last stages of solidification by the ProCAST software are in good agreement with that obtained experimental results.

8 OUTLOOK

- This thesis has predicted the hot tearing tendency of binary alloys based on Clyne and Davies' model. The predicted tendencies correlated well with experimental results. However, it is practical importance to able to predict the hot tearing tendency for multicomponent alloys. In order to predict hot tearing tendency for the multi-component system, it is necessary to modify the Clyne and Davies' model.
- Future work should improve hot tearing theories. The theories may lead to establishment of new predicted models that can be evaluable to all alloy systems.
- A standard hot tearing test system needs to be established and developed which is applicable to all casting alloys and types. In order to quantify the hot tearing tendency, a consistent approach should be agreed upon.

9 REFERENCES

[1] A. Luo. Magnesium: Current and potential automotive applications. JOM: Journal of Minerals, Metals and Materials Society, 2002, 54(2): 42-48.

[2] D.Q. Li, Q.D. Wang, W.J. Ding. Effects of heat treatments on microstructure and mechanical properties of Mg-4Y-4Sm-0.5Zr alloy. Materials Science and Engineering A, 2007, 448 (1-2): 165-170.

[3] Z.H. Huang, Y. Zhang, R.S. Chen, E.H. Han. Hot tearing susceptibility of Mg-Y-Zn-Zr alloys. Foundry, 2009, 58(8): 788-792

[4] G.K. Sigworth. Hot tearing of metals. Transactions of the American Foundrymen's Society, 1996, 104: 1053-1062.

[5] D.G. Eskin, Suyitno, L. Katgerman. Mechanical properties in the semi-solid state and hot tearing of aluminum alloys. Progress in Materials Science, 2004, 49(5): 629-711.

[6] J. Campbell. Castings (Second Edition). Oxford, UK: Butterworth-Heinemann, 2003.

[7] M. Pekguleryuz, P. Labelle, D. Argo, E. Baril. Magnesium diecasting alloy AJ62X with superior creep resistance, ductility and diecastability. In: H.I. Kaplan, editor, Magnesium Technology 2003, TMS, San Diego, California, USA, 2003: 201-206.

[8] Y.S. Wang, Q.D. Wang, G.H. Wu, Y.P. Zhu, W.J. Ding. Hot-tearing susceptibility of Mg-9Al-xZn alloy. Materials Letters, 2002, 57(4): 929-934.

[9] G. Cao, C. Zhang, H. Cao, Y.A. Chang, S. Kou. Hot-tearing susceptibility of ternary Mg-Al-Sr alloy castings. Metallurgical and Materials Transactions A, 2010, 41(3): 706-716.

[10] G. Cao, S. Kou. Hot tearing of ternary Mg-Al-Ca alloy castings. Metallurgical and Materials Transactions A, 2006, 37(12): 3647-3663.

[11] D. Argo, M. Pekguleryuz, P. Labelle, M. Dierks, T. Sparks, T. Waltemate. Die castability and properties of Mg-Al-Sr based alloys. In: J.N. Hryn, editor, Magnesium Technology 2001, TMS, New Orleans, Louisiana, USA, 2001: 181-186.

[12] D. Argo, M. Pekguleryuz, P. Labelle, P. Vermette, R. Bouchard, M. Lefebvre. Process parameters and diecasting of noranda's AJ52 high temperature Mg-Al-Sr alloy. In: H.J. Kaplan, editor, Magnesium Technology 2002, TMS, Seattle, Washington, USA, 2002: 87-93.

[13] Z. Zhen, M. Qian, S. Ji, Z. Fan. The effects of rheo-diecasting on the integrity and mechanical properties of Mg-6Al-1Zn. Scripta Materialia, 2006, 54(2): 207-211.

[14] N. Hort, H. Dieringa, H. Frank, K.U. Kainer. Hot tearing of magnesium alloys. Transactions of the Indian Institute of Metals, 2005, 58(4): 703-708.

[15] J. Campbell. Castings. Oxford, UK: Butterworth-Heinemann, 1991.

[16] I.I. Novikov. Hot shortness of non-ferrous metals and alloys. Nauka, Moscow, Russian, 1966.

[17] S. Bozorgi, K. Haberl, C. Kneissl, T. Pabel, P. Schumacher. Effect of alloying elements (Magnesium and Copper) on hot cracking susceptibility of AlSi7MgCu alloys. In: M. Tiryakioglu, J. Campbell, P.N. Crepeau, editors, Shape Casting: 4th International Symposium, TMS, San Diego, California, USA, 2011: 113-120.

[18] A.A. Gokhale. Solidification Cracking: A Review. Transaction of the Indian Institute of Metals, 1986, 39: 153-164.

[19] H.F. Bishop, C.G. Ackerlind, W.S. Pellini. Investigation of metallurgical and mechanical effects in the development of hot tearing. Transactions of the American Foundry Society, 1957, 65: 247-258.

[20] Y.S. Wang, Q.D. Wang, C.J. Ma, W.J. Ding, Y.P. Zhu. Effects of Zn and RE additions on the solidification behavior of Mg-9Al magnesium alloy. Materials Science and Engineering A, 2003, 342(1-2): 178-182.

[21] W.C. Zheng, S.S. Li, B. Tang, D.B. Zeng, X.T. Guo. Effect of rare earths on hot cracking resistant property of Mg-Al alloys. Journal of Rare Earths, 2006, 24 (3): 346-351.

[22] L. Zhou, Y.D. Huang, P.L. Mao, K.U. Kainer, Z. Liu, N. Hort. Investigations on hot tearing of Mg-Zn-(Al) alloys. In: W.H. Sillekens, S.R. Agnew, N.R. Neelameggham, S.N. Mathaudhu, editors, Magnesium Technology 2011, TMS, San Diego, California, USA, 2011: 125-130.

[23] L. Zhou, Y.D. Huang, P.L. Mao, K.U. Kainer, Z. Liu, N. Hort. Influence of composition on hot tearing in binary Mg-Zn alloys. Proceedings of the 8th Pacific Rim International Conference on Modeling of Casting and Solidification Process (MCSP8-2010), 2010: 97-104.

[24] A. Singh, A.P. Tsai. On the cubic W phase and its relationship to the icosahedral phase in Mg-Y-Zn alloys. Scripta Materialia, 2003, 49 (2): 143-148.

[25] A.R.E Singer, P.H. Jennings. Hot-shortness of some aluminium-iron-silicon alloys of high purity. Journal of the Institute of Metals, 1946, 73: 273-284.

[26] W.I. Pumphrey, J.V. Lyons. Cracking during the casting and welding of the more common binary aluminum alloys. Journal of the Institute of Metals, 1948, 74: 439-455.

[27] J.M. Drezet, M. Rappaz. Study of hot tearing in aluminum alloys using the ring mould test. Modeling of Casting, Welding and Advanced Solidification Processes VIII. In: B.G. Thomas, C. Beckermann, editors, TMS, San Antonio, Texas, USA, 1998: 883-890.

[28] A.R.E. Singer, P.H. Jennings. Hot-shortness of the aluminum silicon alloys of commercial purity. Journal of the Institute of Metals, 1947, 73: 197-212.

[29] D. Warrington, D.G. McCartney. Hot-cracking in aluminum alloys 7050 and 7010-a comparative study. Cast Metals, 1991, 3: 202-208.

[30] D. Warrington, D.G. McCartney. Development of a new hot-cracking test for aluminum alloys. Cast Metals, 1989, 2: 134-143.

[31] I.I. Novikov, O.E. Grushko. Hot cracking susceptibility of Al-Cu-Li and Al-Cu-Li-Mn alloys. Materials Science and Technology, 1995, 11 (9): 926-932.

[32] P. Gunde, A. Schiffl, P. J. Uggowitzer. Influence of yttrium additions on the HTS of magnesium-zinc alloys. Materials Science and Engineering A, 2010, 527(26): 7074-7079.

[33] T.W. Clyne, G.J. Davies. A quantitive solidification test for casting and an evaluation of cracking in Aluminium-Magnesium alloys. The British Foundryman. 1975, 68: 238-244.

[34] T.W. Clyne, G.J. Davies. The influence of composition on solidification cracking susceptibility in binary alloy systems. The British Foundryman, 1981, 74: 65-73.

[35] Z. Zhen, N. Hort, Y.D. Huang, N. Petri, O. Utke, K.U. Kainer. Quantitative determination on hot tearing in Mg-Al binary alloys. Materials Science Forum, 2009, 618-619: 533-540.

[36] S. Li. Hot tearing in cast Aluminum alloys: Measures and effects of process variables. PhD thesis, Worcester Polytechnic Institute, 2010.

[37] S. Instone, D.H. StJohn, J.F. Grandfield. New apparatus for characterizing tensile strength development and hot cracking in the mushy zone. International Journal of Cast Metals Research, 2000, 12(6): 441-456.

[38] D.M. Viano, D.H. StJohn, C.H. Cáceres, J.F. Grandfield. Hot tearing of aluminium-copper Alloys. Light Metals Technology Conference, 2003: 247-250.

[39] C.H. Dickhaus, L. Ohm, S. Engler. Mechanical properties of solidifying shells of aluminum alloys. Transactions of the American Foundry Society, 1994, 101: 677-684.

[40] D.J. Lahaie, M. Bouchard. Physical modeling of the deformation mechanisms of semisolid bodies and a mechanical criterion for hot tearing. Metallurgical and Materials Transactions B, 2001, 32(4): 697-705.

[41] B. Magnin, L. Katgerman, B. Hannart. Physical and numerical of aluminium alloys. Modeling of Casting, Welding and Advanced Solidification Processes VII, In: M. Cross, J. Campbell, editors, TMS, Warrendale, Pennsylvania, USA, 1995: 303-310.

[42] B. Magnin, L. Maenner, L. Katgerman, S. Engler. Ductility and Rheology of Al-4.5% Cu alloy from room temperature to coherency temperature. Materials Science Forum, 1996, 217-222: 1209-1214.

[43] I. Farup, A. Mo. Two-phase modeling of mushy zone parameters associated with hot tearing. Metallurgical and Materials Transactions A, 2000, 31(5): 1461-1472.

[44] L. Zhao, B. Wang, V. Sahajwalla, R.D. Pehlke. The rheological properties and hot tearing behaviour of an Al-Cu alloy. International Journal of Cast Metals Research, 2000, 13(3): 167-174.

[45] B. Commet, A. Larouche. An integrated approach to control hot tearing in sheet ingot casting. In: T.J. Galloway, editor, Light Metals 2006, TMS, San Antonio, Texas, USA, 2006: 833-838.

[46] A. Stangeland, A. Mo, M. M'Hamdi, D. Viano, C. Davidson. Thermal strain in the mushy zone related to hot tearing. Metallurgical and Materials Transactions A: Physical Metallurgy and Materials Science, 2006, 37(3): 705-714.

[47] W.S. Pellini. Strain theory of hot tearing. Foundry, 1952, 80: 125-199.

[48] W.S. Pellini, H.F. Bishop. C.G. Ackerlind. Metallurgy and mechanics of hot tearing. Transactions of the American Foundry Society, 1952, 60: 818-833.

[49] J. Zhang, R.F. Singer. Hot tearing of nickel-based superalloys during directional solidification. Acta Materialia, 2002, 50(7): 1869-1879.

[50] M. Rappaz, J.M. Drezet, M. Gremaud. A new hot-tearing criterion. Metallurgical and Materials Transaction A, 1999, 30(2): 449-455.

[51] M. Braccini, C.L. Martin, M. Suery, Y. Brechet. Relation between mushy zone rheology and hot tearing phenomena in Al-Cu alloys. Modeling of Casting, Welding and Advanced Solidification Processes-IX. Aachen, Germany, 2000: 18-24.

[52] U. Feurer. Influence of alloy composition and solidification conditions on dendrite arm spacing, feeding and hot tearing properties of aluminum alloy. Quality Control of Engineering Alloys and the Role of Metals Science. Delft, The Netherlands: Delft University of Technology, 1977: 131-145.

[53] T.W. Clyne, G.J. Davies. A comparison of experimental results and theoretical predictions relating to the dependence of solidification cracking on composition. Solidification and Casting of Metals, The Metals Society, London, UK, 1979: 275-278.

[54] G. Cao, S. Kou. Hot cracking of binary Mg-Al alloy castings. Materials Science and Engineering A, 2006, 417(1-2): 230-238.

[55] L. Katgerman. A mathematical model for hot cracking of aluminum alloys during DC casting. Journal of the Minerals Metals and Materials Society, 1982, 34(20): 46-49.

[56] W.H. Suyitno, L. Katgerman. Evaluation of mechanical and non-mechanical hot tearing criteria for DC casting of an aluminum alloy. In: P. Crepeau, editor, Light Metals 2003, TMS, San Diego, California, USA, 2003: 753-758.

[57] D.G. Lees, M.A. Member. The hot-tearing tendencies of Aluminum casting alloys. The Journal of the Institute of Metals, 1946, 72: 343-364.

[58] S.A. Metz, M.C. Flemings. A fundamental study of hot tearing. Transactions of the American Foundry Society. 1970, 78: 453-460.

[59] G. Upadhya, S. Cheng, U. Chandra. A mathematical model for prediction of hot tears in castings. In: J.W. Evans, editor, Light Metals 1995, TMS, Warrendale, Pennsylvania, USA, 1995, 1: 101-106.

[60] M. Sadayappan, M. Sahoo, M. Shkuka, B.J. Yang, R.W. Smith. Effect of melt processing and magnetic field on the hot tearing of Al-Cu alloy A201. Transactions of the American Foundry Society. 2002, 110: 407-415.

[61] M. Easton, H. Wang, J. Grandfield, D. StJohn, E. Sweet. An analysis of the effect of grain refinement on the hot tearing of Aluminum alloys. Materials Science Forum, 2004, 28: 224-229.

[62] M. Easton, J. Grandfield, D. StJohn, B. Rinderer. The effect of grain refinement and cooling rate on the hot tearing of wrought Aluminum alloys. Materials Science Forum, 2006, 30: 1675-1680.

[63] J.M. Middleton, H.T. Protheroe. The hot-tearing of steel. Journal of the Iron and Steel Institute, 1951, 168: 384-397.

[64] L. Bichler, K. Lee, A. Elsayed. Effect of mould and pouring temperatures on the hot tearing of AZ91D Magnesium alloy. International Journal of Metal Casting, 2008, 1(2): 43-56.

[65] J.A. Spittle, A.A. Cushway. Influence of superheat and grain structure on hot-tearing susceptibilities of Al-Cu alloy castings. Metals Technology, 1983, 10: 6-13.

[66] Z. Zhen, N. Hort, O. Utke, Y.D. Huang, N. Petri, K.U. Kainer. Investigations on hot tearing of Mg-Al binary alloys by using a new quantitative method. In: E.A. Nyberg, S. R. Agnew, N.R. Neelameggham, M.O. Pekguleryuz, editors, Magnesium Technology 2009, TMS, San Francisco, California, USA, 2009: 105-110.

[67] R.A. Dodd, W.A. Pollard, J.W. Meier. Hot tearing of magnesium casting alloys. Transactions of the American Foundry Society, 1957, 65: 100-118.

[68] R.A. Rosenberg, M.C. Flemings, H.F. Taylor. Nonferrous binary alloys hot tearing. Transactions of the American Foundry Society, 1960, 68: 518-528.

[69] L. Zhou, Y.D. Huang, P.L. Mao, K.U. Kainer, Z. Liu, N. Hort. Influence of composition on hot tearing in binary Mg-Zn alloys. International Journal of Cast Metals Research, 2011, 24: 170-176.

[70] A. Srinivasan, Z. Wang, Y. D. Huang, F. Beckmann, K. U. Kainer, N. Hort. Hot tearing characteristics of binary Mg-Gd alloy castings. Metallurgical and Materials Transactions A, 2013, 44(5): 2285-2298.

[71] S.S. Li, B. Tang, X.Y. Jin, D.B. Zeng. An investigation on hot crack mechanism of Sr addition into Mg-6Al-0.5Mn alloy. Journal of Materials Science, 2012, 47(4): 2000-2004.

[72] U. Chandra, A. Ahmed. Stress analysis. Modeling for casting and solidification processing, 2002: 55-93.

[73] R.W. Lewis, K. Ravindran. Finite element simulation of metal casting. International Journal for Numerical Methods in Engineering, 2000, 47(1-3): 29-59.

[74] R.W. Lewis, E.W. Postek, Z.Q. Han, D.T. Gethin. A finite element model of the squeeze casting processes. International Journal of Numerical Methods for Heat and Fluid Flow 2006, 16(5): 539-572.

[75] E.W. Postek, R.W. Lewis, D.T. Gethin. Finite element modeling of the squeeze casting process. International Journal of Numerical Methods for Heat and Fluid Flow, 2008, 18(3-4): 325-355.

[76] S. Koric, L.C. Hibbeler, B.G. Thomas. Explicit coupled thermomechanical finite element model of steel solidification. International Journal for Numerical Methods in Engineering, 2009, 78 (1): 1-31.

[77] J.Z. Zhu, J. Guo, M.T. Samonds. Numerical modeling of hot tearing formation in metal casting and its validations. International Journal for Numerical Methods in Engineering, 2011, 87(1-5): 289-308.

[78] ProCAST 2010.0 User Manual, ESI Group Inc., 2010.

[79] A.L. Gurson. Continuum theory of ductile rupture by void nucleation and growth: part 1-yield criteria and flow rules for porous ductile media. Journal of Engineering Materials and Technology, 1977, 99(1): 2-15.

[80] V. Tvergaard, A. Needleman. Analysis of the cup-cone fracture in a round tensile bar. Acta Metallurgica, 1984, 32(1): 157-169.

[81] A. Needleman, V. Tvergaard. An analysis of ductile rupture modes at a crack tip. Journal of the Mechanics and Physics of Solids, 1987, 35(2): 151-183.

[82] Z.L. Zhang, C. Thaulow, J. Odegard. A complete Gurson model approach for ductile fracture. Engineering Fracture Mechanics, 2000, 67(2): 155-168.

[83] C. Monroe. Development of hot tearing indicator for steel castings. Ph.D. thesis, University of Iowa, Iowa City, USA, 2008

[84] E.B. Marin, D.L. McDowell. A semi-implicit integration scheme for rate-dependent and rate-independent plasticity. Computers and Structures, 1997, 63(3): 579-600.

[85] M. G. Pokorny. Prediction of hot tearing formation for binary magnesium-aluminum alloys in a permanent mould, Master's thesis, 2009.

[86] S. Sandlöbes, M. Friák, S. Zaefferer, A. Dick, S. Yi, D. Letzig, Z. Pei, L.-F. Zhu, J. Neugebauer, D. Raabe. The relation between ductility and stacking fault energies in Mg and Mg-Y alloys. Acta Materialia, 2012, 60(6-7): 3011-3021.

[87] B.L. Wu, Y.H. Zhao, X.H. Du, Y.D. Zhang, F. Wagner, C. Esling. Ductility enhancement of extruded magnesium via yttrium addition. Matreial Science and Engineering A, 2010, 527(16-17): 4334-4340.

[88] Q.M. Peng, J. Meng, Y. Li, Y.D. Huang, N. Hort. Effect of yttrium addition on lattice parameter, Young's modulus and vacancy of magnesium. Matreial Science and Engineering A, 2011, 528(4): 2106-2109.

[89] X. Zhang, K. Zhang, X. Deng, H.W. Li, Y.J. Li, M.L. Ma, N. Li, Y.L. Wang. Corrosion behavior of Mg-Y alloy in NaCl aqueous solution. Progress in Natural Science: Materials International, 2012, 22(2): 169-174.

[90] A.P. Tsai, Y. Murakami, A. Niikura. The Zn-Mg-Y phase diagram involving quasicrystals. Philosophical Magazine A, 2000, 80(5): 1043-1054.

[91] S. Yi, E.S. Park, J.B. Ok, W.T. Kim, D.H. Kim. (Icosahedral phase+α-Mg) two phase microstructures in the Mg-Y-Zn ternary system. Matreial Science and Engineering A, 2001, 300(1-2): 312-315.

[92] I.G. Watson, P.D. Lee, R.J. Dashwood, P. Young. Simulation of the mechanical properties of an aluminum matrix composite using X-ray micro-tomography. Metallurgical and Materials Transaction. A, 2006, 37(3): 551-558.

[93] J. Alkemper, P.W. Voorhees. Three dimensional characterization of dendritic microstructures. Acta Meterialia, 2001, 49(5): 897-902.

[94] D. Bernard, D. Gendron, J-M. Heintz, S. Bordere, J. Etourneau. First direct 3d visualization of microstructural evolutions during sintering through X-ray computed micro-tomography. Acta Materialia, 2005, 53(1): 121-128.

[95] E. Maire, J.Y. Buffiere, L. Salvo, J.J. Blandin, W. Ludwig, J.M. Letang. On the application of X-ray micro-tomography in the field of materials science. Advanced Engineering Materials, 2001, 3(8): 539-546.

[96] R.W. Hamilton, D. See, S. Butler, P.D. Lee. Multiscale modeling for the prediction of casting defects in investment cast aluminum alloy. Materials Science and Engineering A, 2003, 343(1-2): 290-300.

[97] E. Maire, J.C. Grenier, D. Daniel, A. Baldacci, H. Klocker, A. Bigot. Quantitative 3D characterization of intermetallic phases in an Al-Mg industrial alloy by X-ray micro-tomography. Scripta Materialia, 2006, 55(2): 123-126.

[98] A.A. Nayeb-Hashemi, J.B. Clark. Phase diagram of binary magnesium alloys. Metal Park, OH: ASM International, USA, 1988: 43-46.

[99] H.D. Zhao, G.W. Qin, Y.P. Ren, W.L. Pei, D. Chen, Y. Guo. The maximum solubility of Y in α-Mg and composition range of $Mg_{24}Y_{5-x}$ and Mg_2Y_{1-x} intermetallic phases in Mg-Y binary system. Journal of Alloys and Compounds, 2011, 509(3): 627-631.

[100] PanEngine 7 User's Guide, CompuTherm LLC, 2000-2007.

[101] Y.D. Huang, Z. Wang, A. Srinivasan, K.U. Kainer, N. Hort. Metallurgical characterization of hot tearing curves recorded during solidification of magnesium alloys. Acta Physica Polonica A, 2012, 122(3): 497-500.

[102] M. Paliwal, Y.B. Kang, E. Essadiqi, I.H. Jung. Solidification studies of Mg-Al alloys. In: S.N. Mathaudhu, W.H. Sillekens, N.R. Neelameggham, N. Hort, editors, Magnesium Technology 2012, TMS, Orlando, Florida, USA, 2012: 175-178.

[103] A.K. Dahle, L. Arnberg. The rheological properties of solidifying aluminum foundry alloys. JOM, 1996, 48(3): 34-37.

[104] S. Lin, C. Aliravci, M.O. Pekguleryuz. Hot-tear susceptibility of alumimum wrought alloys and the effect of grain refining. Metallurgical and Materials Transactions A, 2007, 38(5): 1056-1068.

[105] K. Kim, H.N. Han, T. Yeo, Y. Lee, K.H. Oh, D.N. Lee. Analysis of surface and internal cracks in continuously cast beam blank. Iron Making and Steel Making, 1977, 24(3): 249-256.

[106] Pandat-Phase Diagram Calculation Software Package for Multicomponent Systems, Computherm LLC, Madison, WI.

[107] PanMg-Database for Mg Alloys, CompuTherm LLC, Madison, WI.

[108] E.L. Glasson, E.F. Emley. Heterogeneous nucleation in the solidification of aluminum and magnesium alloys. Solidification of metals, Iron and Steel Institute, London, 1968: 1-9.

[109] D.H. Stjohn, Q. Ma, M.A. Easton, P. Cao, Z. Hildebrand. Grain refinement of magnesium alloys. Metallurgical and Materials Transactions A, 2005, 36(7): 1669-1679.

[110] H. Ding, H.Z. Fu, Z.Y. Liu, R.Z. Chen, Z.G. Zhong, D.Z. Tang. Compensation of solidification contraction and hot cracking tendency of alloys. Acta Metallurgica sinica, 1997, 33(9): 921-926.

[111] L. Zhou. Investigations on hot tearing susceptibility and mechanism for Mg-Zn-(Al) alloys. PhD thesis, Shenyang University of Technology, 2011.

[112] G. Cao, I. Haygood, S. Kou. Onset of hot tearing in ternary Mg-Al-Sr alloy castings. Metallurgical and Materials Transactions A, 2010, 41(8): 2139-2150.

[113] V.N. Saveiko. Theory of Hot Tearing. Russian Castings Production, 1961, 11: 453-456.

[114] I. Farup, J.M. Drezet, M. Rappaz. In situ observation of hot tearing formation in succinonitrile-acetone. Acta Materialia, 2001, 49(7): 1261-1269.

10 PUBLICATION LIST

Journal papers

- **Z. Wang**, Y.D. Huang, A. Srinivasan, Z. Liu, F. Beckmann, K.U. Kainer, N. Hort. Experimental and numerical analysis of hot tearing susceptibility for Mg-Y alloys. Journal of Materials Science, 2014, 49: 353-362.
- **Z. Wang**, Y.D. Huang, A. Srinivasan, Z. Liu, F. Beckmann, K.U. Kainer, N. Hort. Hot tearing susceptibility of binary Mg-Y alloy castings. Materials and Design, 2013, 47: 90-100.
- A. Srinivasan, **Z. Wang**, Y.D. Huang, F. Beckmann, K.U. Kainer, N. Hort. Hot tearing Characteristics of binary Mg-Gd alloy castings. Metallurgical and Materials Transactions A, 2013, 44: 2285-2298.
- A. Srinivasan, **Z. Wang,** Y.D. Huang, F. Beckmann, K.U. Kainer, N. Hort. Hot tearing susceptibility of Magnesium-Gadolinium binary alloys. Transactions of the Indian Institute of Metals. 2012, 65(6): 701-706.
- Y.D. Huang, **Z. Wang**, A. Srinivasan, K.U. Kainer, N. Hort. Metallurgical characterization of hot tearing curves recorded during solidification of magnesium alloys. Acta Physica Polonica A, 2012, 122(3): 497-500.

Conference contributions

- **Z. Wang**, Y.D. Huang, Z.S. Zhen, Z. Liu, K.U. Kainer, N. Hort. Hot tearing of magnesium alloys. International Magnesium Association 70th Annual World Magnesium Conference. Xian, China, 2013, 53-63 (Full paper).
- **Z. Wang**, Y.D. Huang, A. Srinivasan, Z. Liu, K.U. Kainer, N. Hort. Influences of Y additions on the hot tearing susceptibility of Mg-1.5wt.% Zn alloys. Light Metals Technology, Old Windsor, United Kingdom, 2013, 306-310 (Full paper).
- **Z. Wang**, Y.D. Huang, A. Srinivasan, Z. Liu, K.U. Kainer, N. Hort. Prediction of hot tearing tendency for binary Mg-Y alloys. In: J.T. Cieslinski, J.A. Szymczyk (Eds.): Developments in mechanical engineering. Strasund, Germany, 2012, 5: 191-197 (Full paper).

CURRICULUM VITAE

Personal information

First name: Zhi

Last name: Wang

Gender: Female

Date of birth: 08.03.1983

Email: wangzhi8303@163.com

Education

2010-2014 Doctoral Candidate at Institute of Metallurgy, Clausthal University of Technology, Germany

2006-2009 Master Degree at School of Materials Science and Engineering, Shenyang University of Technology

2002-2006 Bachelor Degree at School of Materials Science and Engineering, Shenyang University of Technology

Professional experience

2010-2014 Research assistant at Magnesium Innovation Centre, Helmholtz-Zentrum Geesthacht (HZG), Germany

Signature:

Date: